# Accepted Manuscript


U-Pb and Lu-Hf zircon geochronology of the Cañadón Asfalto Basin, Chubut, Argentina: Implications for the magmatic evolution in central Patagonia

N. Hauser, N.G. Cabaleri, O.F. Gallego, M.D. Monferran, D. Silva Nieto, C. Armella, M. Matteini, P.A. Aparicio González, M.M. Pimentel, W. Volkheimer, W.U. Reimold

PII: S0895-9811(16)30154-7

DOI: 10.1016/j.jsames.2017.05.001

Reference: SAMES 1702

To appear in: *Journal of South American Earth Sciences*

Received Date: 22 August 2016

Revised Date: 1 May 2017

Accepted Date: 3 May 2017

Please cite this article as: Hauser, N., Cabaleri, N.G., Gallego, O.F., Monferran, M.D., Silva Nieto, D., Armella, C., Matteini, M., Aparicio González, P.A., Pimentel, M.M., Volkheimer, W., Reimold, W.U., U-Pb and Lu-Hf zircon geochronology of the Cañadón Asfalto Basin, Chubut, Argentina: Implications for the magmatic evolution in central Patagonia, *Journal of South American Earth Sciences* (2017), doi: 10.1016/j.jsames.2017.05.001.

# U-Pb and Lu-Hf zircon geochronology of the Cañadón Asfalto Basin, Chubut, Argentina: implications for the magmatic evolution in central Patagonia.

N. Hauser[(1)*], N.G. Cabaleri[(2)], O.F. Gallego[(3)], M.D. Monferran[(3)], D. Silva Nieto[(4)], C. Armella[(2)], M. Matteini[(1)], P.A. Aparicio González[(2)], M.M. Pimentel[(1)], W. Volkheimer[(5)], W.U. Reimold[(1,6,7)]

*(1) Laboratory of Geochronology, Instituto de Geociências, Universidade de Brasília, 70910 900 Brasília, DF, Brazil,*

*(2) Instituto de Geocronología y Geología Isotópica, Consejo Nacional de Investigaciones Científicas y Técnicas, Universidad de Buenos Aires, Ciudad Universitaria, C1428EHA Buenos Aires, Argentina*

*(3) Centro de Ecología Aplicada del Litoral, Asignaturas Geología Histórica-Micropaleontología (Área Ciencias de la Tierra) - CECOAL-CCT-Nordeste-CONICET, Departamento de Biología, FaCENA-UNNE, C.C.128, C.P. 3400 Corrientes, Argentina.*

*(4) Servicio Geológico Minero Argentino, Instituto de Geología y Recursos Minerales, Av. Julio A. Roca 651, 10° Piso, C1067ABB Buenos Aires, Argentina*

*(5) Instituto Argentino de Nivología, Glaciología y Ciencias Ambientales. Centro Científico Tecnológico Mendoza, Consejo Nacional de Investigaciones Científicas y Técnicas, C.C. 330. (5500) Mendoza, Argentina.*

*(6) Museum für Naturkunde – Leibniz-Institute for Evolution and Biodiversity Research, Invalidenstrasse 43, 10115 Berlin, Germany*

*(7) Humboldt Universität zu Berlin, Unter den Linden 6, 10099 Berlin, Germany.*

**Corresponding author: e-mail address*: *nataliah@unb.br* (Natalia Hauser)

*Universidade de Brasilia-IG-Laboratorio de Geocronología*

*Fax/tel.: +55 031 3559 1861*

Keywords: zircon geochronology; U-Pb and Hf isotopes; Middle Jurassic; Cañadón Asfalto basin; Central Chubut; Magmatic evolution.

## Abstract

The Cañadón Asfalto basin, central Chubut, Argentina, comprises a volcano-sedimentary sequence related to the opening of the Atlantic Ocean during Mesozoic times. The Lonco Trapial, Cañadón Asfalto and Cañadón Calcáreo formations are the main units related to the evolution of this basin. The Las Chacritas and Puesto Almada members are distinguished in the Cañadón Asfalto Formation. LA-HR-ICP-MS U-Pb and Lu-Hf data on zircon were obtained on these units. The Lonco Trapial Formation gave a weighted average age of 172.3±1.8 Ma. A pyroclastic level from the Las Chacritas Member gave a weighted average age of 168.2±2.2 Ma. Two U-Pb concordant ages of 160.3±1.7 Ma on a laminated tuffite and 158.3±1.3 Ma on a pyroclastic level were obtained for the Puesto Almada Member. Two maximum depositional ages constrain the sedimentary provenance areas for the basin: 1) A sample from the Sierra de la Manea range, where a

controversial unit related either to the Cañadón Asfalto or to the Cañadón Calcáreo formation occurs, gave an age of 176.6±1.0 Ma. Two younger zircon crystals indicate that this unit may be related to the Cañadón Calcáreo Formation. 2) A sandstone with cross-stratification from the Puesto Almada Member gave a maximum depositional age of 173.6±6.4 Ma. In terms of U-Pb and Lu-Hf isotopes, two magmatic events are identified in central Patagonia: the *Mamil Choique magmatic event* characterized by negative $\varepsilon_{Hf}$ values around -5.0 and representing recycling during Permian times of Mesoproterozoic crust ($T_{DM}$ of ~1.5 Ga), and the *Cañadón Asfalto magmatic event* with negative (-8.2) to positive (+4) $\varepsilon_{Hf}$ values and Meso- to Neoproterozoic $T_{DM}$ between 1.5 and 0.8 Ga. The younger event is characterized by three main cycles: C1 related to the Lonco Trapial magmatism, C2 to the Las Chacritas volcanism, and C3 to the Puesto Almada volcanism. These cycles are related with Marifil, Chon Aike and El Quemado formations volcanics events of Patagonia and the Neuquén Basin during the Mesozoic.

## 1. Introduction

Since the Triassic and during the Jurassic the Gondwana continent was generally affected by extension, which resulted in thinning of the lithospheric crust (e.g., Cortiñas, 1996). The basement was fragmented into rotated and basculated blocks, showing evidence of extensional phases with superimposed compressional faults (Figari et al., 1996), as in the Middle Chubut area of southern Argentina. Cuneiform basins developed that are delimited by profound normal and listric faults (ibid).

One of these (Figari and Courtade, 1993; Cortiñas, 1996) is the Early Jurassic Cañadón Asfalto basin in the southern part of the North Patagonian Massif (Argentina), to the north of the Deseado Massif, and to the east of the Subcordilleran Plutonic Belt (SPB, Fig. 1a) (Zaffarana and Somoza 2012). This basin is composed of asymmetric graben-type sub-basins as a result of strong extensional activity (Figari et al, 1996; Silva Nieto et al., 2002a, b; Figari, 2005; Figari et al., 2015).

The main lithostratigraphic units associated with the evolution of this basin (Fig. 1b, 2) are the volcanic Lonco Trapial Formation (Lesta and Ferello, 1972) and the continental volcano-sedimentary sequences of the Cañadón Asfalto (Stipanicic et al., 1968) and Cañadón Calcáreo formations (Proserpio, 1987).

The Cañadón Asfalto Formation, that includes basalts and pyroclastic rocks intercalated with lacustrine-fluvio deltaic sequences, is particularly important, as it contains the most diverse continental Jurassic fossil record of South America in terms of vertebrate, invertebrate and plant remains (Rauhut, 2006; Escapa et al., 2008; Gallego et al., 2011; Cúneo et al., 2013). Cabaleri et al. (2010b) defined three sub-basins (Fig. 1b) known as the *Cerro Cóndor* (around the middle Chubut River), *Fossati* (southwest of Gan Gan village), and *El Portezuelo-Llanquetruz* (southwest of Gastre village) sub-basins. The age of the

formation has been variably constrained with paleontological data (Volkheimer et al., 2008; Cabaleri et al., 2010b; Gallego et al., 2011; Olivera et al., 2015) and stratigraphic relationships (Silva Nieto, 2005; Cabaleri et al., 2010a; Figari et al., 2015).

Different geochronological data sets on the Lonco Trapial (Zaffarana and Somoza, 2012), Cañadón Asfalto (Nullo, 1983; Silva Nieto, 2005; Salani, 2007; Cabaleri et al., 2010b; Hauser et al., 2012; Cúneo et al., 2013; Hauser et al., 2014), and Cañadón Calcáreo (Cúneo et al., 2013) formations were used to elucidate the basin development. However, between the different groups working in this area, there is still a lack of agreement regarding: 1) the stratigraphic position for the base of the Cañadón Asfalto Formation, 2) the stratigraphic division of this formation, and 3) the stratigraphic relations between the Lonco Trapial, Cañadón Asfalto, and Cañadón Calcáreo formations, respectively.

Regarding the first problematic, a basalt at the base of the Las Chacritas Member in the Cerro Cóndor sub-basin was given a Bajocian age (170 Ma, Salani, 2007), whereas Cúneo et al. (2013) reported a mid to late Toarcian to Aalenian (perhaps even Bajocian?) age for a tuff level. The age of the underlying Lonco Trapial Formation was variably constrained to the mid to late Toarcian and Aalenian (Nullo, 1983; Silva Nieto, 2005), Pliensbachian (Zaffarana and Somoza, 2012), or Pliensbachian and Toarcian (Cúneo et al., 2013).

With respect to the stratigraphic division of the Cañadón Asfalto Formation (Lizuaín and Silva Nieto, 2005), some authors restrict this stratigraphic term only to the intercalated lacustrine, fluvio-deltaic and tuffaceous rocks defined first by Stipanicic et al. (1968). The division into two members made by Silva Nieto et al. (2003) and then followed by Cabaleri et al. (2010a) was based on the transitional contact between the lacustrine sequence and the fluvio-lacustrine sequence, whereby the former was assigned to the Las Chacritas Member and the latter to the Puesto Almada Member. The contact between these two members is well exposed to the south of Cerro Cóndor sub-basin (Fig. 1b). The problem to either assign the fluvio-lacustrine sequence to the Cañadón Asfalto Formation or to integrate it with the mainly fluvial sequence of the Cañadón Calcáreo Formation led some authors to create a new stratigraphic unit, the La Manea Formation (Figari, 2011). This formation outcrops in the Sierra de la Manea Range (in the following termed “La Manea Range”) in the Cerro Cóndor sub-basin (Fig. 1b).

The stratigraphic relation between the Lonco Trapial and Cañadón Asfalto formations was interpreted by Cabaleri et al. (2010a) as a discontinuity. Other authors (Figari et al., 2015) interpreted a transitional contact from the upper part of the Lonco Trapial Formation to the lower part of the Cañadón Asfalto Formation. Concerning the contact between the Cañadón Asfalto and Cañadón Calcáreo formations, Volkheimer et al. (2009) discussed a tectonic contact in the eastern part of the Chubut River area.

In order to assist with the clarification of the chronostratigraphy of the units related with the evolution of the Cañadón Asfalto basin, new LA-HR-ICP-MS U-Pb in zircon from volcanic units of the Lonco Trapial Formation, as well as the Las Chacritas and Puesto Almada members of the Cañadón Asfalto Formation, sampled in the Cerro Cóndor and Fossati sub-basins, were obtained for this contribution. The geochronological framework for the Cañadón Asfalto Basin can then be used to compare with the paleontological record of the different sedimentary sequences related with the evolution of the basin.

Furthermore, the stratigraphic position of the volcano-sedimentary sequence that outcrops in the La Manea Range (Fig. 3) is currently doubtful due to the complexity of tectonic features in that region. A tuffaceous sample from this sequence has, thus, been investigated as well. At the La Manea Range locality and in the Fossati sub-basin, the potential sediment source areas have been characterized in order to discuss the tectonic evolution and magmatic events of central Patagonia.

Hafnium isotope data on zircon crystals, from the volcanic and sedimentary sequences, previously dated by U-Pb were collected to better understand the regional geological evolution in terms of crustal reworking. An attempt is also made to correlate the volcanic units of the Cañadón Asfalto basin with the Mesozoic magmatic events recognized in Patagonia.

## 2. Geological setting

Figure 2 represents a stratigraphic column for the study area after Cabaleri et al. (2010a). The basement of the Cañadón Asfalto Basin is mainly formed by two magmatic units, the Cushamen Formation (Volkheimer, 1964) and the Mamil Choique Formation (Ravazzoli and Sesana, 1977). The Cushamen Formation is composed of metamorphic and intrusive rocks of Devonian-Carboniferous age (Zaffarana et al., 2013), and the Mamil Choique

Formation comprises migmatites and granitoids including tonalite (Sesana, 1968) of Permian-Triassic age (a K-Ar age of 250±5 Ma; López de Luchi and Rapalini, 2002; López de Luchi and Cerredo, 2008). Granitoids from the *El Portezuelo-Llanquetruz* and *Fossati* sub-basins and from the Pichiñanes Range (Fig. 1b) were dated to 318±2 Ma (Pankhurst et al., 2006). The main outcrop of the Mamil Choique Formation is located in the *El Portezuelo-Llanquetruz* sub-basin, near Gastre village (see Fig. 1). Scarce outcrops of this unit are observed to the east of the Pichiñanes Range and near El Escorial (Fig. 1b).

The Mamil Choique Formation is unconformably overlain by the sedimentary sequences of the Las Leoneras Formation (Nakayama, 1973), the age of which this author assigned to the Hettangian to mid Toarcian, but that could also be Sinemurian to Pliensbachian (Cúneo et al., 2013) or Early Jurassic (Escapa et al., 2008). The Las Leoneras Formation, in turn, is unconformably overlain by Toarcian to Aalenian (Silva Nieto, 2005) mesosilicic lava flows of andesitic/basaltic composition, and by continental sedimentary rocks (Fig. 3) of the Lonco Trapial Formation (Lesta and Ferello, 1972). This formation was included into the Jurassic Large Igneous Province (LIP), the Chon Aike Province (Kay et al., 1989), straddling South America and the Antarctic Peninsula with a total volume of 235,000 $km^3$ (e.g., Pankhurst et al., 1998). As introduced by these authors, the principal silicic volcanic units in extra-Andean Patagonia are the Marifil and Chon Aike formations, and in the Andean Cordillera the El Quemado and Tobífera, as well as the Ibañez, formations in Argentina and Chile, respectively (Fig. 1a).

In the study area (Fig. 1b), the Lonco Trapial Formation is separated from the younger volcano-sedimentary sequence of the Cañadón Asfalto Formation by a regional unconformity (Cabaleri et al., 2010a; Gallego et al., 2011) or exhibits a gradual contact (Figari et al., 2015). The Cañadón Asfalto Formation (Stipanicic et al., 1968), representing the main infill of the basin, was divided into the Las Chacritas and Puesto Almada members (Silva Nieto et al., 2003; Cabaleri et al., 2010a and Gallego et al., 2011).Other authors (Cúneo et al., 2013; Figari et al., 2015) prefer to restrict the Cañadón Asfalto Formation only to the lower part of the unit. In this work, we follow the twofold stratigraphic division proposed by Cabaleri et al. (2010a).

The three sub-basins defined by Cabaleri et al. (2010a) have similar tectonic and sedimentary styles, indicating lacustrine sedimentation prograding to fluvial deposition

(Fig. 3; Cabaleri and Armella, 1999; Cabaleri et al., 2005, 2010a, 2013). Locally, this transition may be truncated by a very smooth angular unconformity, as mentioned by Scasso et al. (2013). Also, diachronism between different sub-basins of the Middle Chubut River and Gastre-Gan Gan areas was recognized (Silva Nieto et al., 2007). These sub-basins record a complete continental sedimentary sequence (Cabaleri et al., 2010a) - including rift phases (Figari et al., 2015), each of which is coeval with acid and basic volcanism (Uliana et al., 1985; Zaffarana et al., 2013).

Located in the southwestern part of the Cañadón Asfalto basin near Cerro Cóndor village (Fig. 1b), the *Cerro Cóndor sub-basin* is limited to the west by the Lonco Trapial Range (type locality for the Lonco Trapial Formation). In this sub-basin, the Las Chacritas Member is characterized by lacustrine sediments (Cabaleri and Armella, 2005; Cabaleri et al., 2010a) interbedded with pyroclastic deposits. Olivine basalt flows, sills and dykes (Cabaleri et al., 2010a) are common at the base of the unit (Fig. 3).

The lacustrine levels are composed mainly of silicified limestones with chert nodules, limestones with planar stromatolites, algal boundstones, conglomerates, sandstones, siltstones, black shales, claystones, and evaporites (Cabaleri et al., 2005, 2010a). Limestones with mudcracks and symmetric ripple cross-stratification occur frequently at the top of this member. In the same section occur well-sorted, fine-grained sandstones with planar cross-stratification and bioturbation that alternate with tuffaceous sandstones, and very fine-grained, massive, yellowish-grey to white, silicified tuffs that have been associated with fluvial channel systems (Silva Nieto et al., 2002b; Cabaleri et al., 2010a). At the Las Chacritas creek locality (Figs. 1b and 3), hyperpicnic flow deposits with vertebrate remains are observed in the middle section of this member (Cabaleri and Armella, 1999).

The succession of the Las Chacritas Member is relevant by fossil content (Fig. 3). This includes spinicaudatans (Tasch and Volkheimer, 1970; Vallati, 1986; Gallego and Cabaleri, 2005), bivalves (Martínez et al., 2007), ostracodes (Musacchio, 1995), palynomorphs (Volkheimer et al., 2008), as well as megaflora (Escapa, 2009) and vertebrates (Rauhut et al., 2002; Rauhut, 2005, 2006; Rougier et al., 2007; Sterli, 2008; Sterli et al., 2010; Gaetano and Rougier, 2011; Pol et al., 2011). Palynomorphs and spinicaudatan (“conchostracans”)

196 and ostracod associations support an early Bajocian to early Bathonian age for this member
197 (Musacchio, 1995, 2001; Martínez, 2002; Volkheimer et al., 2008; Cabaleri et al., 2010a).
198 The upper part of the Cañadón Asfalto Formation was named the Puesto Almada
199 Member. Some authors have related this member to the Cañadón Calcáreo Formation
200 (Cúneo et al., 2013; Zavattieri et al., 2010; Figari et al., 2015), indicating that these two
201 units could be at least partially equivalent. In the type profile, the Cerro Bandera locality
202 (Fig. 3), the Puesto Almada Member consists of tuff and tuffite levels interbedded with
203 dark-grey limestones with ripple cross-stratification and mudcracks. They are interbedded
204 with thin shale and grey claystone beds that contain spinicaudatans. In the lower section of
205 the unit, grey tuff and tuffites, limestones, rhythmites with fish remains, and medium- to
206 coarse-grained sandstones with carbonatic cement and planar cross-stratification occur
207 (Cabaleri et al., 2010a).
208 At the top of the section occurs an intercalation of sandstones with silicified tree trunks
209 in life position (Cabaleri et al., 2010a). Tuffs, sandy tuffites, and red, laminated sandstones
210 and rhythmites with fish remains (López-Arbarello, 2004; López-Arbarello et al., 2013)
211 cover these sandstones. The Puesto Almada Member has been bracketed between the
212 Callovian and the Tithonian (Cabaleri et al., 2010b; Gallego et al., 2011; Hauser et al.,
213 2012), which is supported by dinosaur remains, ostracods and spinicaudatan associations
214 from the Late Jurassic (Musacchio et al., 1990; Musacchio, 1989, 1995, 2001; Rich et al.,
215 1999; Rauhut et al., 2005; Gallego et al., 2011; Monferran et al., 2013).
216 In the *Fossati* sub-basin, the Las Chacritas member is constituded entirely of limestones
217 and basalts, and the Puesto Almada member shows similar lithological characteristics as
218 found in the *Cerro Cóndor sub-basin* (Fig. 3). Details of the sedimentary environments in
219 these sub-basins were presented by Cabaleri and Benavente (2013) and Cabaleri et al.
220 (2013).
221 In the Puesto Almada Member spinicaudatans (Gallego et al., 2010; Monferran et al.,
222 2013), bivalves (Martínez et al., 2007), gastropods (Gallego et al., 2011), ostracods
223 (Musacchio, 1995; Ballent and Díaz, 2011), and Trichoptera (Caddisflies) (Gallego et al.,
224 2011) were identified. The vertebrate content includes tetrapods, amphibians, turtles,
225 dinosaurs, and mammals (Bonaparte, 1979a, b; Rich et al., 1999; Sterli, 2008; Rauhut et al.,
226 2002, 2005; Martin and Rauhut, 2005; Rougier et al., 2007; Báez and Nicoli, 2008; Escapa

et al., 2008; Pol and Rauhut, 2012), and fish remains (Bochino, 1967; Bordas, 1943; López Albarello et al., 2013). The member also includes megaplants (equisetaleans, ferns, and conifers - Frenguelli 1949; Cortés and Baldoni, 1984; Escapa et al., 2008) and gymnosperm and cheirolepidiacean pollen grains (Cabaleri et al., 2013).

The age of the Cañadón Calcáreo Formation has been debated for a long time. Volkheimer et al. (2009) on the basis of palynological evidence placed this entire formation into the Lower Cretaceous between the Berriasian and Hauterivian (Fig. 2), whereas Cúneo et al. (2013) proposed an Oxfordian-Kimmeridgian, perhaps even Tithonian, age. The main difference between Cañadón Asfalto and Cañadón Calcáreo formations is the nearly total absence of calcareous rocks and the relatively weaker faulting and folding in the Cañadón Calcáreo Formation. Proserpio (1987) proposed that to the east of the Chubut River, these two formations, occurs in tectonic contact. Both the Cañadón Asfalto and the Cañadón Calcáreo formations have an angular unconformity to the overlying Los Adobes and Cerro Barcino formations of the Chubut Group of Barremian to Santonian age (Lesta, 1968; Codignotto et al., 1979; Marveggio and Llorens, 2013). The main difference of the Cañadón Calcáreo Formation from the upper Chubut Group is that the latter was not affected by synsedimentary deformation (Proserpio, 1987).

The Cretaceous Chubut Group is composed of pelite, sandstone, conglomerate, tuff, and tuffite of continental origin, deposited during a phase of tectonic stability or thermal subsidence (sag stage; Ranalli et al., 2011). Above the Chubut Group several formations occur (Fig. 2): The Campanian sequences of the Lefipán Formation (Lesta and Ferello, 1972) are represented by fossiliferous sandstone, siltstone, and claystone of an estuarine environment. Campanian to Maastrichtian sandstones and quartzitic conglomerate of the Paso del Sapo Formation (Lesta and Ferello, 1972) correspond to littoral marine environments and braided rivers of delta plains (Page et al., 1999). The Salamanca Formation (Lesta et al., 1980) of Maastrichtian to Paleocene age is composed of sandy limestones and shell beds representing shallow marine environments.

The Eocene to Miocene is represented by tuffs and yellowish-white, sandy tuffites of the Sarmiento Group (Simpsom, 1941). Outcrops of Miocene basalt of the El Mirador Formation (Volkheimer, 1964) are recognized along the northern to middle Chubut River (Turner, 1983). During the Pliocene-Pleistocene, large stratovolcanoes were built along the

North Patagonian Cordillera (Rapela et al., 1988). The Quaternary is represented by old piedmont and colluvial deposits accumulated by mass wasting, as well as alluvial and eolian deposits (Fig. 2).

## 3. Samples and methods

### *3.1 Characteristics of the analyzed samples*

U-Pb and Lu-Hf isotope data for zircon grains were obtained for samples of the stratigraphic units related to the evolution of the Cañadón Asfalto basin. The data are compiled in Tables 1 and 2. Four stratigraphic units were sampled in the Cerro Cóndor sub-basin:

**Sample LT-CT-1** (43º 30´ 59´´ S and 69º 23´ 05´´ W) is a volcanic breccia collected in the Lonco Trapial Range section, at the type locality Puesto César Torres (Figs. 1b and 3). The sample was collected to better constrain the age of the base of the Cañadón Asfalto Formation. In this area the Lonco Trapial Formation is represented by central volcanic edifices (Fig. 4a). The outcrop of LT-CT-1 consists of a purplish-gray volcanic breccia, characterized by pink clasts of andesitic composition (Fig. 4a inset) enclosed in a gray groundmass of the same composition. In thin section, the rock is composed by plagioclase, quartz, and biotite phenocrysts in groundmass of the same mineralogy. Thirty-three zircon crystals, mostly short or long prismatic, up to 500 µm in length (Table 1), with magmatic zonation and some inherited cores (Fig. 5c), were analyzed for their U-Pb isotopic compositions.

**Sample CAV-40** (43º 30´ 22.57´´ S and 69º 10´ 33.7´´ W) was taken in the middle section of the Las Chacritas Member from the lower part of the Cañadón Asfalto Formation in the Asfalto Creek locality (Fig. 3). It is a pyroclastic level of about 20 cm thickness that occurs 10 m below the basal olivine basalt with columnar structure (Fig. 4b). The sample is characterized by angular vitroclastics (shards and pumice fragments), cristalloclastics, and plant remains that are concentrated along the top of the stratum. Sixteen euhedral and long to normal prismatic zircon crystals (Table 1), up to 450 µm in length with magmatic zonation (Fig. 5d), were analyzed for their U-Pb isotopic compositions.

**Sample SCN-2** (43º 16´ 49.2” S and 69º 07´ 45.3” W) was collected from the Puesto Almada Member at the Estancia La Sin Rumbo locality (Fig. 3). It is a yellow, laminated

tuffite level (Fig. 4c) of approximately 40 cm thickness (Gallego et al., 2011). The base of the profile lies on the Lonco Trapial Formation (Fig. 3) with an erosional unconformity; the contact with the overlying unit was not observed. Eight mostly prismatic zircon crystals, up to 150 µm in length (Table 1) with magmatic zonation (Fig. 5d), were analyzed for their U-Pb isotopic compositions.

**Sample LA-Manea-1** (42° 48' 09.7" S and 68° 29' 1.5" W) is a tuffaceous sandstone (Fig. 4d) from the La Manea Range locality. As pointed out above, the sampled unit (Fig. 3) has been variably related to the Cañadón Calcáreo Formation (Prosepio, 1987; Figari et al., 2015) or the Puesto Almada Member of the Cañadón Asfalto Formation (Cabaleri et al., 2010a; Cabaleri et al., 2011). The zircon crystals collected from this sample are up to 400 µm in length, long to short prismatic (Table 1), and generally subrounded (Fig. 6c, inset). In order to constrain the maximum depositional age for this controversial unit, thirty-nine U-Pb analyses on single zircon grains were carried out.

For the *Fossati sub-basin* it was only possible to analyze the Puesto Almada Member, because in this area the Las Chacritas Member is entirely made up of a limestone succession. The Puesto Almada Member has been identified at the Cerro Bandera locality (Fig. 1b), 7.5 km to the east-northeast of Estancia Fossati (Cabaleri et al, 2013). Here, the formation is covered unconformably by Cretaceous fluvial deposits of the Chubut Group. Two samples (Fig. 3) were collected for U-Pb zircon analysis (Table 1) : CAF-8 and CAF-6.

**Sample CAF-8** (42° 48’ 16.72” S and 68° 28’ 51.55” W) was derived from a 60 cm thick, whitish, cross-bedded pyroclastic level (Fig. 4f). The zircon crystals from this sample are up to 400 µm in length, euhedral, and long-prismatic (Fig. 5h).

**Sample CAF-6** (42º 48´ 58.7´´ S and 68° 29’ 58.28´´ W) corresponds to a whitish, medium-grained sandstone with cross-stratification (Fig. 4e). This sample was obtained 20 meters beneath the CAF-8 level. The zircon grains are subrounded to long/short prismatic and up to 300 µm in length (Fig. 6d inset). This sample was collected to determine the maximum age of deposition and to constrain the provenance during deposition of the Puesto Almada Member.

For every sample, representative zircon grains/crystals were analyzed for their Hf isotopic composition (Table 2).

320

321 *3.2 Separation and preparation procedures*

322 Zircon concentrates were extracted from 1-10 kg rock samples by panning at different
323 sizes (100 to 400 µm) and magnetic separation using a Frantz isodynamic separator. After
324 separation, the grains were placed on epoxy mounts, polished to approximately half
325 thickness, and characterized by back-scattered electron and cathodoluminescence imaging
326 using a JEOL QUANTA 450 scanning electron microscope at the Laboratory of
327 Geochronology of Brasilia University. The images provided the basis for selecting
328 locations for laser ablation analysis. The mounts were cleaned with 3% nitric acid before
329 analysis.

330

331 *3.3 U-Pb and Lu-Hf LA-MC-ICP-MS analysis*

332 U-Pb and Lu-Hf isotopic analyses were performed on zircon using a Thermo-Fisher
333 Neptune HR-MC-ICP-MS coupled with a Nd:YAG UP213 New Wave laser ablation
334 system, also at the Laboratory of Geochronology of the University of Brasilia. The U-Pb
335 analyses (Table 1, Fig. 5, 6 and 7) were carried out by the standard-sample bracketing
336 method (Albarède et al., 2004) using the GJ-1 standard zircon (Jackson et al., 2004) in
337 order to quantify the amount of ICP-MS fractionation. The tuned masses were 238, 207,
338 206, 204 and 202. The integration time was 1 second and the ablation time was 40 second.
339 A 30 µm spot size was used and the laser setting was 10 Hz and 2-3 J/cm$^2$. Two to four
340 unknown grains were analyzed between GJ-1 analyses. $^{206}Pb/^{207}Pb$ and $^{206}Pb/^{238}U$ ratios
341 were time corrected. On smaller zircon crystals (about 50 µm), single-spot laser-induced
342 fractionation of the $^{206}Pb/^{238}U$ ratio was corrected using the linear regression method
343 (Košler et al., 2002). The raw data were processed off-line and reduced using an Excel
344 worksheet (Buhn et al., 2009). During the analytical sessions the zircon standard Temora-2
345 (Black et al., 2004) was also analyzed as an unknown.

346 Common $^{204}Pb$ was monitored using the $^{202}Hg$ and ($^{204}Hg$+$^{204}Pb$) masses. Common Pb
347 corrections were not done due to very low signals for $^{204}Pb$ (< 30 cps) and high $^{206}Pb/^{204}Pb$
348 ratios. Reported errors are propagated by quadratic addition $[(2SD^{\wedge 2}+2SE^{\wedge 2})^{1/2}]$ (SD =
349 standard deviation; SE = standard error) of external reproducibility and within-run
350 precision. External reproducibility is represented by the standard deviation obtained from

repeated analyses (*n*=20, ~1.1 % for $^{207}Pb/^{206}Pb$ and up to ~2 % for $^{206}Pb/^{238}U$) of the GJ-1 zircon standard during the analytical sessions, and the within-run precision is the standard error calculated for each analysis. Concordia diagrams (2σ error ellipses) and weighted average ages were calculated using the Isoplot-3/Ex software (Ludwig, 2003). The geologic time scale applied follows that of Cohen et al. (2013; updated).

Zircon crystals previously analyzed for U-Pb isotopes and that show concordant to slightly concordant data (concordance of 6/8 and 7/5 ages between 90 and 110%) were selected for Lu-Hf analysis (Table 2, Fig. 7c). Lu-Hf isotopic data were collected over 40-50 seconds of ablation time and using a 40-50 µm spot size. Measurement spots were carefully positioned in the same growth area but not onto the same spot analyzed for U-Pb data. The signals of the interference-free isotopes $^{171}Yb$, $^{173}Yb$ and $^{175}Lu$ were monitored during analysis in order to correct for isobaric interferences of $^{176}Yb$ and $^{176}Lu$ on the $^{176}Hf$ signal. The $^{176}Yb$ and $^{176}Lu$ contributions were calculated using the isotopic abundance of Lu and Hf proposed by Chu et al. (2002). Contemporaneous measurements of $^{171}Yb$ and $^{173}Yb$ provide a method to correct for mass-bias of Yb using a $^{173}Yb/^{171}Yb$ normalization factor of 1.132685 (Chu et al., 2002). The Hf isotope ratios were normalized to $^{179}Hf/^{177}Hf$ of 0.7325 (Patchett, 1983).

Before the Hf isotope measurements, replicate analyses of a 200 ppb Hf JMC 475 standard solution doped with Yb (Yb/Hf=0.02) were carried out ($^{176}Hf/^{177}Hf$=0.282162±13 2s, n=4). During the analytical sessions, replicate analyses of the GJ-1 standard zircon were executed obtaining an average $^{176}Hf/^{177}Hf$ ratio of 0.282006±16 (2σ; n=25), in good agreement with the reference value for the GJ standard zircon by Morel et al. (2008).

$Hf_{(t)}$ was calculated using the decay constant λ=1.865*10-11 proposed by Scherer et al. (2006) and the $^{176}Lu/^{177}Hf$ and $^{176}Hf/^{177}Hf$ CHUR values of 0.0332 and 0.282772 proposed by Blichert-Toft and Albarède (1997). Two-stage model ages ($T_{DM}$) were calculated from the initial Hf-isotopic composition of the zircon, using an average crustal Lu/Hf ratio (Nebel et al., 2007; Gerdes and Zeh, 2009). The values of $^{176}Lu/^{177}Hf$ = 0.0384 and $^{176}Hf/^{177}Hf$ = 0.28325 were used for depleted mantle (Chauvel and Blichert-Toft, 2001), and $^{176}Lu/^{177}Hf$ = 0.0113 for average crust (Taylor and McLennan, 1985; Wedepohl, 1995).

The initial Hf composition of zircon represents the $^{176}Hf/^{177}Hf$ value calculated for the time of zircon crystallization. For concordant to slightly concordant analyses (%

concordance of 6/8 and 7/5 ages between 90 and 110%), the $^{206}Pb/^{238}U$ and $^{207}Pb/^{206}Pb$ ages were used for the recalculation of Hf isotopic compositions at <1 Ga and >1 Ga grains, respectively.

## 4. Results

### 4.1. *Cerro Cóndor sub-basin*

*Lonco Trapial Formation*

The youngest zircon population of sample **LT-CT-1** shows (Fig. 5a, 7a) a continuous trend of concordant U-Pb ages from 179 to 166 Ma (in gray in Table 1). A weighted average $^{206}Pb/^{238}U$ age of **172.3±1.8 Ma** (MSWD=37) is interpreted as the crystallization age for this unit (Fig. 5a inset). The inherited populations, mostly subrounded grains, are represented by Cambrian-Neoproterozoic crystals. Five zircon crystals (with ages between 166 and 174 Ma) yielded $\varepsilon_{Hf}$ from -2 to +0.9, with Mesoproterozoic $T_{DM}$ of 1.2-1.0 Ga. Two older (536, 580 Ma) crystals have positive $\varepsilon_{Hf}$ (about +2) and also Mesoproterozoic $T_{DM}$ of 1.3 Ga (Fig. 7c).

*Las Chacritas Member*

Fifteen zircon crystals from sample **CAV-40** show a continuous concordant to slightly discordant age trend between 164 Ma and 183 Ma (Fig. 5b and 7a). The nine younger crystals gave a weighted average $^{206}Pb/^{238}U$ age of **168.2±2.2 Ma** (MSWD=2.4), which can be interpreted as the crystallization age**.** Only one zircon has a slightly older age of ca. 230 Ma, due to inheritance from an older source. Seven magmatic zircon crystals (with ages between 164 and 174 Ma) yielded negative $\varepsilon_{Hf}$ values between -9.2 and -6.6 and Mesoproterozoic $T_{DM}$ between 1.6 and 1.4 Ga (Fig. 7c), whereas one zircon with an age of 174 Ma has a negative $\varepsilon_{Hf}$ value of -8.4 and also a Mesoproterozoic $T_{DM}$ of 1.5 Ga.

*Puesto Almada Member*

The analyzed crystals from sample **SCN-2** show concordant to nearly concordant ages between 159 and 182 Ma (Fig. 5g and 7a). Four euhedral and prismatic crystals (in gray in Table 1) gave a concordant age of **160.3±1.7 Ma** (MSWD=3.1), which is interpreted as the crystallization age for the Puesto Almada Member tuffite (Fig. 5e). Two magmatic zircon

grains yielded slightly positive $\varepsilon_{Hf}$ values of 0.6 and 0.1 and Meso- to Neoproterozoic $T_{DM}$ of ~1.0 Ga. One older zircon (Z5: 177 Ma) yielded a negative $\varepsilon_{Hf}$ value of -1.6 and Mesoproterozoic $T_{DM}$ of 1.1 Ga (Fig. 7c).

*The La Manea Range*

The data for **La Manea-1** correspond to a continuous zircon age distribution with populations crystallized between 171 and 206 Ma (97% of the grains), with two main peaks at 177 and 187 Ma (Fig. 6a and 7a). Two younger zircon crystals with ages of 165 and 156 Ma were also analyzed. The weighted average $^{206}Pb/^{238}U$ age for the twenty younger grains (not including the two youngest one) is **176.6±1.0 Ma** (MSWD=1.5) - interpreted as the maximum depositional age of this unit. Twenty-four zircon grains representative of the main U-Pb age populations were analyzed for their Lu-Hf isotopic compositions (Table 2). Zircon grains with ages between 172 and 224 Ma show variable $\varepsilon_{Hf}$ values from -16.1 to +1.3 (compare Fig. 7c), with $T_{DM}$ between 1.9 and 0.9 Ga.

### 4.2. *Fossati sub-basin*

*Puesto Almada Member*

Eleven long-prismatic zircon crystals (Fig. 5h) from sample **CAF-8** gave a concordant age of **158.3±1.3 Ma** (MSWD=0.52), which is interpreted as the crystallization age for this pyroclastic level (Fig. 5f). Seven magmatic zircon crystals with ages between 153 and 160 Ma show negative $\varepsilon_{Hf}$ values between -5.6 and -0.2, with Mesoproterozoic $T_{DM}$ from 1.3 to 1.1 Ga (Fig. 7c).

From the twenty-five zircon grains analyzed from sample **CAF-6**, five grains with concordance below 88 % were discarded (Table 1). In terms of shape and other characteristics, several types of grains were identified (Fig. 6d inset): long, euhedral and prismatic, short and prismatic, fractured, subhedral and prismatic, and subrounded crystals (Fig. 6d inset and Table 1). There is no obvious correlation between these characteristics and the obtained age populations.

The 20 concordant zircon data (concordance between 88-110%) form a bimodal zircon age distribution, with the main population (50 %) yielding two peaks at ~287 and 303 Ma (Fig. 6d). The secondmost important population (25 % of the grains) has two age peaks at

444 172 and 185 Ma. Scattered ages (25 % of grains) between 359 and 418 Ma were also
445 obtained. The weighted average $^{206}Pb/^{238}U$ age (Fig. 6f) for the three youngest grains (Z28,
446 5 and 6 and gray in Table 1) gave a maximum depositional age of **173.6±6.4 Ma**
447 (MSWD=1.7).

448 Grains from the main population (between 287 and 305 Ma) have $\varepsilon_{Hf}$ of -6.0 to -3.5
449 values and Mesoproterozoic $T_{DM}$ of 1.5-1.3 Ga (Fig. 7c); those from the second population
450 display positive to negative $\varepsilon_{Hf}$ values between -2.2 and +4.0 and $T_{DM}$ between 1.9 and 0.8
451 Ga. Four Devonian zircon crystals gave negative $\varepsilon_{Hf}$ values between -4.8 and +0.3, with
452 $T_{DM}$ between 1.5 and 1.2 Ga.

453

454 **5. Discussion**

455 *5.1 Age constraints for the lithological units of the Cañadón Asfalto basin*

456 For the Lonco Trapial Formation a continuous range of concordant U-Pb data on zircon
457 between 180 and 164 Ma was obtained. The twenty younger crystals display a weighted
458 average age of 172.3±1.8 Ma that is interpreted as the crystallization age for the Lonco
459 Trapial Formation at its type locality. The analyzed zircon crystals have magmatic
460 zonation, and some of them display inherited cores, a possible reason for the observed data
461 scatter.

462 Interestingly, Pankhurst and Rapela (1995) obtained a similar age (169±6 Ma, Rb-Sr
463 age) on a rhyolite intercalated with the Lonco Trapial Formation in the Río Chubut area.
464 Several K-Ar ages were obtained on bulk rock samples from different locations of this
465 widely distributed Patagonian unit, at 176±4 Ma (Stipanicic and Bonetti, 1970), 167±5 Ma
466 (Lesta et al., 1980), and 173±9 Ma (Silva Nieto, 2005). More recently, a $^{40}Ar/^{39}Ar$ age of
467 ca. 185 Ma (Zaffarana and Somoza, 2012) was obtained for a sample from north of the
468 study area. Cúneo et al. (2013) bracketed the age for this unit between 189 and 177 Ma
469 (Pliensbachian-Toarcian).

470 Our new U-Pb age (172.3±1.8 Ma) for a volcanic breccia from the Lonco Trapial
471 Formation in its type locality, allows to extend this Jurassic volcanic event to the Bajocian.
472 This result also provides a new age for the base of the Cañadón Asfalto Formation.

473 The CAV-40 sample from the *Cerro Cóndor sub-basin* gave a U-Pb weighted average
474 age of 168.2±2.2 Ma that constrains the age of the lower Las Chacritas Member. This age is

similar to a K-Ar age of 170±4 Ma obtained for the oldest basalt of this unit (Salani, 2007) - and younger than a U-Pb age of 178.766±0.092 Ma (Cúneo et al., 2013). These authors (p. 1269) stated that the dated sample "is from a distinct, 10 cm-thick tuff bed in the stratigraphic interval between the two lower basalt flows of the lower Cañadón Asfalto Formation (transition with the underlying Lonco Trapial Formation) at the Cañadón Lahuincó locality in the Cerro Cóndor area". As is obvious from Figure 7a, the concordant and nearly concordant U-Pb zircon data for the Lonco Trapial Formation and the Las Chacritas Member overlap strongly.

The two ages obtained for the Puesto Almada Member, one for a tuffite level in the *Cerro Cóndor* sub-basin (SCN-2: 160.3±1.7 Ma) and another for a pyroclastic level in the *Fossati* sub-basin (CAF-8: 158.3±1.3 Ma) (Table 1), are very similar within analytical errors, indicating an average age of ~159 Ma for the upper part of the Cañadón Asfalto Formation.

Similar ages were obtained by Cúneo et al. (2013) for tuff samples from the Cañadón Calcáreo Formation. Taking into account that these authors do not subscribe to the division of the Cañadón Asfalto Formation into two members (Las Chacritas and Puesto Almada; Cabaleri et al., 2010b), the synchronicity of their and our ages does not exclude the possibility that the samples were taking from thesame, continuous sequence. However, as Cúneo et al. (2013) did not provide a detailed stratigraphic profile for the sampling site, this possible correlation can, at this point, not be verified. Volkheimer et al. (2009) interpreted field evidence to indicate the presence of a tectonic contact between the Puesto Almada Member and the Cañadón Calcáreo Formation at the type locality. This locality is obviously of crucial importance for any interpretation of the chronostratigraphy of the sequence under investigation, and further geochronological work will be concentrated on this.

Taking into account the K-Ar age of 147±3.3 Ma (Cabaleri et al., 2010a) for a tuff level at the Punta Biotita locality, some 1000 m west of the Estancia El Torito locality (López-Albarello et al., 2013), the current age range for the Puesto Almada Member embraces the period from the Oxfordian to the Tithonian (Fig. 8). The fauna of the La Manea locality includes the spinicaudatan *Congestheriella rauhuti* (Gallego et al., 2010), and fish species, *Luisiella feruglioi* (Bordas, 1943) and *Condorlepis groeberi* (Bordas, 1943) (López-

Arbarello et al., 2013; Monferran et al., 2016). This fossil record is also consistent with an Oxfordian to Tithonian age.

*5.2 Fossil constraint*

In addition to the U-Pb data (Table 1) there is paleontological evidence for the areas studied here, which is summarized in Figure 8. This paleontological evidence may be useful in assessing correlation between study sites and controversy with respect to stratigraphic interpretation.

The fossil record of the Asfalto Creek locality comprises spinicaudatans ?*Euestheria taschi* (Vallati, 1986) (Eosestheriidae), '*Lioestheria' patagoniensis* (Tasch and Volkheimer 1970) (Triglyptidae); Darwinuloid ostracods and bivalves (Cabaleri et al., 2010a; Monferran, 2015). Other records for the fauna of the Las Chacritas Member comprise species of Euestheriidae, Eosestheriidae, and Anthronestheriidae that support an age that cannot be much younger than Early Jurassic to early Late Jurassic (Cabaleri et al., 2010a; Monferran, 2015). The new U-Pb datum of 168.2 Ma for sample CAV-40 supports an extension of this association to the Middle Jurassic (Bajocian-Bathonian).

This fauna is also related to the Middle Jurassic (Bajocian-Bathonian) *Euestheria ziliujingensis* fauna (=*Triglypta-Qaidamestheria*) from China (Li and Masuoka, 2012), the *Skyestheria* fauna (Bathonian or Callovian, Great Estuarine Group) from Scotland (Chen and Hudson, 1991), and the *Carapacestheria* fauna from the late Early Jurassic to basal Middle Jurassic of the Ferrar Group from Antarctica (Chen, 1994).

Based on the ostracod association of *Penthesilenula magna-P. sarytirmenensis* and charophytes, Musacchio (1995), offered an age range from the Lower Jurassic to Middle Jurassic for the levels close to the La Angostura creek, south of the Cerro Cóndor locality, that corresponds to the Lahuincó Creek locality (see profile description in Volkheimer et al, 2008). This association is characteristic for the Middle Jurassic of northern China (Musacchio, 1995, 2001; Pang and Chen, 1996). Volkheimer et al. (2008) studied also palynomorphs from black shales at the Lahuincó Creek locality and noted that these morphospecies belong to the *Microcachryidites castellanosii* sub-biozone defined by Martínez (2002) that corresponds to the latest early Bajocian to early Bathonian.

The fossil record of the Puesto Almada Member at the La Sin Rumbo locality comprises the spinicaudatan *Wolfestheria smekali* (Monferran et al., 2013) (Fushunograptidae), the ostracods *Penthesilenula sarytirmanensis* Sharapova, *Theriosynoecum barrancalensis minor* (Musacchio et al., 1990), and *Mandelstamia* sp., bivalves cf. *Diplodon*, and insect remains. The *Wolfestheria* species (Fushunograptidae - Monferran et al., 2013) from the Puesto Almada Member resembles the components of the Late Jurassic "*Eosestheriopsis* fauna" from the Oxfordian-Kimmeridgian of southwestern China and the *Qinghaiestheria-Mangyalimnadia* fauna of the Kimmeridgian of northwestern China (Li and Matsuoka, 2012). Also, two ostracod species *Theriosynoecum barrancalensis minor (*Musacchio et al., 1990) and *Penthesilenula sarytirmenensis* Sharapova recorded in the Puesto Almada Member belong to the *Theriosynoecum barrancalensis* Zone of the Late Jurassic (Oxfordian-Tithonian; Musacchio, 1989, 2001). On the other hand, the presence of *Congestheriella rauhuti* (Afrograptidae) supports previous ideas about the Late Jurassic to Early Cretaceous age of the Puesto Almada Member (Gallego et al., 2010).

On the basis of the new U-Pb age of 160.3±1.7 Ma and the previous 147 Ma K-Ar age (Cabaleri et al., 2010a) this paleontological association can be bracketed between the Oxfordian and Tithonian stages (compare Fig. 7).

*5.3 Implications from the new provenance data*

The provenance areas during the deposition of the Puesto Almada Member (Fossati sub-basin) were investigated through the zircon populations in sandstone CAF-6. The weighted average age of 173.6±6.4 Ma interpreted here as the maximum depositional age for the Puesto Almada Member seems reasonable, considering that the stratigraphic age of the Puesto Almada Member was constrained by the 158 Ma pyroclastic level (CAF-8) sampled 20 m above the CAF-6 sandstone (Fig. 3).

Fifty percent of the analyzed grains from sample CAF-6 yielded Middle Devonian to early Permian ages (between 386 and 286 Ma), that correspond very well with the basement lithologies. Granitoids from the North Patagonian Massif to the north of the Cañadón Asfalto basin were dated between 289 and 394 Ma (Pankhurst et al., 2006). They also dated a deformed leucogranite exposed to the south of the basin, at 289 Ma. These rocks were grouped together by Ramos (2008) as the Western Magmatic and Metamorphic

Belt. This belt extends from San Martin de Los Andes (Neuquén province) to Paso de Indios (south of the Cañadón Asfalto basin, in the Chubut region). Our three older zircon grains with Lower Devonian ages (~415 Ma) can be related to the plutonic rocks dated by Basei et al. (2005) between 420 and 380 Ma in the same belt.

Our early to middle Jurassic ages (Pliensbachian-Aalenian) for zircon grains in CAF-6 could relate to a source that was part of the Lonco Trapial Formation or of the Las Chacritas Member (Fig. 7a). This indicates that these units were possibly exposed at 158 Ma ago (i.e., there was a phase of regional uplift) and contributed material to the deposition of the Puesto Almada Member.

The weighted average age for the tuffaceous sandstone (La Manea-1) from the La Manea Range is 176.6±1.0 Ma. In addition, there are two younger zircon crystals with concordant ages of 156 and 165 Ma. This could indicate that the dated level belongs either to the Puesto Almada Member or that the analyzed section is younger than 156 Ma. While the Puesto Almada Member (CAF-6) shows a bimodal zircon provenance pattern from Paleozoic sources and Mesozoic terranes, the sample from the La Manea Range (La Manea-1) only yielded a provenance pattern from Mesozoic terranes (from 206 to 171 Ma, this paper), besides some younger zircons. If the unit that crops out in the Sierra de la Manea Range is correlated with the upper Puesto Almada Member, the subtle difference in the provenance patterns in both sub-basins can be explained easily by different source areas having contributed to different parts of the basin.

Alternatively, the difference in the provenance patterns plus the presence of the two younger zircons in the unit sampled in the La Manea Range, for which zircon grains of equivalent age were not found in the CAF-6 sandstone, could indicate that this unit should not be correlated with the Puesto Almada Member but is actually younger than it. If the analyzed level of the La Manea Range would be younger than the Puesto Almada Member, it could be correlated with the Cañadón Calcáreo Formation that was assigned to the Kimmeridgian-Valanginian (from ~157 to ~137 Ma; Cohen et al., 2013; updated) by Proserpio (1987), or alternatively with the basal part of the Cretaceous Chubut Group (Cabaleri et al., 2011; Marveggio and Llorens, 2013). In this scenario, the two younger zircons indicate that during the deposition of the La Manea sequence, the Puesto Almada Member could have resided in an area of positive topography that shed material into the

598 younger basin. The main population of zircon ages between 171 and 206 Ma for the La
599 Manea sample (Fig. 7a) indicates that the main source were Jurassic precursors, such as the
600 Las Leoneras, Lonco Trapial, or Cañadón Asfalto formations.
601 Our observations and the above discussion imply inversion tectonics to have affected the
602 Cañadón Asfalto basin - possible as early as Middle Jurassic times, after 158 Ma. Notably,
603 the only previous reference about inversion tectonics for this basin delimited this tectonic
604 phase to Paleocene-Eocene times (Figari et al., 2015). Additional work on the La Manea
605 Range is obviously desirable.
606
607 *5.4 Crustal growth in central Chubut, Patagonia*
608 Figure 7b shows a bimodal U-Pb zircon age distribution of all analysed zircon
609 crystal/grains of this study. Two magmatic events can be distinguished: an older event with
610 Carboniferous-Permian ages and a younger event with Jurassic ages.
611
612 *The Mamil Choique magmatic event*
613 The older event is named here the *Mamil Choique magmatic event* (between 359 and
614 230 Ma). The name refers to data from the basement of the area, the Mamil Choique
615 Formation. Zircon grains from this unit were "sampled" by the CAF-6 sandstone from the
616 Fossati sub-basin. This eventis well characterized in terms of Hf data (negative $\varepsilon_{Hf}$ values
617 between -6.0 and -3.5 and $T_{DM}$ between 1.5 and 1.3 Ga, Fig. 7c). This event represents
618 recycling, during Permian times, of a Mesoproterozoic crust with $T_{DM}$ of ~1.5 Ga (Fig. 7c).
619 According to Pankhurst et al. (2006) and Fanning et al. (2011), this event coincides with
620 the large-scale crustal melting in the North Patagonian Massif due to a break-off of
621 subducted slab in a post-collisional setting. Hafnium data obtained by Fanning et al. (2011)
622 in zircon crystals from one sample of Mamil Choique granodiorite (MAC-128) from the
623 western part of the North Patagonian Massif indicate Hf characteristics similar to those
624 registered by our sample from the *Fossati* sub-basin (Fig. 7c).
625
626 *The Cañadón Asfalto magmatic event*
627 The younger magmatic event, here named the *Cañadón Asfalto magmatic event*
628 (between 200-150 Ma), combines the data obtained from the Lonco Trapial and Cañadón

Asfalto formations and from the La Manea-1 sandstone. As shown in Figure 7b and in more detail in Fig. 9, three main cycles (or phases) can be distinguished: **C1** between 172-180 Ma, with a main peak at 176 Ma referring mainly to Lonco Trapial magmatism, **C2** between 166-169 Ma with two peaks at 166 and 169 Ma, related to the volcanic deposits of the Las Chacritas Member, and **C3** between 155-162 Ma, with a main peak at 158 Ma corresponding to ages for the pyroclastic levels in the Puesto Almada Member (SCN-2 and CAF-8 samples).

The **C1**, so-called *Lonco Trapial magmatic cycle*, is characterized by a prominent peak at 176 Ma, recorded by zircon crystals from the Lonco Trapial andesite LT-CT-1 and some detrital zircon grains from the CAF-6 sandstone from the Fossati sub-basin. This magmatic cycle is well constrained by Hf isotopic compositions on zircon showing negative and positive $\varepsilon_{Hf}$ values between -2.2 to +4.0 and Meso- to Neoproterozoic $T_{DM}$ between 1.2 and 0.8 Ga (Fig. 7c). With respect to our data, andesitic magmas with positive and negative $\varepsilon_{Hf}$ values may be generated (see Fig. 7c) by: (I) juvenile magmas strongly contaminated with old crust, or by (II) partial melting of old lower crust or fossilized lithospheric mantle (Pankhurst and Rapela 1995), in this case of Neoproterozoic-Mesoproterozoic age (~1.0 Ga).

The first possibility (I, Fig. 7c) is in agreement with the presence - at about 176 Ma to the west of the Lonco Trapial Formation - of a cordilleran type magmatic arc, the so-called "Sub-Cordilleran Plutonic Belt" (Haller et al., 1999) (Fig. 1a), with granites of I-type characteristics. Mixing of juvenile magmas, possibly generated by extension behind the arc, with old crust could have generated magmas with hybrid isotopic characteristics (Fig. 7c), as suggested by this study. It is interesting to note that at least 40 % of the new data correspond to inherited zircon, indicating that this juvenile magma was contaminated with older crust of Paleozoic, Neoproterozoic, and Paleoproterozoic ages.

The second possibility (II, Fig. 7c) is supported by Nd model ages (between 1.2 and 1.5 Ga) for several Paleozoic and Jurassic granitoids and metasedimentary rocks of Patagonia (Pankhurst and Rapela, 1995). These authors interpreted their data to indicate the possible involvement of fossilized lithospheric mantle or partial melting of lower crust to form juvenile Jurassic magmas with such Nd $T_{DM}$ ages. Our Hf $T_{DM}$ ages allow for this possibility as well. Geochemical data for our LT-CT-1 sample (e.g., La/Ta=44.5 and

Ba/La=15.7 - N. Hauser, unpublished results) indicate that the Lonco Trapial Formation has arc affinity in agreement with Page and Page (1993).

Following the discussion of Page and Page (1993), Pankhurst et al. (1996), and Zaffarana et al. (2014), the geochemical character of the Lonco Trapial volcanics variably favors affinity to an extensional setting (Uliana et al., 1985; Figari et al., 2015), an arc setting (Page and Page 1993; Pankhurst et al. 1996), or a mixed extensional and arc setting (Zaffarana et al., 2014). Uliana et al. (1985) proposed that basalts of the Lonco Trapial Formation were generated in an extensional setting related to injection of mantle-derived magmas into the lower crust. Zaffarana et al. (2014) interpreted that this crust had arc affinity, so that the resulting melts were arc-crust contaminated. The hybrid magmas would have reached the surface through normal faults in an extensional regime, producing big volumes of pyroclastic material. Figari et al. (2015) postulated that the volcanism of the Lonco Trapial Formation was generated in a half-graben associated with extension.

The **C2** magmatic cycle is represented by the *acid volcanics* (pyroclastic rocks) *of the Las Chacritas Member* (168 Ma, Fig. 7c). This cycle is isotopically well constrained by Hf isotopic compositions of zircon crystals - of negative $\varepsilon_{Hf}$ values with a peak at -8.2. Therefore, one possible interpretation is that the Las Chacritas magmatism represents crustal reworking during Jurassic times of an old crust with $T_{DM}$ between 1.4 and 1.55 Ga. As shown by Figure 7c, this old crust is also similar in terms of Hf isotopic character to the *Mamil Choique magmatic event*, denoting that possibly the same Mamil Choique basement was recycled at ~168 Ma during C2, in still unknown source areas.

The last magmatic cycle **C3** is represented by the *acid volcanism (pyroclastic rocks) of the Puesto Almada Member* (SCN-2+CAF-8 = ca. 159 Ma) and two zircon grains from the La Manea-1 sample. It shows mixed Hf isotope characteristics (Fig. 7c), namely, negative to slightly positive $\varepsilon_{Hf}$ values between -5.6 and 2.1 and $T_{DM}$ between 1.3 and 0.9 Ga (Fig. 7c). One explanation for these findings could be that a juvenile magma with Lonco Trapial Hf isotope characteristics was highly contaminated with old crust (compare Fig. 7c), maybe the Mamil Choique basement.

*5.5 Relationship between the Cañadón Asfalto magmatic event and the main volcanic cycles of Patagonia*

691 Regarding geochronological data previously obtained for Jurassic igneous rocks of
692 Patagonia and Antarctica, Pankhurst et al. (2000, Fig. 9) recognized three main magmatic
693 phases of volcanism: V1 (188-178 Ma), V2 (172-168 Ma), and V3 (157 and 153 Ma).
694 These phases overlap partially with our main cycles of the *Cañadón Asfalto magmatism*
695 (Fig. 9). Our *Lonco Trapial magmatic cycle* (between 172-180 Ma) is bracketed by the V1
696 and V2 phases. The *Las Chacritas volcanic cycle* (166-169 Ma) overlaps exactly with the
697 V2 phase, and the *Puesto Almada volcanic cycle* partially overlaps with the V3 phase.
698 The V1 phase is contemporaneous with the emplacement of rhyolite and ignimbrite of
699 the Marifil Formation (Pankhurst et al., 2000) that outcrops in central Patagonia to the east
700 of the study area, along the Atlantic coast (Fig. 1a). These authors related this magmatism
701 to the Gondwana break-up. Today this phase is well exposed in Antarctica (the Ferrar
702 Supergroup), Australia (Tasmanian dolerite), and South Africa (Karoo province). The
703 V1volcanic cycle is also contemporaneous with arc activity in the Subcordilleran Batholith
704 of Patagonia (Fig. 1a) that lasted until 180 Ma (Rapela *et al*., 2005), as well as with the
705 early stages of the Andean magmatic arc in the Neuquén Basin (Saini-Eidukat *et al*., 2002;
706 Castro *et al.*, 2011). This arc has been implicated as the likely source of ash material
707 produced from the Pliensbachian up to the Toarcian/Aalenian boundary (Llambías and
708 Leanza, 2005).
709 The second ignimbrite volcanism event, V2, occurred in the eastern part of the Deseado
710 Massif in southern Patagonia, and was related to the Chon Aike Formation of Argentina
711 and the Mapple Formation in Antarctica (Pankhurst et al., 2000). Finally, the V3 event was
712 related to the ignimbrites and associated granites of the eastern Andes (El Quemado
713 Formation of Argentina and Ibañez Formation of Chile - Fig. 1a).
714 Based on Figure 9, it can be speculated also whether the Lonco Trapial Formation could
715 be related to the widespread magmatism that took place with the opening of the Atlantic
716 Ocean over a somewhat extended period from 188 until 172 Ma (this work). If the
717 pyroclastic rocks of the Las Chacritas and Puesto Almada cycles are not generated inside
718 the basin, they could represent air fall from the extensive ignimbrite production of the Chon
719 Aike Formation (V2) as found in the Deseado Massif and the El Quemado Formation (V3)
720 of the Andes. The characteristics of the analyzed zircon crystals from the Las Chacritas and

Puesto Almada members, long-prismatic with smooth marks of sedimentary reworking, also support this interpretation.

## 6. Conclusions

New U-Pb geochronological results on zircon combined with a Hf isotopic study on lithological units related to the Cañadón Asfalto basin in Central Chubut (Argentina) yielded important information about the evolution of the basin. The main conclusions are as follows:

1) The age for the base of the Cañadón Asfalto Formation is doubly constrained to ~171 Ma by new data for the Las Chacritas Member (168.2±2.2 Ma) and the Lonco Trapial Formation (172.3±1.8 Ma).

2) The two members of the Cañadón Asfalto Formation are different in age and Hf characteristics. The age of the Las Chacritas Member is constrained to 168.2 Ma; this member is characterized by negative $\varepsilon_{Hf}$ values. ThePuesto Almada Member is constrained by two U-Pb data of 158.3 (CAF-8) and 160.3 (SCN-2) Ma, and mostly slightly negative $\varepsilon_{Hf}$ data.

3) The relatively younger age obtained in this work for the Lonco Trapial Formation (172.3 Ma) for a sample from the type locality, in comparison to the $^{40}Ar$-$^{39}Ar$ data (~185 Ma) for the same unit further to the north (Zaffarana and Somoza 2012), confirms the diachronism of the unit that is younging to the south. The Hf data of this study indicate that the unit has more affinity to an arc than to an extensional setting.

4) Considering that our age for the Puesto Almada Member is the same as the age for the Cañadón Calcáreo Formation by Cúneo et al. (2013), it remains unclear at this point whether the Cañadón Calcáreo sandstones are part of the Puesto Almada Member, or vice versa. Further field work to resolve this remaining problematic is mandatory.

5) Two main magmatic events with different Hf ratios are identified in this work: the *Mamil Choique* (359-230 Ma) and the so-called *Cañadón Asfalto* (200-150 Ma) magmatic events

6) The *Cañadón Asfalto* magmatic event seems to have been episodic between 200 and 150 Ma. Previous data obtained by Pankhurst et al. (2006) for volcanic and plutonic rocks of Patagonia and the Antarctic Peninsula corroborate this argument.

752 7) For the Lonco Trapial magmatic cycle the Hf isotopic data suggest that these magmas
753 either were formed by reworking of Meso- to Neoproterozoic crust or by the mixing
754 between a juvenile source with older crust.
755 8) The three main cycles recognized here partially overlap in age with the Marifil, Chon
756 Aike, and El Quemado/Ibañez formations that represent the main volcanic events
757 associated with the Atlantic opening in Patagonia. The Lonco Trapial cycle (C1) could be
758 related with the Subcordilleran Batholith in Patagonia and the Andean magmatic arc in the
759 Neuquén Basin.
760

761 **Acknowledgements**

762 The LA-MC-ICP-MS facility at the Universidade de Brasília (UnB) was installed with
763 funds provided by PETROBRAS and the Ministério de Minas e Energia do Brasil. This
764 study was supported by grants from the Consejo Nacional de Investigaciones Científicas y
765 Técnicas (CONICET) Nº 5760, 112-201001-00034 (NC) and 5581 (OFG). The authors
766 acknowledge the Comisión Nacional de Energía Atómica (CNEA) for logistic support at
767 the Campamento Los Adobes during field trips. G. Giordanengo is thanked for some
768 drafting support. Mr. and Mrs. Fossati are thanked for providing access to Estancia Fossati.
769 Mrs. Ana Marcela Sanchez is acknowledged for assistance in the preparation of the
770 bibliography, and Mrs Luciana Pereira (UnB, Brazil) for assistance with
771 cathodoluminescence imaging. WUR contributed to this project while on sabbatical at the
772 Geochronology Laboratory at UnB. We are very grateful to two reviewers, Carita
773 Augustsson and an anonymous referee, and the Associate Editor, Reinhardt Fuck, for
774 providing essential guidance that improved our manuscript considerably.
775

776 **References**

777 Albarède, F., Telouk, S. Blichert-Toft, J., Boyet, M., Agranier, A., Nelson, B., 2004.
778 Precise and accurate isotopic measurements using multiple-collector ICPMS.
779 Geochimica et Cosmochimica Acta 68, 2725–2744.
780 Baéz, A.M., Nicoli, L., 2008. A new species of *Notobatrachus* (Amphibia, Salienta) from
781 the Middle Jurassic of northwestern Patagonia. Journal of Paleontology 82, 372–376.

782 Ballent, S.C. and Díaz, A.R., 2011. Contribution to the taxonomy, distribution and
783 paleoecology of the early representatives of Penthesilenula Rossetti & Martens, 1998
784 (Crustacea, Ostracoda, Darwinulidae) from Argentina, with the description of a new
785 species. Hydrobiologia 2011, 1-14.
786 Basei, M.A., Varela, R., Passarelli, C., Siga Jr., O., Cingolani, C., Sato, A., Gonzalez, P.D.,
787 2005. The crystalline basement in the north of Patagonia: isotopic ages and regional
788 characteristics. In: Pankhurst, R., Veiga, G. (Eds.), Gondwana 12: Geological and
789 Biological Heritage of Gondwana, Abstracts, Academia Nacional de Ciencias, Córdoba,
790 p.62.
791 Black, L.P., Kamo, S.L., Allen, C.M., Davis, D.W., Aleinikoff, J.N., Valley, J.W., Mundil,
792 R., Campbell, I.H., Korsch, R.J., Williams, I.S., Foudoulis, C. 2004. Improved
793 $^{206}Pb/^{238}U$ microprobe geochronology by the monitoring of a trace element-related
794 effect; SHRIMP, ID-TIMS, ELA-ICP-MS and oxygen isotope documentation for a
795 series of zircon standards. Chemical Geology, 205, 115-140.
796 Blichert-Toft, J., Albarède, F., 1997. The Lu–Hf isotope geochemistry of chondrites and the
797 evolution of the mantle–crust system. Earth and Planetary Science Letters 148, 243–258.
798 Bochino, R., 1967. Luisícllú ínexcutalu gen. et sp. nov. (Pisces, Clupeiformes,
799 Dussumieriidae) del Jurásico superior de la Provincia del Chubut, Argentina.
800 Ameghiniana 4, 91-100.
801 Bonaparte, J.F., 1979a. Dinosaurs: a Jurassic assemblage from Patagonia. Science 205,
802 1377–1379.
803 Bonaparte, J.F., 1979b. Faunas y paleobiogeografía de los tetrápodos Mesozoicos de
804 América del Sur. Ameghiniana 16, 217–238.
805 Bordas, A.F., 1943. Peces del Cretácico del Río Chubut (Patagonia). Physis 19, 313–318.
806 Buhn, B, Pimentel M.M., Matteini M., Dantas E.L., 2009. High spatial resolution analysis
807 of Pb and U isotopes for geochronology by laser ablation multi-collector inductively
808 coupled plasma mass spectrometry (LA-MC-ICPMS). Annals of the Brazilian Academy
809 of Sciences 81, 99–114.
810 Cabaleri, N.G., Armella C., 1999. Facies lacustres de la Formación Cañadón Asfalto
811 (Caloviano-Oxfordiano) en la quebrada Las Chacritas, Cerro Cóndor, provincia del
812 Chubut. Asociación Geológica Argentina Revista 5, 377–388.

Cabaleri, N.G., Armella, C., 2005. Influence of the biohermal belt on the lacustrine sedimentation of Cañadón Asfalto Formation (Upper Jurassic), Chubut province, southern Argentina. Geologica Acta 3, 205–214.

Cabaleri, N.G., Benavente, C.A., 2013. Sedimentology and paleoenvironments of the Las Chacritas carbonate paleolake, Cañadón Asfalto Formation (Jurassic), Patagonia, Argentina. Sedimentary Geology 284–285, 91–105.

Cabaleri, N.G., Armella, C., Silva Neto, D.G., 2005. Saline lakes of Cañadón Asfalto Formation (Middle-Upper Jurassic), Cerro Condor, Chubut Province (Patagonia), Argentina. Facies 51, 350–364. doi:10.1007/s 10347-004-0042-5.

Cabaleri, N.G., Volkheimer, W., Armella, C., Gallego, O.F, Silva Nieto, D.G, Páez, M.A, Cagnoni, M., Ramos, A., Panarello, H., Koukharsky, M., 2010a. Estratigrafía, análisis de facies y paleoambientes de la Formación Cañadón Asfalto en el depocentro jurásico Cerro Cóndor, provincia del Chubut. Revista de la Asociación Geológica Argentina 66, 349–367.

Cabaleri, N.G., Volkheimer, W., Silva Nieto, D.G, Armella, C., Cagnoni, M., Hauser, N., Matteini, M., Pimentel, M.M., 2010b. U-Pb ages in zircons from Las Chacritas and Puesto Almada members of the Jurassic Cañadón Asfalto Formation, Chubut province, Argentina (Abstract). VII. South American Symposium on Isotope Geology, Universidade de Brasilia, Brasilia, pp. 190–193.

Cabaleri, N.G., Armella, C., Benavente, C.A., Monferran, M., Cagnoni, M., Gallego, O.F., Volkheimer, W., Silva Nieto, D.G., Páez, M.A., 2011. Evento carbonático multicíclico en el Jurásico Medio lacustre de la Patagonia central (Abstract). Actas XVIII. Congreso Geológico Argentino, Asociación Geológica Argentina, Neuquén, Argentina, 2 p.

Cabaleri, N.G., Benavente, C.A., Monferran, M.D., Narváez , P.L., Volkheimer, W., Gallego, O.F., Do Campo, M.D., 2013. Sedimentology and palaeontology of the Upper Jurassic Puesto Almada Member (Cañadón Asfalto Formation, Fossati sub-basin), Patagonia Argentina: Palaeoenvironmental and climatic significance. Sedimentary Geology 296, 103–121.

Carballido, J.L., Rauhut, O.W.M., Pol, D., Salgado, L., 2011. Osteology and phylogenetic relationships of *Tehuelchesaurus benitezii* (Dinosuaria, Sauropoda) from the Upper Jurassic of Patagonia. Zoological Journal of Linnean Society 163, 605–662.

844 Castro, A., Moreno-Ventas, I., Fernández, C., Vujovich, G., Gallastegui, G., Heredia, N.,
845 Martino, R.D., Becchio, R., Corretgé, L.G., Díaz-Alvarado, J., Such, P., García-Arias,
846 M., Liu, D.Y., 2011. Petrology and SHRIMP U/Pb zircon geochronology of Cordilleran
847 granitoids of the Bariloche area, Argentina. Journal of South American Earth Sciences
848 32, 508-530.
849 Chauvel. C., Blichert-Toft, J.E., 2001. A hafnium isotope and trace element perspective on
850 melting of the depleted mantle. Earth and Planetary Science Letters 190, 137–151.
851 Chen, P.J., 1994. Cretaceous conchostracan faunas of China. Cretaceous Research 15, 259–
852 269.
853 Chen, P.J., Hudson, J.D., 1991. The Conchostracan Fauna of the Great Estuarine Group,
854 Middle Jurassic, Scotland. Palaeontology 15, 515–545.
855 Chen, P.J., Li, G., Batten, D.J., 2007. Evolution, migration and radiation of late Mesozoic
856 conchostracans in East Asia. Geological Journal 142, 391–413.
857 Chu, N.C., Taylor, R.N., Chavagnac, V., Nesbitt, R.W., Boella, R.M., Milton, J.A.,
858 German, C.R., Bayon, G., Burton, K., 2002. Hf isotope ratio analysis using multi-
859 collector inductively coupled plasma mass spectrometry: an evaluation of isobaric
860 interference corrections. Journal of Analytical Atomic Spectrometry 17, 1567–1574.
861 Codignotto, J., Nullo, F., Panza,J., Proserpio, C., 1979. Estratigrafía del Grupo Chubut
862 entre Paso de Indios y Las Plumas, provincia del Chubut, Argentina (Abstract). 7°
863 Congreso Geológico Argentino, Actas 1, 471–480
864 Cohen, K.M., Finney, S.C., Gibbard, P.L., Fan, J.-X. (2013, updated). The ICS
865 International Chronostratigraphic Chart. Episodes 36, 199-204.
866 Cortés, J.M., Baldoni, A., 1984. Plantas fósiles jurásicas del sur del Río Chubut medio.
867 Actas 9º Congreso Geológico Argentino. Tomo 4, 432–443.
868 Cortiñas, J.S., 1996. La cuenca de Somuncurá-Cañadón Asfalto; sus límites, ciclos
869 evolutivos del relleno sedimentario y posibilidades exploratorias (Abstract). XIII
870 Congreso Geológico Argentino, Actas 1, 147–163.
871 Cúneo, R., Ramezani, J., Scasso, R., Pol, D., Escapa, I., Zavattieri, A.M., Bowring, S.,
872 2013. High precision U-Pb geochronology and a new chronostratigraphy for the
873 Cañadón Asfalto Basin, Chubut, central Patagonia: implications for terrestrial faunal and
874 floral evolution in Jurassic. Gondwana Research 24, 1267–1275.

875 Escapa, I.H. 2009. La tafoflora de la Formación Cañadón Asfalto, Jurásico Medio Superior
876 de Chubut: taxonomía, bioestratigrafía y paleofitogeografía. Ph.D. Thesis (unpublished).
877 Universidad Nacional del Comahue, Bariloche, Argentina.
878 Escapa, I.H., Sterli, J., Pol, D., Nicoli, L., 2008. Flora y tetrápodos del jurásico de la
879 Formación Cañadón Asfalto en el área de Cerro Cóndor, provincia de Chubut (Abstract).
880 Revista de la Asociación Geológica Argentina 63, 613–624.
881 Fanning, C., Herve, F., Pankhurst, R., 2011. Lu-Hf isotope evidence for the provenance of
882 Permian detritus in accretionary complexes of western Patagonia and the northem
883 Antarctic Penninsula region. Journal of South American Earth Sciences 32, 485–496.
884 Figari, E.G., 2005. Evolución tectónica de la cuenca de Cañadón Asfalto (zona del Valle
885 Medio del Río Chubut). Universidad de Buenos Aires, Ph.D. Thesis (unpublished).
886 Universidad de Buenos Aires, 176pp.
887 Figari, E.G, Courtade, S.F., 1993. Tectosedimentaria de la cuenca de Cañadón Asfalto,
888 Chubut, Argentina (Abstract). Actas del Congreso Geológico Argentino 12, 66–77.
889 Figari, E.G., Courtade, S.F., Constantini, L.A., 1996. Stratigraphy and tectonis of Cañadón
890 Asfalto Basin, lows of Gastre and Gan Gan, north of Chubut province, Argentina. In:
891 Riccardi, A.C. (Ed.), Advances in Jurassic Research, pp. 359–368.
892 Figari, E.G., Scasso, R.A., Cúneo, R.N., Escapa, I., 2015. Estratigrafía y evolución de la
893 Cuenca de Cañadón Asfalto, provincia del Chubut, Argentina. Latin American Journal
894 of Sedimentology and Basin Analysis 22, 135–169.
895 Frenguelli, J., 1949. Los estratos con "*Estheria*" en el Chubut (Patagonia). Revista
896 Asociación Geológica Argentina 4, 11–24.
897 Gaetano, L.C., Rougier, G.W., 2011. New materials of *Argentoconodon fariasorum*
898 (Mammaliaformes, Triconodontidae) from the Jurassic of Argentina and its bearing on
899 triconodont phylogeny. Journal of Vertebrate Paleontology 31, 829–843.
900 Gallego, O.F., Cabaleri, N.G., 2005. Conchóstracos de la Formación Cañadón Asfalto
901 (Jurásico Medio – Superior): análisis preliminar de su distribución estratigráfica
902 (Abstract). II Simposio Argentino del Jurásico (Buenos Aires). Ameghiniana 51, p.42.
903 Gallego, O.F., Shen, Y.B., Cabaleri, N., Hernandez, M., 2010. The genus *Congestheriella*
904 Kobayashi, 1954 (Conchostraca, Afrograptioidea): redescription and new combination

905 to Isaura olsoni Bock from Venezuela and a new species from Argentina (Upper
906 Jurassic). Alavesia 3, 11–24.
907 Gallego, O.F., Cabaleri, N.G., Armella, C., Volkheimer, W., Ballent, S.C., Martínez, S.,
908 Monferran, M.D., Silva Nieto, D.G., Páez, M.A., 2011. Paleontology, sedimentology
909 and paleoenvironment of a new fossiliferous locality of the Jurassic Cañadón Asfalto
910 Formation, Chubut Province, Argentina. Journal of South American Earth Sciences 31,
911 54–68.
912 Gerdes A., Zeh, A., 2009. Zircon formation versus zircon alteration - New insights from
913 combined U–Pb and Lu–Hf in-situ LA-ICP-MS analyses, and consequences for the
914 interpretation of Archean zircon from the Central Zone of the Limpopo Belt. Chemical
915 Geology 261, 230-243.
916 Haller, M.J.; Linares, E., Ostera, H.A., Page, S.M., 1999. Petrology and geochronology of
917 the sub-cordilleran plutonic belt of Patagonia. 2nd SSAGI, South American Symposium
918 on Isotope Geology, Córdoba, 210-214.
919 Hauser, N., Matteini, M. Cabaleri, N. G., Volkheimer, W., Armella, C., Gallego, O.,
920 Monferran, M.D., 2012. New U-Pb ages on a pyroclastic level from the Fossati
921 depocenter of the Jurassic Cañadon Asfalto basin, Chubut, Argentina. 8th SSAGI, South
922 American Symposium on Isotope Geology, Medellin, 124–125.
923 Hauser, N., Matteini, M. Cabaleri, N. G., Volkheimer, W., Silva Nieto, D.G., Gallego, O.F,
924 Monferran, M.D., Pimentel, M., 2014. New U-Pb age and Hf isotopes data from Jurassic
925 Cañadón Asfalto rift basin, Chubut, Argentina: implications on the crustal evolution of
926 Central Patagonia (Abstract). 9th SSAGI, South American Symposium on Isotope
927 Geology, Sao Paulo, 1p.
928 Jackson, S.E., Pearson, N.J., Griffina, W.L., Belousova, E.A., 2004. The application of
929 *laser* ablation-inductively coupled plasma-mass spectrometry to in situ U–Pb zircon
930 geochronology. Chemical Geology 211, 47–69.
931 Kay, S.M., Ramos, V.A., Mpodozis, C., Sruoga, P., 1989. Late Paleozoic to Jurassic silicic
932 magmatism at the Gondwana margin: analogy to the Middle Proterozoic in North
933 America? Geology 17, 324–328.

Košler, J., Fonneland, H., Sylvester, P., Tubrett, M., Pedersen, R.B., 2002. U–Pb dating of detrital zircons for sediment provenance studies, a comparison of laser ablation ICP-MS and SIMS techniques. Chemical Geology 182, 605–618.

Lesta, P., 1968. Estratigrafía de la cuenca del Golfo de San Jorge. 3 Jornadas Geológicas Argentinas 2, Asociación Geológica Argentina, Buenos Aires, 187–289.

Lesta, P., Ferello, R., 1972. Región extraandina de Chubut y norte de Santa Cruz. In: Leanza, A. (Ed.), Geología Regional Argentina, Academia Nacional Ciencias Córdoba, Córdoba, pp.601–653.

Lesta, P., Ferello, R., Chebli, G., 1980. Chubut extraandino. In J.C.M. Turner (Ed.), Simposio Geología Regional Argentina. Academia Nacional de Ciencias de Córdoba 2, 1307-1387.

Li, G., Matsouka, A., 2012. Jurassic clam shrimp ("conchostracan") faunas in China. Scientific Reports of the University of Niigata (Geology) 27, 73–88.

Lizuaín, A., Silva Nieto, D., 2005. Observaciones Geológicas en la región de Río Chico, Gastre, río Chubut Medio, provincia del Chubut. 16º Congreso Geológico Argentino, La Plata, Actas 1, 133-139.

Llambías, E.J., Leanza, H.A., 2005. Depósitos laháricos en la Formación Los Molles (Jurásico) en Chacay Melehue, Neuquén: evidencia de volcanismo jurásico en la Cuenca Neuquina. Revista de la Asociación Geológica Argentina 62, 552-558.

López-Arbarello, A., 2004. The record of Mesozoic fishes of Gondwana (excluding India and Madagascar). In: Arriata, G., Tintori, A. (Eds.), Mesozoic Fishes 3. Systematics, Paleoenvironments and Biodiversity. Verlag Dr Friedrich Pfeil, Germany, pp.497–624.

López-Arbarello, A., Sferco, E., Rauhut, O.W.M., 2013. A new genus of coccolepidid fishes (Actinopterygii, Chondrostei) from the continental Jurassic of Patagonia. Palaeontologia Electronica, 16, No. 1, checked March 2015.

López de Luchi, M.G., Cerredo, M.E., 2008. Geochemistry of the Mamil Choique granitoids at Rio Chico, Río Negro, Argentina: Late Paleozoic crustal melting in the North Patagonian Massif. Journal of South American Earth Sciences 25, 526–546.

Lopez de Luchi, M.G, Rapalini, A.E., 2002. Middle Jurassic dyke swarms in the North Patagonian Massif: the Lonco Trapial Formation in the Sierra de Mamil Choique, Río Negro province, Argentina. Journal of South American Earth Sciences 15, 625-641.

965 Ludwig, K.R., 2003. User's Manual for Isoplot 3.0: a geochronological toolkit for
966 Microsoft Excel. Berkeley Geochronology Center, Special Publication 4, 71pp.
967 Martin, T., Rauhut, O.W.M., 2005. Mandible and dentition of *Asfaltomylos patagonicus*
968 (Australosphenida, Mammalia) and the evolution of tribosphenic teeth. Journal of
969 Vertebrate Paleontology 25, 414–425.
970 Martínez, M.A., 2002. Palynological zonation of the Lajas Formation (Middle Jurassic) of
971 the Neuquén Basin, Argentina. Ameghiniana 39, 221–240.
972 Martínez, S., Gallego, O.F., Cabaleri, N.G, 2007. Nueva fauna de moluscos de la
973 Formación Cañadón Asfalto (Jurásico Medio a Superior) Chubut, Argentina (Abstract).
974 Ameghiniana 44, p.96R.
975 Marveggio, N., Llorens, M., 2013. Nueva edad de la base del grupo Chubut en la mena
976 uranífera Cerro Solo, provincia del Chubut. Revista Asociación Geológica Argentina 70,
977 318–378.
978 Monferran, M.D., 2015. Análisis Paleoecológico de los conchostracos (Spicaudata) de la
979 Formación Cañadón Asfalto, Chubut, Argentina. Ph.D. Thesis (unpublished),
980 Universidad de Buenos Aires, Buenos Aires, 299pp.
981 Monferran, M.D., Gallego, O.F., Cabaleri, N.G., 2013. First record of the family
982 Fushunograptidae (“Conchostraca”, Spinicaudata) of the Cañadón Asfalto Formation
983 (upper jurassic), Patagonia, Argentina. Ameghiniana 50, 447–459.
984 Monferran, M.D., Cabaleri, N.G., Gallego, O.F., Armella, C. and Cagnoni, M., 2016
985 Spinicaudatans from the Upper Jurassic of Argentina and their paleoenvironments.
986 Palaios 31: 405-420.
987 Morel, M.L.A., Nebel, O., Nebel-Jacobsen, Y.L., Miller, J.S., Vroon, P.Z., 2008. Hafnium
988 isotope characterization of the GJ-1 zircon reference material by solution and laser-
989 ablation MC-ICPMS. Chemical Geology 255, 231–235.
990 Musacchio, E.A., 1989. Biostratigraphy of the Non-marine Cretaceous of Argentina based
991 on Calcareous Microfossils. In: Wiedmann, J. (Ed.), Cretaceous of the western Tethys.
992 Proceedings, Third International Cretaceous Symposium, Tübingen,, pp.811-851.
993 Musacchio, E.A., 1995. Estratigrafía y micropalentología del Jurásico y el Cretácico en la
994 comarca del Valle Medio del Río Chubut, Argentina (Abstract). 6º Congreso Argentino
995 de Paleontología y Bioestratigrafía Actas. Trelew, Argentina, 179–187.

996 Musacchio, E.A., 2001. Relaciones paleobiogeográficas de los ostrácodos no marinos del
997 Jurásico yel Cretácico de Patagonia. Acta Geologica Leopoldensia 24, 293-310.
998 Musacchio, E.A., Beros, C., Pujana, I., 1990. Microfósiles continentales del Jurásico y el
999 Cretácico en Chubut y su contribution a la bioestratigrafia de la Cuenca del Golfo de San
1000 Jorge, Argentina. Bioestratigrafía de los Sistemas Regionales del Jurásico y el Cretácico
1001 de América del Sur 2, 355-383.
1002 Nakayama, C., 1973. Sedimentitas pre-Bayocianas en el extremo austral de la Sierra de
1003 Taquetrén, Chubut (Argentina). Pre-Bajocian sedimentary rocks in the southern extreme
1004 of Sierra de Taquetrón, Chubut, Argentina. Actas de las Jornadas Geológicas
1005 Argentinas, 66, 269–277.
1006 Nebel, O., Nebel-Jacobsen, Y., Mezger, K., Berndt, J., 2007. Initial Hf isotope
1007 compositions in magmatic zircon from early Proterozoic rocks from the Gawler Craton,
1008 Australia: A test for zircon model ages. Chemical Geology 241, 23–37.
1009 Nullo, F.E., 1983. Descripción geológica de la Hoja 45c. Pampa de Agnia, provincia del
1010 Chubut. Servicio Geológico, Buenos Aires, Boletín 199, p.94.
1011 Olivera D. E., Zavattieri, A. M., Quattrocchio, M. E., 2015. The palynology of the Cañadón
1012 Asfalto Formation (Jurassic), Cerro Cóndor depocentre, Cañadón Asfalto Basin,
1013 Patagonia, Argentina: palaeoecology and palaeoclimate based on ecogroup analysis.
1014 Palynology 39, 362-386.
1015 Page, R., Page, S., 1993. Petrología y significado tectónico del Jurásico volcánico de
1016 Chubut central. Revista de la Asociación Geológica Argentina 1, 174–176.
1017 Page, R., Ardolino, A., de Barrio, R.E., Franchi, M., Lizuain, A., Page S., Silva Nieto D.G
1018 1999. Estratigrafía del Jurásico y Cretácico del Macizo de Somún Curá, provincias de
1019 Río Negro y Chubut. In: Caminos, R. (Ed.) Geología Regional Argentina, Servicio
1020 Geológico Minero Argentino, Buenos Aires, Instituto de Geología y Recursos
1021 Minerales, Anales 29: 460-488.
1022 Pankhurst, R.J., Rapela, C.W., 1995. Production of Jurassic rhyolite by anatexis of the
1023 lower crust of Patagonia. Earth and Planetary Science Letters 134, 23-36.
1024 Pankhurst, R.J., Leat, P.T., Sruoga, P., Rapela, C.W., Márquez, M., Storey, B.C., Riley,
1025 T.R., 1998. The Chon Aike province of Patagonia and related rocks in West Antarctica:

1026 a silicic large igneous province. Journal of Volcanology and Geothermal Research 81,
1027 113–136.
1028 Pankhurst, R.J., Riley, T.R., Fanning, C.M., Kelley, S.P., 2000. Episodic silicic volcanism
1029 in Patagonia and the Antarctic Peninsula: Chronology of magmatism associated with the
1030 break-up of Gondwana. Journal of Petrology 41, 605-625.
1031 Pankhurst, R.J., Rapela, C.W., Fanning, C.M., Márquez, M., 2006. Gondwanide continental
1032 collision and the origin of Patagonia. Earth-Sciences Reviews 76, 235–257.
1033 Patchett, P.J., 1983. Importance of the Lu–Hf isotopic system in studies of planetary
1034 chronology and chemical evolution. Geochimica and Cosmochimica Acta 47,
1035 doi.10.1016/0016-7037(83)90092-3.
1036 Pol, D., Rauhut, O.W.M., 2012. A Middle Jurassic abelisaurid from Patagonia and the early
1037 diversification of theropod dinosaurs. Proceedings of the Royal Society B, 1-6,
1038 doi:10.1098/rspb.2012.0660.
1039 Pol, D., Rauhut, O.W.M., Becerra, M. 2011. A Middle Jurassic heterodontosaurid dinosaur
1040 from Patagonia and the evoution of heterodontosaurids. Naturwissenchaften 98, 369–
1041 379.
1042 Proserpio, C.A. 1987. Descripción geológica de la Hoja 44e, Valle General Racedo.
1043 Dirección Nacional de Minería y Geología, Buenos Aires, Boletín 201,108pp.
1044 Ramos, V.A., 2008. Patagonia: A paleozoic continental adrift? Journal of South American
1045 Earth Sciences 26, 235-251.
1046 Ranalli, J.N., Peroni, G.O., Boggetti, D.A., Manolo, R., 2011. Cuenca Cañadón Asfalto.
1047 Modelo tectosedimentario (Abstract). VIII Congreso de Exploración y Desarrollo de
1048 Hidrocarburos. Simposio Cuencas Argentinas: visión actual. Instituto Argentino del
1049 Petróleo y del Gas, Mar del Plata, Argentina, pp.185-215.
1050 Rapela, C.W, Spalletti, L. A., Merodio, J. C., Aragon, E. 1988. Temporal evolution and
1051 spatial variation of early Tertiary volcanism in the Patagonian Andes (40ºS-42º30'S).
1052 Journal of South American Earth Sciences 1, 75-88.
1053 Rapela, C.W., Pankhurst, R.J., Fanning, C.M., Hervé, F., 2005. Pacific subduction coeval
1054 with the Karoo mantle plume: the early Jurassic Subcordilleran belt of northwestern
1055 Patagonia. In: Vaughan, A.P.M., Leat, P.T., Pankhurst, R.J. (Eds.), Terrane Processes at

1056 the Margins of Gondwana. Geological Society of London, Special Publications 246,
1057 217-239.
1058 Rauhut, O.W.M., 2005. Osteology and relationships of a new theropod dinosaur from the
1059 Middle Jurassic of Patagonia. Palaeontology 48, 87–110.
1060 Rauhut, O.W.M., 2006. A brachiosaurid sauropod from the Late Jurassic Cañadón Calcáreo
1061 Formation of Chubut, Argentina. Fossil Record — Mitteilungen aus dem Museum für
1062 Naturkunde in Berlin 9, 226–237.
1063 Rauhut, O.W.M., Martin, E., Ortiz-Jaureguizar, Puerta, P., 2002. A Jurassic mammal from
1064 South America. Nature 416, 165–168.
1065 Rauhut, O.W.M., Remes, K., Fechner, R., Cladera, G., Puerta, P., 2005. Discovery of a
1066 short-necked sauropod dinosaur from the Late Jurassic period of Patagonia. Nature 435,
1067 670–672.
1068 Ravazzoli, I.A., Sesana, F.L., 1977. Descripción Geológica de la Hoja 41c, Río Chico.
1069 Provincia de Río Negro. Servicio Geológico Nacional, Buenos Aires, Boletín Nº 148,
1070 p.79.
1071 Rich, T.H., Vickers-Rich, P., Giménez, O., Cuneo, R., Puerta, P., Vacca, R., 1999. A new
1072 Sauropod dinosaur from Chubut Province, Argentina. In: Tomida, Y., Rich, T.H.,
1073 Vickers-Rich, P. (Eds.), Second Gondwanan Dinosaur Symposium. National Science
1074 Museum Monographs, Tokyo, pp.61–84.
1075 Rougier, G.W., Martinelli, A.G., Forasiepi, A.M., Novacek, M.J., 2007. New Jurassic
1076 mammals from Patagonia, Argentina: a reappraisal of australosphenidan morphology
1077 and interrelationship. American Museum Novitates 3566, 1–54.
1078 Saini-Eidukat, B., Migueles, N., Gregori, D.A., Bjerg, E.A., Beard, B.L., Johnson, C.M.,
1079 2002. The Alessandrini Complex: Early Jurassic magmatism in Northern Patagonia,
1080 Argentina (Abstract). 15º Congreso Geológico Argentino, Calafate, Actas 2: 253-258.
1081 Salani, F.M., 2007. Aporte a la edad de la Formación Cañadón Asfalto, Chubut, Argentina
1082 (Abstract). Resúmenes III Simposio Argentino Jurásico, Mendoza, Argentina, p.71.
1083 Scasso, R.A., Escapa, I.H., Damborenea, S., Pagani, A., 2013. Geology and Paleontology in
1084 the Cañadon Asfalto Basin. V Simposio Argentino del Jurásico, Guía de Campo, Museo
1085 Egidio Feruglio, Trelew, Chubut, 1-26.

1086 Scherer, E., Münker, C., Mezger, K., 2006. Calibration of the lutetium-hafnium clock.
1087 Science 293, 683–687.
1088 Sesana, F.L., 1968. Rasgos petrológicos de la comarca de Río Chico, Río Negro. II
1089 Jornadas Geológicas Argentina Actas 3, pp.99–105.
1090 Silva Nieto, D.G, 2005. Hoja Geológica 4369-III, Paso de Indios. Escala 1:250.000. Boletín
1091 del Instituto de Geología y Recursos Minerales, Servicio Geológico Minero Argentino,
1092 Buenos Aires, Argentina, Boletín 265, 1-72.
1093 Silva Nieto, D.G, Cabaleri, N.G, Salani, F., Coluccia, A., 2002a. Cañadón Asfalto, una
1094 cuenca de tipo "Pull Apart" en el área de Cerro Cóndor, Provincia del Chubut
1095 (Abstract). 15º Congreso Geológico Argentino, Asociación Geológica Argentina,
1096 Buenos Aires, Argentina, pp.238-243.
1097 Silva Nieto, D.G., Cabaleri, N., Salani, F.M., González Díaz, E., Coluccia, A., 2002b. Hoja
1098 Geológica 4368-27 Cerro Cóndor, provincia del Chubut, escala 1:100,000. Instituto de
1099 Geología y Recursos Minerales, Servicio Geológico Minero Argentino, Buenos Aires,
1100 Boletín 328, 68pp.
1101 Silva Nieto, D.G., Cabaleri, N.G., Salani, F.M., 2003. Estratigrafía de la Formación
1102 Cañadón Asfalto (Jurásico Superior) provincia del Chubut (Abstract). Ameghiniana
1103 Suplemento 40, p.46.
1104 Silva Nieto, D., Cabaleri, N., Armella, C. Volkheimer, W., Gallego, O., 2007. Hipótesis
1105 sobre la evolución tecto-sedimentaria de la Formación Cañadón Asfalto Provincia del
1106 Chubut. Ameghiniana 44, p.67.
1107 Simpson, G.G., 1941. The Eogene of Patagonia. American Museum Novitates 1120, 1-15.
1108 Stacey, J.S., Kramers, J.D., 1975. Approximation of terrestrial lead isotope evolution by a
1109 two-stage model. Earth and Planetary Science Letters 26, 207–221.
1110 Sterli, J., 2008. A new, nearly complete stem turtle from the Jurassic of South America
1111 with implications for turtle evolution. Biology Letters, 4, 286–289.
1112 doi:10.1098/rsbl.2008.0022
1113 Sterli, J., Pol, D., Rougier, G.W., Rauhut, O.W., Báez, A.M., Carballido, J.L., Nicoli, L.
1114 2010. Nuevos aportes a la diversidad taxonómica de vertebrados de la formación
1115 Cañadón Asfalto (Jurásico Medio) de la provincia del Chubut, Argentina (Abstract). 4º
1116 Simposio Argentino del Jurásico y sus límites, Bahía Blanca, Argentina, p.45.

1117 Stipanicic, P., Rodrigo, F., Baulíes, O.L., Martínez, C.G., 1968. Las formaciones
1118 presenonianas en el denominado Macizo Nordpatagónico y regiones adyacentes. Revista
1119 de la Asociación Geológica Argentina 23, 67–98.
1120 Stipanicic, P., Bonetti, M., 1970. Posiciones estratigráficas y edades de las principales
1121 floras jurásicas argentinas. Floras Liásicas. Ameghiniana 7, 57- 78.
1122 Tasch, P., Volkheimer, W., 1970. Jurassic conchostracans from Patagonia. University of
1123 Kansas Paleontological Contributions 50, 1–23.
1124 Taylor, S.R., McLennan, S.M., 1985. The Continental Crust: its Composition and
1125 Evolution. Blackwell, Oxford, U.K., 312pp.
1126 Turner, J.C., 1983. Descripción geológica de la Hoja 44d, Colan Conhué, Provincia del
1127 Chubut. Servicio Geológico Nacional, Buenos Aires, Boletín Nº 197, 75pp.
1128 Uliana, M.A., Biddle, K.T., Phelps, D.W., Gust, D.A., 1985. Significado del vulcanismo y
1129 extension mesojurásica en el extremo meridional de Sudamérica. Revista de la
1130 Asociación Paleontológica 40, 231–253.
1131 Vallati, P. 1986. Conchóstracos Jurásicos de la Provincia de Chubut, Argentina (Abstract).
1132 4 Congreso Argentino de Paleontología y Bioestratigrafía, Mendoza, 4, 29-38.
1133 Volkheimer, W., 1964. Estratigrafía de la zona extraandina del Departamento deCushamen
1134 (Chubut) entre los paralelos 42º y 42 30´ y los meridianos 70º y 71º. Revista de la
1135 Asociación Geológica Argentina, 19, 85-107.
1136 Volkheimer, W., Quattrocchio, M., Cabaleri, N.G, García, V., 2008. Palynology and
1137 paleoenvironment of the Jurassic lacustrine Cañadón Asfalto Formation at Cañadón
1138 Lahuincó locality, Chubut Province, Central Patagonia, Argentina. Revista Española de
1139 Micropaleontología 40, 77–96.
1140 Volkheimer, W., Gallego, O.F., Cabaleri, N.G., Armella, C., Narvaez, P.L., Silva Nieto,
1141 D.G., Paez, M.A., 2009. Stratigraphy, palynology, and conchostracans of a Lower
1142 Cretaceous sequence at the Canadon Calcareo locality, extra-Andean central Patagonia;
1143 age and palaeoenvironmental significance. Cretaceous Research 30, 270–282.
1144 Wedepohl, K.H., 1995. The compositions of the continental crust. Geochimica et
1145 Cosmochimica Acta 59, 1217–1232.
1146 Zaffarana, C.B., Somoza, R., 2012. Palaeomagnetism and $^{40}Ar/^{39}Ar$ dating from Lower
1147 Jurassic rocks in Gastre, central Patagonia: further data to explore tectonomagmatic

events associated with the break-up of Gondwana. Journal of the Geological Society of London 169, 371-379.

Zaffarana, C.B., Gregori, D., Poma S., Somoza, R., 2013. Comparación geoquímica y esquema tectónico de las unidades magmáticas del Jurásico Temprano de Patagonia Central (Abstract). V Congreso Argentino del Jurásico, Trelew, p.54.

Zaffarana, C.B., Poma S., Lagorio, S.L., Gregori, D., Somoza, R., Busteros, A., Silva Nieto, D., Giacosa, R., 2014. Petrogénesis de las volcanitas Lonco Trapial, magmatismo del Jurásico Temprano de Patagonia Central (Abstract). XIX Congreso Geologico Argentino, Córdoba, 5pp.

Zavattieri, A.M., Escapa, I.H., Scasso, R.A., Olivera, D., 2010. Contribución al conocimiento palinoestratigráfico de la Formación Cañadón Calcáreo en su localidad tipo, provincia del Chubut, Argentina (Abstract). X Congreso Argentino de Paleontología y Bioestratigrafía y VII Congreso Latinoamericano de Paleontología, La Plata, p.20.

**Captions:**

**Figure 1:** a) Schematic map showing the main tectonic units of Central Patagonia during Jurassic times; from west to east: CMC - Chonos accretionary complex; SPB - Subcordilleran Plutonic Belt; PAB - Pampia de Agna Basin; CPB - Late Triassic Central Patagonian Batholith. The main stratigraphic units relevant for this work are: LT - Lonco Trapial volcanic field; MF - Marifil Formation; CA - Chon Aike Formation; EQ - El Quemado Formation, and I - Ibañez Formation. The region around the Cañadón Asfalto Basin is highlighted by the black square. The dotted line represents the axis of the Middle Jurassic to Neogene Patagonian Batholith. Map based on original figures by Zaffarana and Somoza (2012) and Pankhurst et al. (2000). b) Geological map of the study area in the central Chubut Province, with Permian-Triassic to Cenozoic units. Locations of the Cerro Cóndor, Fossati, and Portuzuelo-Llanquetrúz sub-basins are indicated. The sampled areas are in the (1) Cerro Cóndor sub-basin, (2) Sierra de La Manea in Cerro Cóndor sub-basin, and (3) Fossati sub-basins.

**Figure 2:** Stratigraphy of the Cañadón Asfalto Basin based on Cabaleri and Benavente (2013).

**Figure 3:** Sedimentological profiles of the study sites in the Cerro Cóndor and Fossati sub-basins of the Cañadón Asfalto Basin, with the positions of analyzed samples, together with their U-Pb ages. The lithologies referred to the Lonco Trapial Formation are in brown. For the Las Chacritas Member in the Cerro Cóndor and Fossati sub-basins: limestone in light blue, basalts in brown, tuffites in brown, and shales in black. For the Puesto Almada Member in the Cerro Cóndor and Fossati sub-basins: sandstones, limestones, tuffites and tuff in brown, and shales in black. For the Chubut Group: conglomerates are shown in red.

**Figure 4:** *Cerro Cóndor sub-basin:* a) Central volcanic edifices of the Lonco Trapial Formation at the Cañadón Bagual-César Torres locality; width of field of view ca. 10 m. The inset shows volcanic breccia sample LT-CT-1 (hammer for scale 50 cm long). b) The Las Chacritas Member in the Cañadón Asfalto locality; inset: a detail of sample CAV-40 from the pyroclastic level (coin for scale, 2.5 cm wide). c) The Puesto Almada Member, and in the inset, the pyroclastic fall level where sample SCN-2 was taken at the Estancia La Sin Rumbo locality. d) The La Manea Range locality with the tuffaceous sandstone of La Manea-1 (width of field of view estimated at 300 m). *Fossati sub-basin at the Cerro Bandera locality:* e) Alluvial fan conglomerate above medium-grained sandstone with cross-stratification (sample CAF-6). f) A whitish pyroclastic bed of 60 cm thickness (sample CAF-8). The hammer in figures b, c inset, e and f is 35 cm long.

**Figure 5:** Zircon chronology data: a) Tera-Wasserburg diagram for the LT-CT-1 volcanic breccia. In the inset, the 172 Ma weighted average $^{206}Pb/^{238}U$ age obtained for the Lonco Trapial Formation is shown. b) Tera-Wasserburg Concordia diagram for the CAV-40 pyroclastic level from the lower part of the Las Chacritas Member; data for the gray ellipses were used for calculation of the 168 Ma weighted average $^{206}Pb/^{238}U$ age. c) and d) Cathodoluminescence images of selected zircon crystals from LTCT-1 and CAV-40, respectively, showing the magmatic zonation and the position of the spot analyses. The

ages and $\varepsilon_{Hf(t)}$ analysis spots for some zircon grains are shown. e) and f) Ages for the Puesto Almada Member in the Cerro Cóndor and the Fossati sub-basin, respectively. Note that these two ages are overlapping. g) Back-scattered electron image for zircon from sample SCN-2, and h) from sample CAF-8.

**Figure 6:** All U-Pb ages from a) the tuff sandstone from the La Manea Range (sample La-Manea-1) in the Cerro Cóndor sub-basin, and b) the tuff sandstone from the Puesto Almada Member (CAF-6) collected in the Fossati sub-basin. Probability density plots for the c) La Manea and d) Puesto Almada sandstones. Back-scattered electron images of representative zircon crystals with their $^{206}Pb/^{238}U$ ages are given as insets in figures a, b, c and d. On some grains the respective $\varepsilon_{Hf}$ values are given as well. e) and f) Weighted average ages for La Manea-1 and CAF-6, respectively.

**Figure 7:** a) Tera-Wasserburg U-Pb isotope diagram for all data of this study that are related to the evolution of the Cañadón Asfalto basin. Colors refer to the legend in Figure 8c. b) Total U-Pb zircon age distribution indicating two main magmatic events in Central Patagonia: 1 – The Mamil Choique and 2 – the Cañadón Asfalto (CA) magmatism. Inset distinguishes the three volcanic cycles of the younger (CA) event (compare also with Figure 9): C1 (172-180 Ma), C2 (166-169 Ma) and C3 (155-162 Ma). c) $\varepsilon_{Hf}$ vs. Age (Ga) diagram. The Mamil Choique event reworked Mesoproterozoic crust, as indicated by red, dashed lines going towards 1.6-1.3 Ga. The same crust was probably reworked again during the acid volcanism associated with the Las Chacritas cycle. The dashed-dotted orange lines indicate possible crustal reworking of Meso- to Neoproterozoic crust of 1.2-0.8 Ga age, during the magmatism associated with the Lonco Trapial cycle and later during the Puesto Almada cycle. Hf data from the La Manea-1 sandstone interpreted to represent the Cañadón Calcáreo Formation and CAF-6 sandstone belonging to the Puesto Almada Member are also shown. For further detailed discussion of this figure, including the meaning of the I and II interpretations, refer to the text. The crustal evolution trends represent the bulk-rock trends for Mesoproterozoic juvenile crust, calculated using the $^{176}Lu/^{177}Hf$ ratio of 0.0113 (Taylor and McLennan, 1985 and Wedepohl, 1995).

**Figure 8:** Comparison between previously obtained paleontological and geochronological ages and those obtained in this work for the Lonco Trapial Formation, and the Las Chacritas and Puesto Almada members of the Cañadón Asfalto Formation.

**Figure 9:** Cumulative probability curve for the Cañadón Asfalto magmatic event showing the three main cycles suggested by this work. For comparison (cf. Discussion chapter), the silicic volcanic events recognized by Pankhurst et al. (2000) for Patagonia and Antarctica are also shown.

**Table 1:** Zircon U-Pb data for pyroclastic levels and sedimentary rocks of units related with the evolution of the Cañadón Asfalto basin, central Chubut.

**Table 2:** Representative results of in situ Lu-Hf LA-ICP-MS-MC zircon analyses for igneous and sedimentary rocks related to the evolution of the Cañadón Asfalto basin, central Chubut.

Table 1: Zircon U-Pb data for pyroclastic levels and sedimentary rocks of units related with the evolution of Cañadón Asfalto basin, central Chubut.

| | | | | | **Ratios** | | | | | | rho | **Ages** | | | | | | **% Conc |
|---|---|---|---|---|---|---|---|---|---|---|---|---|---|---|---|---|---|---|
| | Morphology | Lenght (um) | Position | Characteristics | $^{207}Pb/^{206}Pb$ | 2σ (%) | $^{207}Pb/^{235}U$ | 2σ (%) | $^{206}Pb/^{238}U$ | 2σ (%) | | $^{207}Pb/^{206}Pb$ | 2σ (Ma) | $^{207}Pb/^{235}U$ | 2σ (Ma) | $^{206}Pb/^{238}U$ | 2σ (Ma) | |
| *Lonco Trapial Range* | | | | | | | | | | | | | | | | | | |
| **LTCT-1 volcanic brecchia from Lonco Trapial Formation** | | | | | | | | | | | | | | | | | | |
| Z5(*) | Long-Prismatic | 300 | Core | Magmatic zonation | 0.04898 | 2.70 | 0.17655 | 2.96 | 0.02614 | 1.22 | 0.41 | 146.7 | 31.4 | 165.1 | 2.3 | 166.4 | 1.1 | 101 |
| Z21 | Short-Prismatic | 200 | Core | Magmatic zonation | 0.04919 | 2.38 | 0.17757 | 2.80 | 0.02618 | 1.47 | 0.52 | 156.9 | 27.6 | 166.0 | 2.2 | 166.6 | 1.3 | 100 |
| Z4 | Prismatic | 300 | Core | Magmatic zonation | 0.04876 | 3.12 | 0.17611 | 3.52 | 0.02619 | 1.62 | 0.46 | 136.4 | 71.3 | 164.7 | 4.9 | 166.7 | 1.4 | 101 |
| Z14 | Short-Prismatic | 200 | Rim | Inher. Core | 0.05082 | 3.95 | 0.18426 | 4.23 | 0.02630 | 1.52 | 0.36 | 232.5 | 91.1 | 171.7 | 6.7 | 167.3 | 2.5 | 97 |
| Z19 | Short-Prismatic | 150 | Core | Magmatic zonation | 0.04975 | 2.68 | 0.18119 | 3.06 | 0.02641 | 1.47 | 0.48 | 183.3 | 30.9 | 169.1 | 2.4 | 168.1 | 1.3 | 99 |
| Z43 | Short-Prismatic | 100 | Core | Magmatic zonation | 0.04893 | 2.33 | 0.17909 | 2.59 | 0.02655 | 1.13 | 0.44 | 144.3 | 27.1 | 167.3 | 2.1 | 168.9 | 1.1 | 101 |
| Z23 | Short-Prismatic | 100 | Core | Magmatic zonation | 0.04931 | 2.87 | 0.18066 | 3.19 | 0.02657 | 1.38 | 0.43 | 162.4 | 65.4 | 168.6 | 4.6 | 169.1 | 1.3 | 100 |
| Z22 | Short-Prismatic | 100 | Core | Magmatic zonation | 0.04973 | 2.16 | 0.18332 | 2.79 | 0.02673 | 1.76 | 0.63 | 182.6 | 50.4 | 170.9 | 4.4 | 170.1 | 3.0 | 100 |
| Z1 | Short-Prismatic | 400 | Core | Magmatic zonation | 0.04972 | 2.15 | 0.18389 | 2.64 | 0.02682 | 1.53 | 0.58 | 181.9 | 24.9 | 171.4 | 2.1 | 170.6 | 1.4 | 100 |
| Z20 | Prismatic-Frat | 500 | Core | Magmatic zonation | 0.04975 | 2.59 | 0.18530 | 2.97 | 0.02701 | 1.46 | 0.49 | 183.4 | 58.9 | 172.6 | 4.3 | 171.8 | 1.4 | 100 |
| Z11 | Short-Prismatic | 150 | Core | Magmatic zonation | 0.05103 | 2.18 | 0.19007 | 2.37 | 0.02701 | 0.93 | 0.39 | 242.2 | 24.9 | 176.7 | 2.0 | 171.8 | 1.0 | 97 |
| Z45 | Short-Prismatic | 150 | Core | Magmatic zonation | 0.04904 | 2.40 | 0.18308 | 2.65 | 0.02708 | 1.12 | 0.42 | 149.7 | 54.7 | 170.7 | 3.9 | 172.2 | 1.1 | 101 |
| Z3 | Prismatic | 300 | Core | Magmatic zonation | 0.04906 | 2.35 | 0.18515 | 2.68 | 0.02737 | 1.27 | 0.48 | 150.7 | 55.2 | 172.5 | 4.2 | 174.1 | 2.2 | 101 |
| Z29 | Prismatic | 200 | Core | Magmatic zonation | 0.05021 | 1.51 | 0.19015 | 1.76 | 0.02746 | 0.91 | 0.51 | 204.9 | 17.4 | 176.8 | 1.5 | 174.7 | 1.0 | 99 |
| Z34 | Short-Prismatic | 200 | Core | Magmatic zonation | 0.04977 | 1.69 | 0.18979 | 1.91 | 0.02766 | 0.89 | 0.47 | 184.2 | 38.3 | 176.4 | 2.8 | 175.9 | 0.9 | 100 |
| Z32 | Short-Prismatic | 200 | Core | Magmatic zonation | 0.05089 | 3.06 | 0.19422 | 3.39 | 0.02768 | 1.47 | 0.43 | 235.7 | 34.9 | 180.2 | 2.8 | 176.0 | 1.4 | 98 |
| Z35 | Short-Prismatic | 250 | Core | Magmatic zonation | 0.05095 | 1.89 | 0.19468 | 2.43 | 0.02771 | 1.52 | 0.63 | 238.7 | 21.7 | 180.6 | 2.1 | 176.2 | 1.4 | 98 |
| Z40 | Subrounded | 200 | Core | Magmatic zonation | 0.05012 | 1.96 | 0.19173 | 2.19 | 0.02775 | 0.99 | 0.45 | 200.5 | 22.6 | 178.1 | 1.9 | 176.4 | 1.0 | 99 |
| Z17 | Prismatic | 150 | Core | Magmatic zonation | 0.04960 | 2.16 | 0.18993 | 2.56 | 0.02777 | 1.36 | 0.53 | 176.2 | 25.1 | 176.6 | 2.1 | 176.6 | 1.3 | 100 |
| Z44 | Prismatic | 200 | Core | Magmatic zonation | 0.05037 | 1.71 | 0.19562 | 2.30 | 0.02817 | 1.54 | 0.67 | 212.0 | 19.7 | 181.4 | 2.0 | 179.1 | 1.5 | 99 |
| Z41 | Short-Prismatic | 150 | Core | Magmatic zonation | 0.05409 | 0.62 | 0.44996 | 1.16 | 0.06033 | 0.99 | 0.85 | 374.9 | 13.9 | 377.2 | 3.7 | 377.6 | 3.6 | 100 |
| Z30 | Subrounded | 100 | Core | Magmatic zonation | 0.05980 | 1.00 | 0.75733 | 1.68 | 0.09185 | 1.35 | 0.80 | 596.5 | 20.4 | 572.5 | 5.3 | 566.4 | 4.0 | 99 |
| Z39 | Prismatic | 150 | Core | Magmatic zonation | 0.05874 | 1.83 | 0.75303 | 2.43 | 0.09297 | 1.60 | 0.66 | 557.6 | 19.8 | 570.0 | 5.5 | 573.1 | 4.7 | 101 |
| Z10 | Prismatic | 400 | Core | Magmatic zonation | 0.06070 | 1.14 | 0.78845 | 1.69 | 0.09421 | 1.25 | 0.74 | 628.6 | 12.3 | 590.3 | 4.0 | 580.4 | 3.9 | 98 |
| Z26 | Subrounded | 200 | Core | Magmatic zonation | 0.05958 | 0.56 | 0.79489 | 2.74 | 0.09676 | 2.68 | 0.98 | 588.4 | 12.1 | 593.9 | 12.3 | 595.4 | 15.3 | 100 |
| Z37 | Prismatic | 250 | Core | Magmatic zonation | 0.10787 | 0.48 | 4.77446 | 1.02 | 0.32101 | 0.89 | 0.88 | 1763.8 | 8.9 | 1780.4 | 8.5 | 1794.7 | 14.0 | 101 |
| Z33 | Subrounded | 200 | Core | Magmatic zonation | 0.13201 | 0.55 | 6.52807 | 1.44 | 0.35864 | 1.33 | 0.92 | 2124.9 | 4.9 | 2049.7 | 6.9 | 1975.7 | 12.5 | 96 |
| Z12 | Subrounded | 400 | Core | Magmatic zonation | 0.13571 | 0.82 | 6.79526 | 1.96 | 0.36315 | 1.78 | 0.91 | 2173.2 | 14.2 | 2085.1 | 17.4 | 1997.1 | 30.7 | 96 |
| Z13(***) | Subrounded | 250 | Core | Inher. Core/Magm Zon Rim | 0.05491 | 1.41 | 0.33476 | 1.69 | 0.04422 | 0.94 | 0.55 | 408.5 | 15.7 | 293.2 | 2.3 | 278.9 | 1.5 | 95 |
| Z15 | Square | 250 | Core | Inher. Core/Magm Zon Rim | 0.05426 | 0.99 | 0.39524 | 1.53 | 0.05283 | 1.16 | 0.76 | 381.7 | 11.2 | 338.2 | 2.4 | 331.9 | 2.1 | 98 |
| Z36 | Prismatic-Frat | 300 | Core | Magmatic zonation | 0.05454 | 1.15 | 0.40403 | 1.75 | 0.05373 | 1.31 | 0.75 | 393.2 | 12.9 | 344.6 | 2.7 | 337.4 | 2.4 | 98 |
| Z27 | Subrounded | 150 | Core | Magmatic zonation | 0.05901 | 1.02 | 0.65631 | 1.38 | 0.08066 | 0.94 | 0.68 | 567.5 | 11.1 | 512.4 | 3.1 | 500.1 | 2.7 | 98 |
| Z16 | Subrounded | 150 | Core | Magmatic zonation | 0.06468 | 1.73 | 0.77375 | 2.11 | 0.08676 | 1.18 | 0.56 | 763.9 | 35.4 | 581.9 | 8.1 | 536.4 | 3.5 | 92 |
| *Cerro Cóndor sub-basin* | | | | | | | | | | | | | | | | | | |
| **CAV-40: Gray pyroclastic level, Las Chacritas Member** | | | | | | | | | | | | | | | | | | |
| Z6(*) | Prismatic | 450 | Core | Magmatic zonation | 0.05205 | 4.70 | 0.18479 | 5.26 | 0.02575 | 2.36 | 0.45 | 287.6 | 107.4 | 172.2 | 8.3 | 163.9 | 3.8 | 95 |
| Z1 | Prismatic | 200 | Rim | Magmatic zonation | 0.05058 | 5.54 | 0.18113 | 6.44 | 0.02597 | 3.29 | 0.51 | 222.0 | 128.2 | 169.0 | 10.0 | 165.3 | 5.4 | 98 |
| Z17 | Prismatic | 170 | Core | Magmatic zonation | 0.05033 | 3.30 | 0.18039 | 3.97 | 0.02600 | 2.21 | 0.56 | 210.1 | 76.6 | 168.4 | 6.2 | 165.4 | 3.6 | 98 |
| Z5 | Prismatic | 150 | Core | Magmatic zonation | 0.05373 | 5.12 | 0.19425 | 5.61 | 0.02622 | 2.31 | 0.41 | 359.9 | 115.4 | 180.3 | 9.3 | 166.8 | 3.8 | 93 |
| Z4 | Prismatic | 300 | Core | Magmatic zonation | 0.05320 | 5.03 | 0.19409 | 5.99 | 0.02646 | 3.24 | 0.54 | 337.3 | 114.1 | 180.1 | 9.9 | 168.4 | 5.4 | 93 |
| Z3 | Prismatic | 450 | Core | Magmatic zonation | 0.05084 | 3.19 | 0.18610 | 4.04 | 0.02655 | 2.48 | 0.61 | 233.6 | 73.6 | 173.3 | 6.4 | 168.9 | 4.1 | 97 |
| Z2 | Short-Prismatic | 150 | Core | Magmatic zonation | 0.05080 | 1.66 | 0.18811 | 2.61 | 0.02686 | 2.02 | 0.77 | 231.6 | 38.4 | 175.0 | 4.2 | 170.9 | 3.4 | 98 |

| | | | | | | | | | | | | | | | | | |
|---|---|---|---|---|---|---|---|---|---|---|---|---|---|---|---|---|---|
| Z16 | Subrounded | 180 | Core | Magmatic zonation | 0.05098 | 3.88 | 0.19008 | 4.45 | 0.02704 | 2.18 | 0.49 | 239.8 | 89.5 | 176.7 | 7.2 | 172.0 | 3.7 | 97 |
| Z15 | Prismatic | 250 | Core | Magmatic zonation | 0.04997 | 3.08 | 0.18633 | 4.00 | 0.02704 | 2.54 | 0.64 | 193.7 | 71.7 | 173.5 | 6.4 | 172.0 | 4.3 | 99 |
| Z12 | Subrounded | 200 | Rim | Magmatic zonation | 0.05225 | 3.95 | 0.19637 | 4.69 | 0.02726 | 2.54 | 0.54 | 296.4 | 90.1 | 182.1 | 7.8 | 173.4 | 4.3 | 95 |
| Z14 | Short-Prismatic | 220 | Core | Magmatic zonation | 0.05172 | 2.98 | 0.19470 | 4.77 | 0.02730 | 3.72 | 0.78 | 272.9 | 68.4 | 180.6 | 7.9 | 173.7 | 6.4 | 96 |
| Z11 | Long-Prismatic | 260 | Rim | Magmatic zonation | 0.05237 | 3.51 | 0.19930 | 4.34 | 0.02760 | 2.55 | 0.59 | 301.6 | 80.0 | 184.5 | 7.3 | 175.5 | 4.4 | 95 |
| Z8 | Short-Prismatic | 150 | Rim | Magmatic zonation | 0.05159 | 3.82 | 0.19695 | 4.48 | 0.02769 | 2.34 | 0.52 | 267.1 | 87.7 | 182.5 | 7.5 | 176.1 | 4.1 | 96 |
| Z18 | Subrounded | 160 | Core | Magmatic zonation | 0.05070 | 4.44 | 0.19405 | 5.70 | 0.02776 | 3.59 | 0.63 | 227.4 | 102.5 | 180.1 | 9.4 | 176.5 | 6.2 | 98 |
| Z13 | Prismatic | 140 | Rim | Magmatic zonation | 0.05003 | 4.16 | 0.19851 | 5.19 | 0.02877 | 3.09 | 0.60 | 196.6 | 96.7 | 183.9 | 8.7 | 182.9 | 5.6 | 99 |
| Z9 | Prismatic | 200 | Rim | Magmatic zonation | 0.05403 | 2.64 | 0.26959 | 3.96 | 0.03619 | 2.95 | 0.75 | 372.4 | 59.4 | 242.4 | 8.5 | 229.2 | 6.6 | 95 |
| **SCN-2: Laminated tuffite, Puesto Almada Member** | | | | | | | | | | | | | | | | | | |
| Z2(*) | Short-Prismatic | 80 | Core | Magmatic zonation | 0.04968 | 2.32 | 0.17162 | 3.30 | 0.02505 | 2.34 | 0.7 | 180.1 | 54.1 | 160.8 | 4.9 | 159.5 | 3.7 | 99 |
| Z8 | Long-Prismatic | 100 | Core | Magmatic zonation | 0.05055 | 4.11 | 0.17469 | 5.27 | 0.02506 | 3.29 | 0.6 | 220.3 | 95.1 | 163.5 | 8.0 | 159.6 | 5.2 | 98 |
| Z10 | Long-Prismatic | 150 | Core | Magmatic zonation | 0.05099 | 2.87 | 0.17680 | 3.41 | 0.02515 | 1.84 | 0.5 | 240.4 | 66.2 | 165.3 | 5.2 | 160.1 | 2.9 | 97 |
| Z11 | Short-Prismatic | 60 | Core | Magmatic zonation | 0.04874 | 3.24 | 0.16992 | 3.69 | 0.02528 | 1.77 | 0.5 | 135.4 | 76.0 | 159.3 | 5.4 | 161.0 | 2.8 | 101 |
| Z12 | Short-Prismatic | 60 | Core | Magmatic zonation | 0.04820 | 2.87 | 0.17345 | 3.61 | 0.02610 | 2.20 | 0.6 | 109.3 | 67.7 | 162.4 | 5.4 | 166.1 | 3.6 | 102 |
| Z5 | Prismatic | 150 | Core | Magmatic zonation | 0.05210 | 5.98 | 0.20078 | 6.95 | 0.02795 | 3.53 | 0.5 | 289.7 | 136.6 | 185.8 | 11.8 | 177.7 | 6.2 | 96 |
| Z4 | Short-Prismatic | 60 | Core | Magmatic zonation | 0.05245 | 3.84 | 0.20729 | 5.20 | 0.02866 | 3.51 | 0.7 | 305.1 | 87.5 | 191.3 | 9.1 | 182.2 | 6.3 | 95 |
| Z7 | Short-Prismatic | 50 | Core | Magmatic zonation | 0.04923 | 4.54 | 0.19501 | 5.17 | 0.02873 | 2.48 | 0.5 | 158.9 | 106.2 | 180.9 | 8.6 | 182.6 | 4.5 | 101 |
| **La Manea-1: A tuff sandstone** | | | | | | | | | | | | | | | | | | |
| Z34 | Prismatic | 240 | Core | Magmatic zonation | 0.05031 | 4.06 | 0.17012 | 4.77 | 0.02453 | 2.51 | 0.53 | 209.2 | 94.0 | 159.5 | 7.0 | 156.2 | 3.9 | 98 |
| Z3CORE | Prismatic | 300 | Core | Magmatic zonation | 0.04933 | 2.23 | 0.17619 | 3.55 | 0.02590 | 2.77 | 0.78 | 163.5 | 52.1 | 164.8 | 5.4 | 164.9 | 4.5 | 100 |
| Z18(*) | Short-Prismatic | 230 | Core | Smooth-Mag. zonation | 0.05222 | 3.83 | 0.19359 | 4.89 | 0.02689 | 3.03 | 0.62 | 295.0 | 87.5 | 179.7 | 8.0 | 171.0 | 5.1 | 95 |
| Z27 | Prismatic | 250 | Rim | Smooth-Mag. zonation | 0.04917 | 3.77 | 0.18311 | 4.57 | 0.02701 | 2.58 | 0.56 | 155.8 | 88.3 | 170.7 | 7.2 | 171.8 | 4.4 | 101 |
| Z35 | Prismatic | 230 | Core | Homogeneous | 0.04912 | 4.15 | 0.18415 | 4.92 | 0.02719 | 2.64 | 0.54 | 153.5 | 97.2 | 171.6 | 7.8 | 172.9 | 4.5 | 101 |
| Z21 | Prismatic | 250 | Rim | Smooth-Mag. zonation | 0.04925 | 3.13 | 0.18591 | 5.08 | 0.02738 | 4.00 | 0.79 | 159.7 | 73.2 | 173.1 | 8.1 | 174.1 | 6.9 | 101 |
| Z16 | Prismatic-Subrounded | 200 | Rim | Smooth-Mag. zonation | 0.05045 | 1.92 | 0.19066 | 3.37 | 0.02741 | 2.77 | 0.82 | 215.9 | 44.5 | 177.2 | 5.5 | 174.3 | 4.8 | 98 |
| Z8 | Long-Prismatic | 300 | Rim | Magmatic zonation | 0.04881 | 5.79 | 0.18457 | 6.60 | 0.02743 | 3.17 | 0.48 | 138.6 | 66.6 | 172.0 | 5.2 | 174.4 | 2.8 | 101 |
| Z11 | Rectangular | 150 | Rim | Magmatic zonation | 0.04902 | 1.78 | 0.18647 | 2.77 | 0.02759 | 2.12 | 0.77 | 148.9 | 41.8 | 173.6 | 4.4 | 175.4 | 3.7 | 101 |
| Z13 | Prismatic | 300 | Rim | Magmatic zonation | 0.04931 | 2.43 | 0.18760 | 3.64 | 0.02759 | 2.70 | 0.74 | 162.8 | 53.8 | 174.6 | 4.4 | 175.5 | 2.4 | 100 |
| Z14 | Prismatic | 250 | Rim | Smooth-Mag. zonation | 0.05207 | 3.20 | 0.19813 | 4.20 | 0.02760 | 2.72 | 0.65 | 288.4 | 73.2 | 183.5 | 7.1 | 175.5 | 4.7 | 96 |
| Z32CORE | Prismatic-Frat | 250 | Core | Smooth-Mag. zonation | 0.05085 | 4.15 | 0.19370 | 4.88 | 0.02763 | 2.57 | 0.53 | 234.1 | 95.8 | 179.8 | 8.0 | 175.7 | 4.5 | 98 |
| Z36 | Prismatic | 250 | Core | Smooth-Mag. zonation | 0.04633 | 6.01 | 0.17686 | 6.82 | 0.02769 | 3.22 | 0.47 | 14.7 | 144.6 | 165.4 | 10.4 | 176.1 | 5.6 | 106 |
| Z9CORE | Prismatic | 250 | Core | Inhereted core | 0.05155 | 4.27 | 0.19683 | 5.23 | 0.02769 | 3.02 | 0.58 | 265.7 | 98.0 | 182.4 | 8.7 | 176.1 | 5.2 | 97 |
| Z25 | Subrounded-Frat | 230 | Rim | Homogeneous | 0.05068 | 3.86 | 0.19441 | 4.63 | 0.02782 | 2.55 | 0.55 | 226.5 | 89.1 | 180.4 | 7.6 | 176.9 | 4.5 | 98 |
| Z28 | Subrounded | 250 | Rim | Smooth-Mag. zonation | 0.05129 | 3.20 | 0.19692 | 4.16 | 0.02784 | 2.66 | 0.64 | 254.1 | 73.6 | 182.5 | 7.0 | 177.0 | 4.6 | 97 |
| Z3RIM | Prismatic-Frat | 250 | Rim | Smooth-Mag. zonation | 0.05615 | 4.82 | 0.21670 | 6.09 | 0.02799 | 3.72 | 0.61 | 458.2 | 52.6 | 199.2 | 5.5 | 178.0 | 3.3 | 89 |
| Z7 | Prismatic-Frat. | 250 | Rim | Homogeneous | 0.04977 | 4.33 | 0.19235 | 4.82 | 0.02803 | 2.09 | 0.44 | 184.4 | 49.7 | 178.6 | 4.0 | 178.2 | 1.9 | 100 |
| Z12 | Rectangular | 130 | Rim | Magmatic zonation | 0.04851 | 3.61 | 0.18775 | 4.25 | 0.02807 | 2.22 | 0.52 | 124.4 | 42.0 | 174.7 | 3.4 | 178.4 | 2.0 | 102 |
| Z10 | Short-Prismatic | 250 | Rim | Zonation | 0.05469 | 2.06 | 0.21169 | 2.96 | 0.02807 | 2.13 | 0.72 | 399.6 | 46.1 | 195.0 | 5.3 | 178.5 | 3.7 | 92 |
| Z24 | Prismatic | 230 | Rim | Homogeneous | 0.05053 | 2.52 | 0.19598 | 3.37 | 0.02813 | 2.23 | 0.66 | 219.6 | 58.4 | 181.7 | 5.6 | 178.8 | 3.9 | 98 |
| Z26 | Prismatic | 250 | Rim | Magmatic zonation | 0.05208 | 5.19 | 0.20269 | 5.72 | 0.02823 | 2.41 | 0.42 | 288.9 | 118.6 | 187.4 | 9.8 | 179.4 | 4.3 | 96 |
| Z6RIM | Long-Prismatic | 350 | Rim | Smooth-Mag. zonation | 0.05089 | 3.09 | 0.20252 | 3.85 | 0.02886 | 2.30 | 0.60 | 235.9 | 71.2 | 187.3 | 6.6 | 183.4 | 4.2 | 98 |
| Z31 | Prismatic-Frat. | 250 | Rim | Magmatic zonation | 0.05080 | 4.78 | 0.20403 | 5.62 | 0.02913 | 2.96 | 0.53 | 231.7 | 110.3 | 188.5 | 9.7 | 185.1 | 5.4 | 98 |
| Z4 | Prismatic | 230 | Rim | Smooth-Mag. zonation | 0.05485 | 3.14 | 0.22050 | 4.17 | 0.02915 | 2.75 | 0.66 | 406.2 | 70.2 | 202.3 | 7.6 | 185.3 | 5.0 | 92 |
| Z38 | Short-Prismatic | 200 | Core | Magmatic zonation | 0.05167 | 4.11 | 0.20981 | 5.03 | 0.02945 | 2.90 | 0.58 | 270.9 | 94.3 | 193.4 | 8.9 | 187.1 | 5.3 | 97 |
| Z1 | Short-Prismatic | 130 | Rim | Homogeneous | 0.05037 | 3.43 | 0.20499 | 4.20 | 0.02951 | 2.42 | 0.58 | 212.3 | 39.3 | 189.3 | 3.7 | 187.5 | 2.3 | 99 |
| Z33 | Prismatic | 230 | Core | Smooth-Mag. zonation | 0.05086 | 6.16 | 0.20759 | 6.75 | 0.02960 | 2.75 | 0.41 | 234.3 | 142.2 | 191.5 | 11.8 | 188.1 | 5.1 | 98 |

| | | | | | | | | | | | | | | | | | |
|---|---|---|---|---|---|---|---|---|---|---|---|---|---|---|---|---|---|
| Z9RIM | Prismatic | 250 | Rim | Magmatic zonation | 0.05738 | 3.09 | 0.23452 | 3.82 | 0.02964 | 2.24 | 0.59 | 506.1 | 68.0 | 213.9 | 7.4 | 188.3 | 4.1 | 88 |
| Z5 | Prismatic | 240 | Rim | Smooth-Mag. zonation | 0.05036 | 2.32 | 0.20860 | 3.38 | 0.03004 | 2.46 | 0.73 | 211.4 | 53.7 | 192.4 | 5.9 | 190.8 | 4.6 | 99 |
| Z23 | Prismatic | 230 | Rim | Magmatic zonation | 0.05217 | 3.51 | 0.21692 | 4.46 | 0.03015 | 2.75 | 0.62 | 293.0 | 80.1 | 199.3 | 8.1 | 191.5 | 5.2 | 96 |
| Z17 | Rectangular | 200 | Rim | Smooth-Mag. zonation | 0.05077 | 4.59 | 0.21111 | 5.45 | 0.03016 | 2.93 | 0.54 | 230.5 | 106.0 | 194.5 | 9.6 | 191.5 | 5.5 | 98 |
| Z15 | Short-Prismatic | 190 | Rim | Homogeneous | 0.05123 | 3.31 | 0.21518 | 4.12 | 0.03047 | 2.45 | 0.60 | 251.0 | 76.1 | 197.9 | 7.4 | 193.5 | 4.7 | 98 |
| Z22 | Subrounded-Prismatic | 150 | Rim | Smooth-Mag. zonation | 0.05564 | 3.10 | 0.23476 | 3.90 | 0.03060 | 2.36 | 0.61 | 438.0 | 69.0 | 214.1 | 7.5 | 194.3 | 4.5 | 91 |
| Z39 | Long-Prismatic | 400 | Core | Magmatic zonation | 0.05123 | 4.40 | 0.21918 | 5.37 | 0.03103 | 3.08 | 0.57 | 251.2 | 101.3 | 201.2 | 9.8 | 197.0 | 6.0 | 98 |
| Z6CORE | Long-Prismatic | 350 | Core | Smooth-Mag. zonation | 0.04984 | 2.12 | 0.21674 | 3.83 | 0.03154 | 3.19 | 0.83 | 187.7 | 49.4 | 199.2 | 6.9 | 200.2 | 6.3 | 100 |
| Z19 | Prismatic | 260 | Rim | Smooth-Mag. zonation | 0.05250 | 2.15 | 0.23375 | 3.32 | 0.03229 | 2.53 | 0.76 | 307.2 | 48.9 | 213.3 | 6.4 | 204.9 | 5.1 | 96 |
| Z2 | Prismatic | 230 | Core | Smooth-Mag. zonation | 0.05169 | 3.35 | 0.23094 | 4.65 | 0.03240 | 3.22 | 0.69 | 271.8 | 38.0 | 211.0 | 4.5 | 205.6 | 3.3 | 97 |
| Z30 | Subrounded-Prismatic | 250 | Rim | Homogeneous | 0.08818 | 1.19 | 3.29341 | 2.82 | 0.27087 | 2.56 | 0.91 | 1386.5 | 22.8 | 1479.5 | 22.0 | 1545.2 | 3.5 | 96 |
| *Fossati sub-basin* | | | | | | | | | | | | | | | | | | |
| **CAF-8: a pyroclastic level** | | | | | | | | | | | | | | | | | | |
| Z1(*) | Long-Prismatic | 300 | Core | Smooth-Mag. zonation | 0.04955 | 2.39 | 0.17103 | 3.42 | 0.02503 | 2.44 | 0.71 | 174.1 | 55.8 | 160.3 | 5.1 | 159.4 | 3.8 | 99 |
| Z2 | Long-Prismatic | 400 | Core | Smooth-Mag. zonation | 0.05061 | 3.13 | 0.17063 | 4.16 | 0.02445 | 2.74 | 0.66 | 223.0 | 72.3 | 160.0 | 6.2 | 155.7 | 4.2 | 97 |
| Z3 | Long-Prismatic | 400 | Core | Smooth-Mag. zonation | 0.04853 | 3.05 | 0.16805 | 4.13 | 0.02512 | 2.78 | 0.67 | 125.0 | 71.9 | 157.7 | 6.0 | 159.9 | 4.4 | 101 |
| Z5 | Long-Prismatic | 250 | Core | Smooth-Mag. zonation | 0.04766 | 3.71 | 0.16154 | 6.00 | 0.02458 | 4.71 | 0.79 | 82.4 | 88.1 | 152.0 | 8.5 | 156.6 | 7.3 | 103 |
| Z6 | Long-Prismatic | 400 | Core | Smooth-Mag. zonation | 0.04833 | 2.75 | 0.16450 | 3.67 | 0.02468 | 2.44 | 0.66 | 115.7 | 64.7 | 154.6 | 5.3 | 157.2 | 3.8 | 102 |
| Z7 | Long-Prismatic | 400 | Core | Smooth-Mag. zonation | 0.05188 | 3.62 | 0.17555 | 4.77 | 0.02454 | 3.11 | 0.65 | 279.9 | 82.8 | 164.2 | 7.2 | 156.3 | 4.8 | 95 |
| Z8 | Long-Prismatic | 350 | Core | Smooth-Mag. zonation | 0.04865 | 2.94 | 0.16816 | 3.90 | 0.02507 | 2.58 | 0.66 | 131.1 | 69.0 | 157.8 | 5.7 | 159.6 | 4.1 | 101 |
| Z9 | Long-Prismatic | 100 | Core | Smooth-Mag. zonation | 0.04986 | 2.64 | 0.17037 | 3.51 | 0.02478 | 2.32 | 0.66 | 188.6 | 61.5 | 159.7 | 5.2 | 157.8 | 3.6 | 99 |
| Z10 | Long-Prismatic | 350 | Core | Smooth-Mag. zonation | 0.05014 | 2.74 | 0.17105 | 3.81 | 0.02474 | 2.65 | 0.70 | 201.7 | 63.5 | 160.3 | 5.6 | 157.5 | 4.1 | 98 |
| Z11 | Long-Prismatic | 400 | Core | Smooth-Mag. zonation | 0.04939 | 4.99 | 0.17154 | 6.37 | 0.02519 | 3.96 | 0.62 | 166.4 | 116.7 | 160.8 | 9.5 | 160.4 | 6.3 | 100 |
| Z12 | Long-Prismatic | 360 | Core | Smooth-Mag. zonation | 0.04895 | 4.59 | 0.17009 | 5.82 | 0.02520 | 3.59 | 0.62 | 145.6 | 107.6 | 159.5 | 8.6 | 160.4 | 5.7 | 101 |
| **CAF-6: tuff sandstone** | | | | | | | | | | | | | | | | | | |
| Z5(*) | Short-Prismatic | 100 | Rim | Magmatic zonation | 0.05033 | 2.30 | 0.18749 | 3.13 | 0.02702 | 2.12 | 0.68 | 210.1 | 52.5 | 174.5 | 5.0 | 171.9 | 3.6 | 99 |
| Z6 | Prismatic | 100 | Rim | Homogeneous | 0.05044 | 2.82 | 0.18881 | 3.77 | 0.02715 | 2.50 | 0.66 | 215.3 | 64.0 | 175.6 | 6.1 | 172.7 | 4.3 | 98 |
| Z24 | Subrounded-Frat | 80 | Rim | Homogeneous | 0.05579 | 2.05 | 0.21376 | 3.13 | 0.02779 | 2.36 | 0.75 | 444.2 | 45.0 | 196.7 | 5.6 | 176.7 | 4.1 | 90 |
| Z26 | Long-Prismatic | 200 | Rim | Homogeneous | 0.05219 | 4.90 | 0.21003 | 5.45 | 0.02919 | 2.38 | 0.44 | 293.8 | 108.1 | 193.6 | 9.6 | 185.5 | 4.4 | 96 |
| Z8 | Rectangular | 150 | Rim | Magmatic zonation | 0.05730 | 3.39 | 0.23179 | 4.08 | 0.02934 | 2.27 | 0.56 | 503.0 | 73.0 | 211.7 | 7.8 | 186.4 | 4.2 | 88 |
| Z27 | Prismatic-Frat | 100 | Core | Smooth-Mag. zonation | 0.05676 | 2.23 | 0.35592 | 3.01 | 0.04548 | 2.03 | 0.67 | 482.1 | 48.5 | 309.2 | 8.0 | 286.7 | 5.7 | 93 |
| Z9 | Prismatic | 150 | Core | Magmatic zonation | 0.05523 | 2.18 | 0.34719 | 3.08 | 0.04560 | 2.17 | 0.71 | 421.3 | 48.7 | 302.6 | 8.1 | 287.4 | 6.1 | 95 |
| Z7 | Subrounded | 100 | Rim | Magmatic zonation | 0.05255 | 2.18 | 0.33054 | 3.15 | 0.04562 | 2.28 | 0.72 | 309.5 | 48.8 | 290.0 | 7.9 | 287.6 | 6.4 | 99 |
| Z2 | Short-SubPrismatic | 150 | Rim | Magmatic zonation | 0.05269 | 3.04 | 0.33399 | 3.72 | 0.04597 | 2.16 | 0.58 | 315.6 | 69.1 | 292.6 | 9.5 | 289.7 | 6.1 | 99 |
| Z1 | Prismatic | 200 | Rim | Magmatic zonation | 0.05250 | 1.53 | 0.33836 | 2.92 | 0.04675 | 2.48 | 0.85 | 307.1 | 34.9 | 295.9 | 7.5 | 294.5 | 7.1 | 100 |
| Z21 | Prismatic-Frat | 200 | Core | Homogeneous | 0.05546 | 2.89 | 0.35930 | 3.98 | 0.04699 | 2.74 | 0.69 | 430.7 | 63.1 | 311.7 | 10.6 | 296.0 | 7.9 | 95 |
| Z17 | Prismatic | 150 | Rim | Smooth-Mag. zonation | 0.05338 | 1.96 | 0.35417 | 3.07 | 0.04812 | 2.35 | 0.77 | 344.8 | 43.8 | 307.9 | 8.1 | 303.0 | 7.0 | 98 |
| Z22 | Rectangular | 150 | Rim | Smooth-Mag. zonation | 0.05203 | 1.52 | 0.34588 | 2.79 | 0.04821 | 2.34 | 0.84 | 286.9 | 34.8 | 301.6 | 7.3 | 303.5 | 6.9 | 101 |
| Z15 | Subrounded | 100 | Core | Homogeneous | 0.05211 | 1.21 | 0.34784 | 2.59 | 0.04842 | 2.29 | 0.88 | 290.1 | 27.3 | 303.1 | 6.8 | 304.8 | 6.8 | 101 |
| Z14 | Long-Subprismatic | 180 | Rim | Smooth-Mag. zonation | 0.05402 | 1.74 | 0.36149 | 2.94 | 0.04853 | 2.36 | 0.80 | 372.0 | 38.8 | 313.3 | 7.9 | 305.5 | 7.0 | 97 |
| Z12 | Long-Prismatic | 200 | Rim | Magmatic zonation | 0.05453 | 2.04 | 0.43063 | 2.97 | 0.05727 | 2.16 | 0.73 | 393.2 | 45.8 | 363.6 | 9.1 | 359.0 | 7.5 | 99 |
| Z11 | Subprismatic | 300 | Rim | Magmatic zonation | 0.05490 | 1.06 | 0.46810 | 2.58 | 0.06184 | 2.35 | 0.91 | 408.2 | 23.8 | 389.9 | 8.3 | 386.8 | 8.8 | 99 |
| Z25 | Rectangular-Frat. | 100 | Core | Magmatic zonation | 0.05481 | 1.55 | 0.49841 | 3.59 | 0.06595 | 3.24 | 0.90 | 404.5 | 34.7 | 410.6 | 12.1 | 411.7 | 12.9 | 100 |
| Z13 | Long-subprismatic | 170 | Rim | Homogeneous | 0.05985 | 4.95 | 0.54955 | 6.20 | 0.06660 | 3.72 | 0.60 | 598.1 | 103.6 | 444.7 | 22.1 | 415.6 | 15.0 | 93 |
| Z3 | Long-subprismatic | 170 | Rim | Magmatic zonation | 0.05793 | 1.52 | 0.53483 | 2.71 | 0.06696 | 2.24 | 0.83 | 527.1 | 33.4 | 435.0 | 9.6 | 417.8 | 9.0 | 96 |
| Z16(***) | Prismatic | 100 | Rim | Smooth-Mag. zonation | 0.07552 | 4.23 | 0.48584 | 5.04 | 0.04666 | 2.74 | 0.54 | 1082.4 | 84.8 | 402.1 | 16.7 | 294.0 | 7.9 | 73 |
| Z23 | Long-Prismatic | 100 | Rim | Homogeneous | 0.06469 | 5.77 | 0.24645 | 6.25 | 0.02763 | 2.40 | 0.38 | 764.3 | 117.1 | 223.7 | 12.5 | 175.7 | 4.2 | 79 |
| Z4 | Subrounded | 100 | Rim | Homogeneous | 0.06634 | 4.84 | 0.39266 | 5.72 | 0.04293 | 3.00 | 0.53 | 817.2 | 98.0 | 336.3 | 16.2 | 270.9 | 8.1 | 81 |

| | | | | | | | | | | | | | | | | | |
|---|---|---|---|---|---|---|---|---|---|---|---|---|---|---|---|---|---|
| Z28 | Subrounded | 200 | Core | Smooth-Mag. zonation | 0.05831 | 2.35 | 0.21603 | 3.21 | 0.02687 | 2.18 | 0.68 | 541.6 | 50.6 | 198.6 | 5.8 | 170.9 | 3.7 | 86 |
| Z19 | Subrounded | 50 | Core | Homogeneous | 0.06091 | 3.14 | 0.36995 | 4.05 | 0.04405 | 2.55 | 0.63 | 636.0 | 67.7 | 319.6 | 11.1 | 277.9 | 6.9 | 87 |

(*) in gray, the data used for calculation of weighted averegare age or concordian age.

(**) the percentage of concordia for every data was calculated using the relation between $^{206}$ Pb/$^{238}$ U and $^{207}$ Pb/$^{235}$ U

(***) discordant data

Table 3: Representative results of in situ Lu-Hf LA-ICP-MS-MC zircon analyses fo
evolution of Cañadón Asfalto basin, centr

| *Sample* | *T (Ga)* | T (Ma) | $(^{176}Lu/^{177}Hf)_{meas}$ | ±2σ | $(^{176}Hf/^{177}Hf)_{meas}$ | ±2σ |
|---|---|---|---|---|---|---|
| | | | | | *Lonco Trapial Range* | |
| **LTCT-1** | | | | | | |
| Z4 | 0.167 | 167 | 0.0609132 | ±0.001285 | 0.282713 | ±0.000026 |
| Z5 | 0.166 | 166 | 0.0608247 | ±0.000518 | 0.282704 | ±0.000030 |
| Z14 | 0.167 | 167 | 0.0935329 | ±0.002385 | 0.282643 | ±0.000048 |
| Z11 | 0.172 | 172 | 0.0364344 | ±0.000525 | 0.282634 | ±0.000020 |
| Z3 | 0.174 | 174 | 0.0278292 | ±0.000124 | 0.282624 | ±0.000017 |
| Z16 | 0.536 | 536 | 0.0599110 | ±0.001878 | 0.282519 | ±0.000023 |
| Z10 | 0.580 | 580 | 0.0297897 | ±0.000401 | 0.282474 | ±0.000019 |
| | | | | | *Cerro Cóndor sub-basin* | |
| **CAV-40** | | | | | | |
| Z4 | 0.172 | 172 | 0.0009568 | ±0.000039 | 0.282459 | ±0.000030 |
| Z14 | 0.168 | 168 | 0.0005840 | ±0.000020 | 0.282441 | ±0.000018 |
| Z3 | 0.174 | 174 | 0.0014928 | ±0.000008 | 0.282463 | ±0.000020 |
| Z15 | 0.168 | 168 | 0.0010224 | ±0.000028 | 0.282421 | ±0.000023 |
| Z6 | 0.169 | 169 | 0.0021392 | ±0.000027 | 0.282490 | ±0.000029 |
| Z17 | 0.164 | 164 | 0.0011385 | ±0.000009 | 0.282433 | ±0.000027 |
| Z1 | 0.165 | 165 | 0.0010426 | ±0.000013 | 0.282499 | ±0.000021 |
| **SCN-2** | | | | | | |
| Z8 | 0.160 | 160 | 0.0012470 | ±0.000036 | 0.282707 | ±0.000031 |
| Z2 | 0.160 | 160 | 0.0014507 | ±0.000023 | 0.282693 | ±0.000024 |
| Z5 | 0.178 | 178 | 0.0032712 | ±0.000088 | 0.282640 | ±0.000050 |
| | | | | | *La Manea Range* | |
| **La Manea-1** | | | | | | |
| Z34 | 0.156 | 156 | 0.0016104 | ±0.000008 | 0.282751 | ±0.000044 |
| Z3CORE | 0.165 | 165 | 0.0012062 | ±0.000033 | 0.282677 | ±0.000022 |
| Z27 | 0.172 | 172 | 0.0014138 | ±0.000014 | 0.282404 | ±0.000026 |
| Z35 | 0.173 | 173 | 0.0014156 | ±0.000017 | 0.282486 | ±0.000028 |
| Z21 | 0.174 | 174 | 0.0006782 | ±0.000004 | 0.282718 | ±0.000015 |
| Z8 | 0.174 | 174 | 0.0016046 | ±0.000013 | 0.282558 | ±0.000027 |
| Z13 | 0.176 | 176 | 0.0011967 | ±0.000026 | 0.282491 | ±0.000021 |
| Z9CORE | 0.176 | 176 | 0.0009853 | ±0.000009 | 0.282439 | ±0.000029 |
| Z36 | 0.176 | 176 | 0.0009126 | ±0.000001 | 0.282359 | ±0.000033 |
| Z28 | 0.177 | 177 | 0.0015562 | ±0.000024 | 0.282452 | ±0.000043 |
| Z7 | 0.178 | 178 | 0.0006917 | ±0.000006 | 0.282481 | ±0.000030 |
| Z12 | 0.178 | 178 | 0.0017838 | ±0.000016 | 0.282615 | ±0.000021 |
| Z24 | 0.179 | 179 | 0.0011268 | ±0.000001 | 0.282470 | ±0.000018 |
| Z26 | 0.179 | 179 | 0.0013490 | ±0.000007 | 0.282468 | ±0.000026 |
| Z4 | 0.185 | 185 | 0.0015254 | ±0.000033 | 0.282439 | ±0.000029 |
| Z38 | 0.187 | 187 | 0.0016577 | ±0.000025 | 0.282508 | ±0.000060 |
| Z1 | 0.188 | 188 | 0.0013851 | ±0.000016 | 0.282576 | ±0.000035 |
| Z23 | 0.192 | 192 | 0.0012489 | ±0.000040 | 0.282453 | ±0.000025 |
| Z15 | 0.194 | 194 | 0.0006840 | ±0.000007 | 0.282454 | ±0.000020 |
| Z39 | 0.197 | 197 | 0.0544359 | ±0.000466 | 0.282415 | ±0.000041 |

| | | | | | | |
|---|---|---|---|---|---|---|
| Z6CORE | 0.200 | 200 | 0.0024479 | ±0.000053 | 0.282398 | ±0.000038 |
| Z19 | 0.205 | 205 | 0.0008463 | ±0.000004 | 0.282457 | ±0.000023 |
| Z30 | 1.479 | 1479 | 0.0014250 | ±0.000004 | 0.282123 | ±0.000045 |
| | | | | | *Fossati sub-basin* | |
| **CAF-8 pyroclastic level** | | | | | | |
| Z7 | 0.156 | 156 | 0.0016642 | ±0.000043 | 0.282536 | ±0.000055 |
| Z6 | 0.157 | 157 | 0.0013138 | ±0.000019 | 0.282548 | ±0.000057 |
| Z9 | 0.158 | 158 | 0.0011957 | ±0.000015 | 0.282565 | ±0.000054 |
| Z8 | 0.159 | 159 | 0.0010977 | ±0.000018 | 0.282647 | ±0.000064 |
| Z5 | 0.157 | 157 | 0.0007659 | ±0.000015 | 0.282652 | ±0.000036 |
| Z1 | 0.159 | 159 | 0.0010662 | ±0.000005 | 0.282664 | ±0.000038 |
| Z3 | 0.160 | 160 | 0.0018739 | ±0.000011 | 0.282687 | ±0.000054 |
| **CAF-6** | | | | | | |
| Z1 | 0.295 | 295 | 0.0009556 | ±0.000024 | 0.282437 | ±0.000032 |
| Z4 | 0.271 | 271 | 0.0005855 | ±0.000010 | 0.282484 | ±0.000017 |
| Z25 | 0.412 | 412 | 0.0010617 | ±0.000027 | 0.282401 | ±0.000015 |
| Z2 | 0.290 | 290 | 0.0020516 | ±0.000073 | 0.282500 | ±0.000045 |
| Z3 | 0.418 | 418 | 0.0017615 | ±0.000017 | 0.282426 | ±0.000028 |
| Z15 | 0.305 | 305 | 0.0009280 | ±0.000036 | 0.282495 | ±0.000019 |
| Z7 | 0.288 | 288 | 0.0008115 | ±0.000006 | 0.282506 | ±0.000020 |
| Z22 | 0.304 | 304 | 0.0009757 | ±0.000012 | 0.282500 | ±0.000016 |
| Z21 | 0.296 | 296 | 0.0010010 | ±0.000015 | 0.282509 | ±0.000014 |
| Z5 | 0.172 | 172 | 0.0012383 | ±0.000016 | 0.282620 | ±0.000021 |
| Z11 | 0.387 | 387 | 0.0006014 | ±0.000004 | 0.282498 | ±0.000017 |
| Z12 | 0.359 | 359 | 0.0010258 | ±0.000025 | 0.282577 | ±0.000019 |
| Z28 | 0.171 | 171 | 0.0038589 | ±0.000067 | 0.282765 | ±0.000024 |
| Z24 | 0.177 | 177 | 0.0036084 | ±0.000040 | 0.282766 | ±0.000029 |
| Z6 | 0.173 | 173 | 0.0018829 | ±0.000038 | 0.282798 | ±0.000021 |

r the igneous and sedimentary rocks related with the
al Chubut.

| $^{176}Hf/^{177}Hf_{(T)}$ | ±2σ | $\varepsilon Hf_{(T)}$ | ±2σ | $T_{DM}$ (Ga) |
|---|---|---|---|---|
| 0.282707 | 0.000026 | 0.9 | 0.9 | 1.0 |
| 0.282699 | 0.000030 | 0.6 | 1.1 | 1.0 |
| 0.282635 | 0.000048 | -1.6 | 1.7 | 1.1 |
| 0.282631 | 0.000020 | -1.7 | 0.7 | 1.1 |
| 0.282622 | 0.000017 | -2.0 | 0.6 | 1.2 |
| 0.282502 | 0.000023 | 1.9 | 0.8 | 1.3 |
| 0.282465 | 0.000019 | 1.6 | 0.7 | 1.3 |
| 0.282417 | 0.000023 | -9.2 | 0.8 | 1.6 |
| 0.282429 | 0.000027 | -8.9 | 0.9 | 1.5 |
| 0.282439 | 0.000018 | -8.4 | 0.6 | 1.5 |
| 0.282456 | 0.000030 | -7.9 | 1.0 | 1.5 |
| 0.282458 | 0.000020 | -7.9 | 0.7 | 1.5 |
| 0.282483 | 0.000029 | -7.1 | 1.0 | 1.4 |
| 0.282495 | 0.000021 | -6.6 | 0.8 | 1.4 |
| 0.282703 | 0.000031 | 0.6 | 1.1 | 1.0 |
| 0.282688 | 0.000024 | 0.1 | 0.9 | 1.0 |
| 0.282629 | 0.000050 | -1.6 | 1.8 | 1.1 |
| 0.282747 | 0.000044 | 2.1 | 1.6 | 0.9 |
| 0.282673 | 0.000022 | -0.3 | 0.8 | 1.1 |
| 0.282400 | 0.000026 | -9.9 | 0.9 | 1.6 |
| 0.282481 | 0.000028 | -6.9 | 1.0 | 1.4 |
| 0.282715 | 0.000015 | 1.4 | 0.5 | 1.0 |
| 0.282552 | 0.000027 | -4.4 | 0.9 | 1.3 |
| 0.282487 | 0.000021 | -6.7 | 0.8 | 1.4 |
| 0.282436 | 0.000029 | -8.5 | 1.0 | 1.5 |
| 0.282356 | 0.000033 | -11.3 | 1.2 | 1.7 |
| 0.282446 | 0.000043 | -8.1 | 1.5 | 1.5 |
| 0.282478 | 0.000030 | -6.9 | 1.1 | 1.4 |
| 0.282609 | 0.000021 | -2.3 | 0.7 | 1.2 |
| 0.282466 | 0.000018 | -7.4 | 0.7 | 1.5 |
| 0.282464 | 0.000026 | -7.4 | 0.9 | 1.5 |
| 0.282433 | 0.000029 | -8.4 | 1.0 | 1.5 |
| 0.282502 | 0.000060 | -5.9 | 2.1 | 1.4 |
| 0.282571 | 0.000035 | -3.4 | 1.2 | 1.3 |
| 0.282448 | 0.000025 | -7.7 | 0.9 | 1.5 |
| 0.282452 | 0.000020 | -7.5 | 0.7 | 1.5 |
| 0.282207 | 0.000041 | -16.1 | 1.4 | 2.0 |

| | | | | |
|---|---|---|---|---|
| 0.282389 | 0.000038 | -9.6 | 1.3 | 1.6 |
| 0.282454 | 0.000023 | -7.2 | 0.8 | 1.5 |
| 0.282082 | 0.000045 | 8.3 | 1.6 | 1.7 |
| | | | | |
| 0.282531 | 0.000055 | -5.6 | 1.9 | 1.3 |
| 0.282544 | 0.000057 | -5.1 | 2.0 | 1.3 |
| 0.282561 | 0.000054 | -4.5 | 1.9 | 1.3 |
| 0.282644 | 0.000064 | -1.5 | 2.3 | 1.1 |
| 0.282650 | 0.000036 | -1.3 | 1.3 | 1.1 |
| 0.282660 | 0.000038 | -0.9 | 1.3 | 1.1 |
| 0.282681 | 0.000054 | -0.2 | 1.9 | 1.1 |
| | | | | |
| 0.282431 | 0.000032 | -6.0 | 1.1 | 1.5 |
| 0.282481 | 0.000017 | -4.8 | 0.6 | 1.4 |
| 0.282393 | 0.000015 | -4.8 | 0.5 | 1.5 |
| 0.282488 | 0.000045 | -4.1 | 1.6 | 1.4 |
| 0.282412 | 0.000028 | -4.0 | 1.0 | 1.5 |
| 0.282490 | 0.000019 | -3.7 | 0.7 | 1.4 |
| 0.282501 | 0.000020 | -3.7 | 0.7 | 1.4 |
| 0.282494 | 0.000016 | -3.6 | 0.6 | 1.4 |
| 0.282503 | 0.000014 | -3.5 | 0.5 | 1.3 |
| 0.282615 | 0.000021 | -2.2 | 0.7 | 1.2 |
| 0.282494 | 0.000017 | -1.8 | 0.6 | 1.3 |
| 0.282569 | 0.000019 | 0.3 | 0.7 | 1.2 |
| 0.282752 | 0.000024 | 2.6 | 0.8 | 0.9 |
| 0.282754 | 0.000029 | 2.8 | 1.0 | 0.9 |
| 0.282791 | 0.000021 | 4.0 | 0.7 | 0.8 |

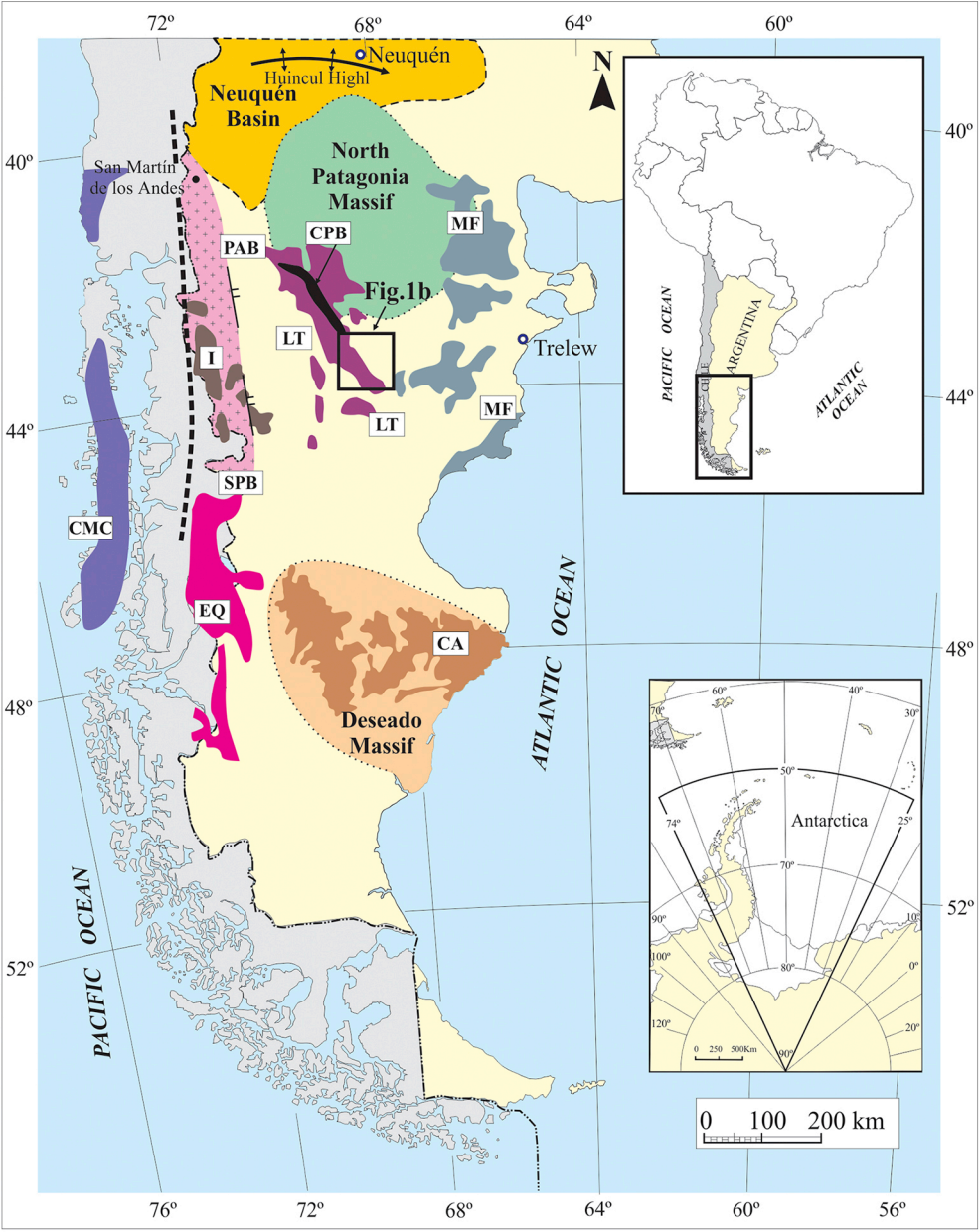
72º
68º
64º
60º
76º
56º
40º
44º
48º
52º
Neuquén
Huincul High
Neuquén Basin
North Patagonia Massif
San Martín de los Andes
PAB
CPB
MF
Fig.1b
LT
I
Trelew
SPB
CMC
EQ
CA
Deseado Massif
ATLANTIC OCEAN
PACIFIC OCEAN
N
PACIFIC OCEAN
ARGENTINA
ATLANTIC OCEAN
Antarctica
0 250 500Km
0 100 200 km

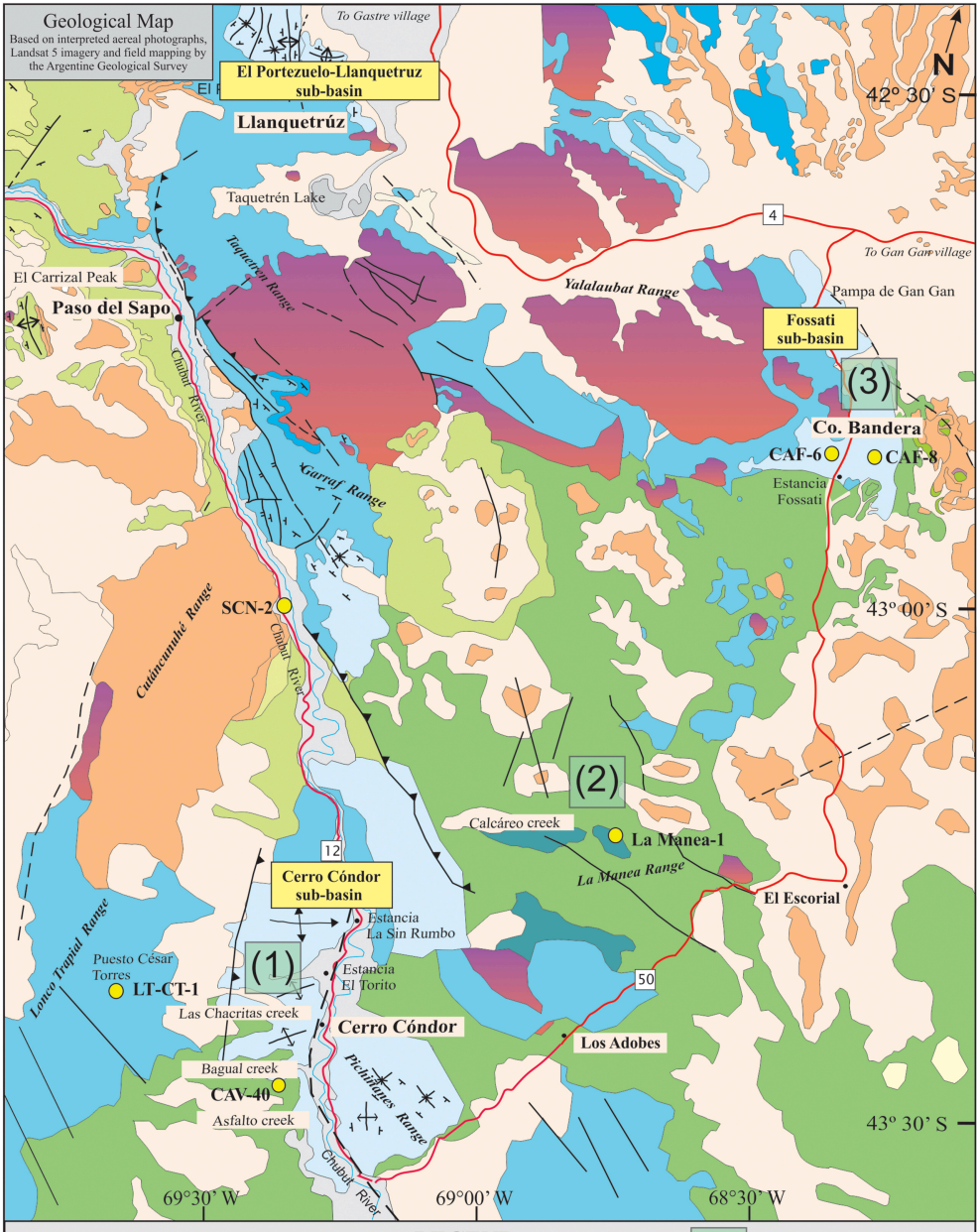
Geological Map
Based on interpreted aereal photographs, Landsat 5 imagery and field mapping by the Argentine Geological Survey
To Gastre village
El Portezuelo-Llanquetruz sub-basin
Llanquetrúz
Taquetrén Lake
Taquetrén Range
El Carrizal Peak
Paso del Sapo
Chubut River
Garraf Range
Yalalaubat Range
To Gan Gan village
Pampa de Gan Gan
Fossati sub-basin
(3)
Co. Bandera
CAF-6
CAF-8
Estancia Fossati
N
42° 30' S
4
Cuáncunuhé Range
SCN-2
Chubut River
43° 00' S
(2)
Calcáreo creek
La Manea-1
La Manea Range
El Escorial
12
Cerro Cóndor sub-basin
Estancia La Sin Rumbo
Lonco Trapial Range
Puesto César Torres
LT-CT-1
(1)
Estancia El Torito
50
Las Chacritas creek
Cerro Cóndor
Los Adobes
Bagual creek
CAV-40
Asfalto creek
Pichiñigües Range
43° 30' S
Chubut River
69°30' W
69°00' W
68°30' W
LEGEND
Quaternary (Alluvial, colluvial and piedmont deposits)
Eocene / Miocene Basalts
Paso del Sapo Fm. (Upper Cretaceous: fluvial sediments)
Lefipán Fm. (Upper Cretaceous: tidal sediments, fine fossiliferous sandstones and conglomerates)
Chubut Gr. (Lower to Upper Cretaceous: fluvial conglomerates, sandstones, tuffs)
Cañadón Calcareo Fm. (Lower Cretaceous: lacustrine limestones, tuffites and tuff)
Cañadón Asfalto Fm. (Middle to Upper Jurassic: lacustrine limestones, shales, evaporites, sandstones, tuffs and basalts)
Lonco Trapial Fm. (Lower to Middle Jurassic: mesosilicic volcanites)
Las Leoneras Fm. (Lower Jurassic: lacustrine sediments and tuffs)
Mamil Choique Fm. (Permian to Triassic: granites and migmatites)
(1) Sampling areas
Samples
Fault
Thrust Fault
Syncline
Strike and Dip
Anticline
10 km

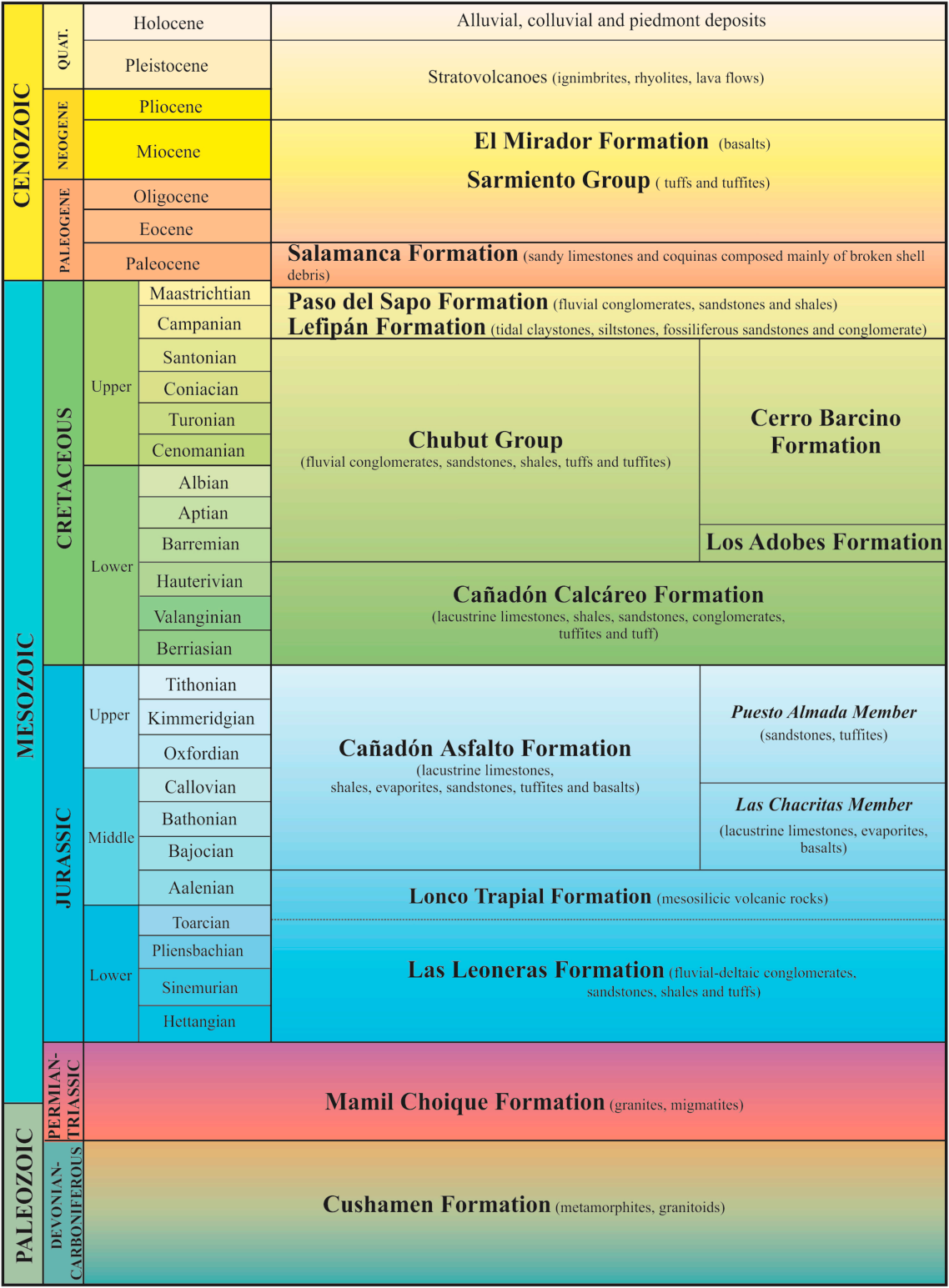
CENOZOIC
MESOZOIC
PALEOZOIC
QUAT.
NEOGENE
PALEOGENE
CRETACEOUS
JURASSIC
PERMIAN-TRIASSIC
DEVONIAN-CARBONIFEROUS
Holocene
Pleistocene
Pliocene
Miocene
Oligocene
Eocene
Paleocene
Upper
Lower
Maastrichtian
Campanian
Santonian
Coniacian
Turonian
Cenomanian
Albian
Aptian
Barremian
Hauterivian
Valanginian
Berriasian
Tithonian
Kimmeridgian
Oxfordian
Callovian
Bathonian
Bajocian
Aalenian
Toarcian
Pliensbachian
Sinemurian
Hettangian
Alluvial, colluvial and piedmont deposits
Stratovolcanoes (ignimbrites, rhyolites, lava flows)
El Mirador Formation (basalts)
Sarmiento Group ( tuffs and tuffites)
Salamanca Formation (sandy limestones and coquinas composed mainly of broken shell debris)
Paso del Sapo Formation (fluvial conglomerates, sandstones and shales)
Lefipán Formation (tidal claystones, siltstones, fossiliferous sandstones and conglomerate)
Chubut Group
(fluvial conglomerates, sandstones, shales, tuffs and tuffites)
Cerro Barcino Formation
Los Adobes Formation
Cañadón Calcáreo Formation
(lacustrine limestones, shales, sandstones, conglomerates, tuffites and tuff)
Cañadón Asfalto Formation
(lacustrine limestones, shales, evaporites, sandstones, tuffites and basalts)
Puesto Almada Member
(sandstones, tuffites)
Las Chacritas Member
(lacustrine limestones, evaporites, basalts)
Lonco Trapial Formation (mesosilicic volcanic rocks)
Las Leoneras Formation (fluvial-deltaic conglomerates, sandstones, shales and tuffs)
Mamil Choique Formation (granites, migmatites)
Cushamen Formation (metamorphites, granitoids)

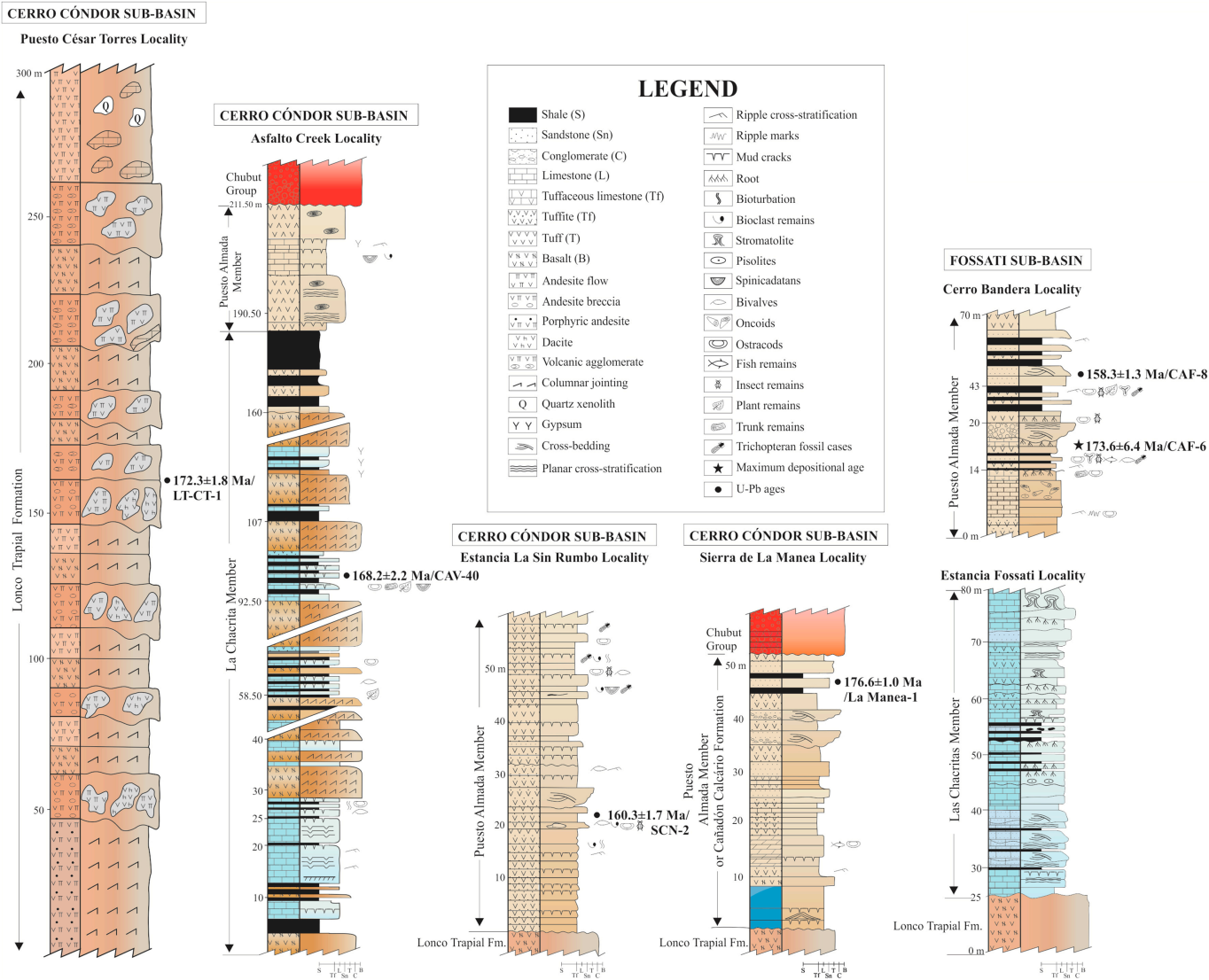
CERRO CÓNDOR SUB-BASIN
Puesto César Torres Locality
300 m
250
200
150
100
50
Lonco Trapial Formation
Q
172.3±1.8 Ma/
LT-CT-1
CERRO CÓNDOR SUB-BASIN
Asfalto Creek Locality
Chubut Group
211.50 m
Puesto Almada Member
190.50
160
107
La Chacrita Member
168.2±2.2 Ma/CAV-40
92.50
58.50
40
30
25
20
10
S Tf Ss C L T B
LEGEND
Shale (S)
Sandstone (Sn)
Conglomerate (C)
Limestone (L)
Tuffaceous limestone (Tf)
Tuffite (Tf)
Tuff (T)
Basalt (B)
Andesite flow
Andesite breccia
Porphyric andesite
Dacite
Volcanic agglomerate
Columnar jointing
Quartz xenolith
Gypsum
Cross-bedding
Planar cross-stratification
Ripple cross-stratification
Ripple marks
Mud cracks
Root
Bioturbation
Bioclast remains
Stromatolite
Pisolites
Spinicadatans
Bivalves
Oncoids
Ostracods
Fish remains
Insect remains
Plant remains
Trunk remains
Trichopteran fossil cases
Maximum depositional age
U-Pb ages
CERRO CÓNDOR SUB-BASIN
Estancia La Sin Rumbo Locality
50 m
40
30
20
10
Puesto Almada Member
160.3±1.7 Ma/
SCN-2
Lonco Trapial Fm.
CERRO CÓNDOR SUB-BASIN
Sierra de La Manea Locality
Chubut Group
50 m
40
30
20
10
Puesto Almada Member or Cañadón Calcário Formation
176.6±1.0 Ma
/La Manea-1
Lonco Trapial Fm.
FOSSATI SUB-BASIN
Cerro Bandera Locality
70 m
43
20
14
0 m
Puesto Almada Member
158.3±1.3 Ma/CAF-8
173.6±6.4 Ma/CAF-6
Estancia Fossati Locality
80 m
70
60
50
40
30
25
0 m
Las Chacritas Member
Lonco Trapial Fm.

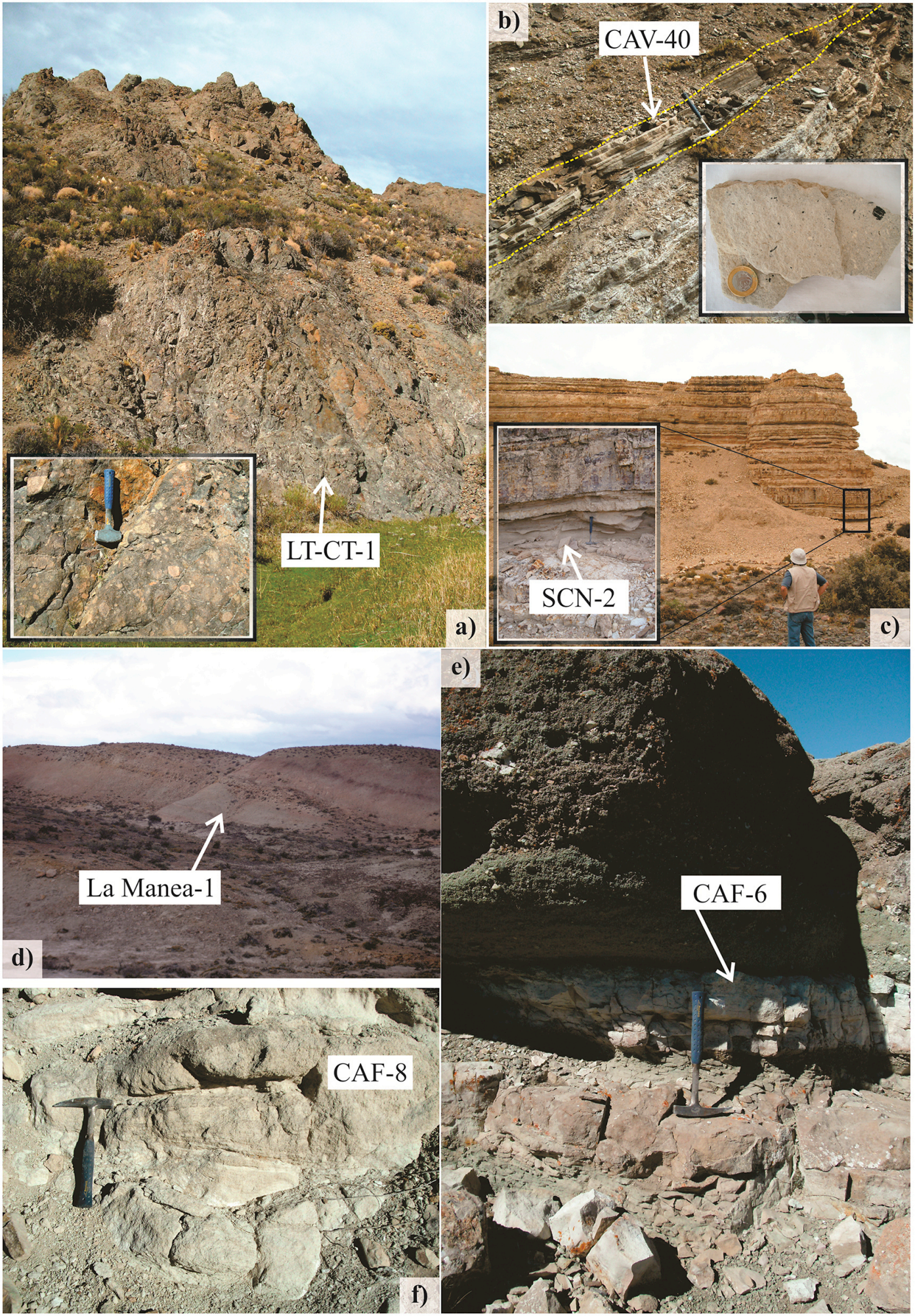
b)
CAV-40
LT-CT-1
a)
SCN-2
c)
La Manea-1
d)
e)
CAF-6
CAF-8
f)

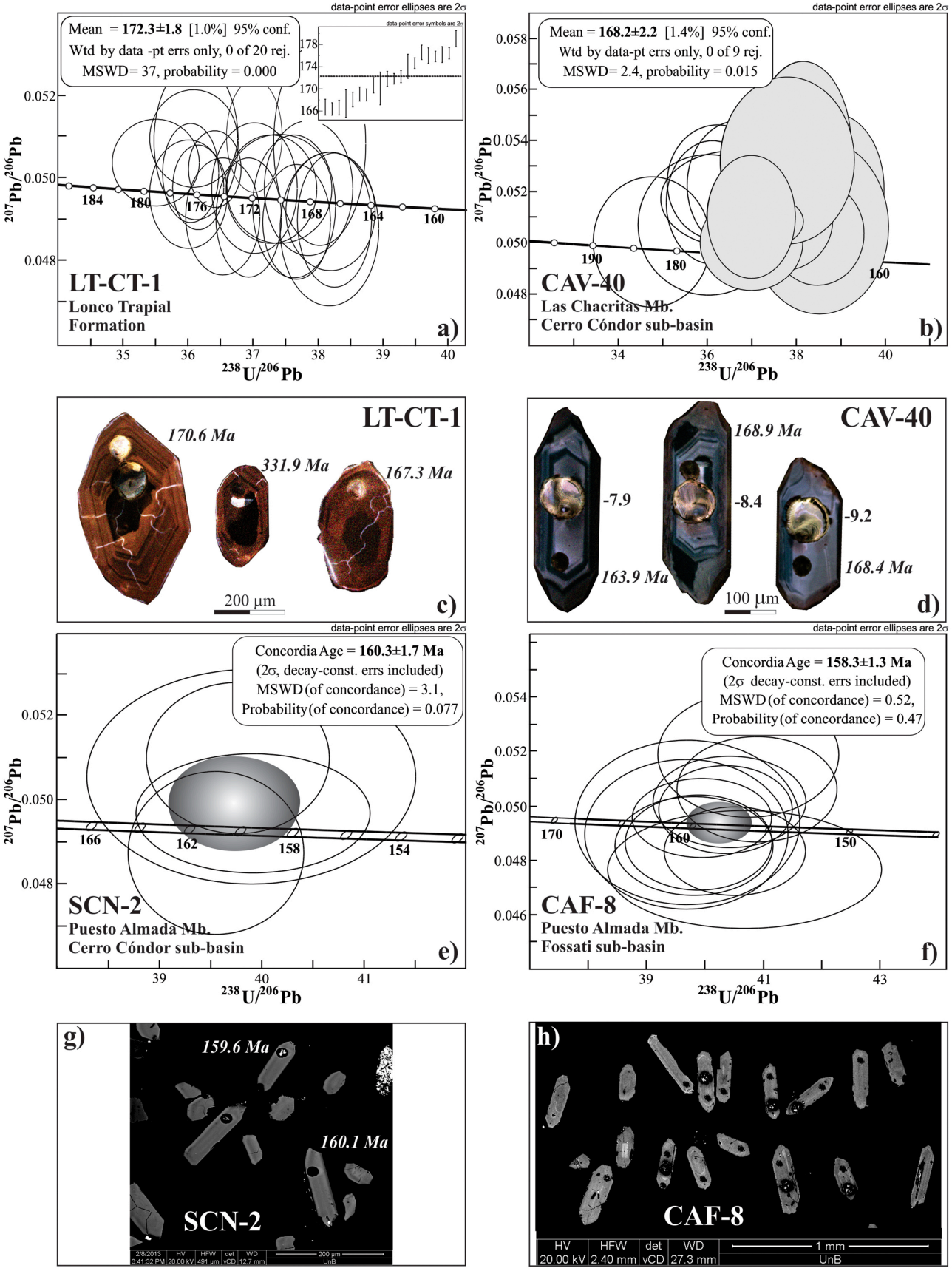
data-point error ellipses are 2σ
Mean = 172.3±1.8 [1.0%] 95% conf.
Wtd by data -pt errs only, 0 of 20 rej.
MSWD= 37, probability = 0.000
data-point error symbols are 2σ
178
174
170
166
0.052
0.050
0.048
207Pb/206Pb
184
180
176
172
168
164
160
LT-CT-1
Lonco Trapial
Formation
a)
35
36
37
38
39
40
238U/206Pb
data-point error ellipses are 2σ
Mean = 168.2±2.2 [1.4%] 95% conf.
Wtd by data-pt errs only, 0 of 9 rej.
MSWD= 2.4, probability = 0.015
0.058
0.056
0.054
0.052
0.050
0.048
207Pb/206Pb
190
180
160
CAV-40
Las Chacritas Mb.
Cerro Cóndor sub-basin
b)
34
36
38
40
238U/206Pb
LT-CT-1
170.6 Ma
331.9 Ma
167.3 Ma
200 µm
c)
CAV-40
168.9 Ma
-7.9
-8.4
-9.2
163.9 Ma
168.4 Ma
100 µm
d)
data-point error ellipses are 2σ
Concordia Age = 160.3±1.7 Ma
(2σ, decay-const. errs included)
MSWD (of concordance) = 3.1,
Probability (of concordance) = 0.077
0.052
0.050
0.048
207Pb/206Pb
166
162
158
154
SCN-2
Puesto Almada Mb.
Cerro Cóndor sub-basin
e)
39
40
41
238U/206Pb
data-point error ellipses are 2σ
Concordia Age = 158.3±1.3 Ma
(2σ decay-const. errs included)
MSWD (of concordance) = 0.52,
Probability (of concordance) = 0.47
0.054
0.052
0.050
0.048
0.046
207Pb/206Pb
170
160
150
CAF-8
Puesto Almada Mb.
Fossati sub-basin
f)
39
41
43
238U/206Pb
g)
159.6 Ma
160.1 Ma
SCN-2
2/8/2013 | HV | HFW | det | WD | 200 µm
3:41:52 PM | 20.00 kV | 491 µm | vCD | 12.7 mm | UnB
h)
CAF-8
HV | HFW | det | WD | 1 mm
20.00 kV | 2.40 mm | vCD | 27.3 mm | UnB

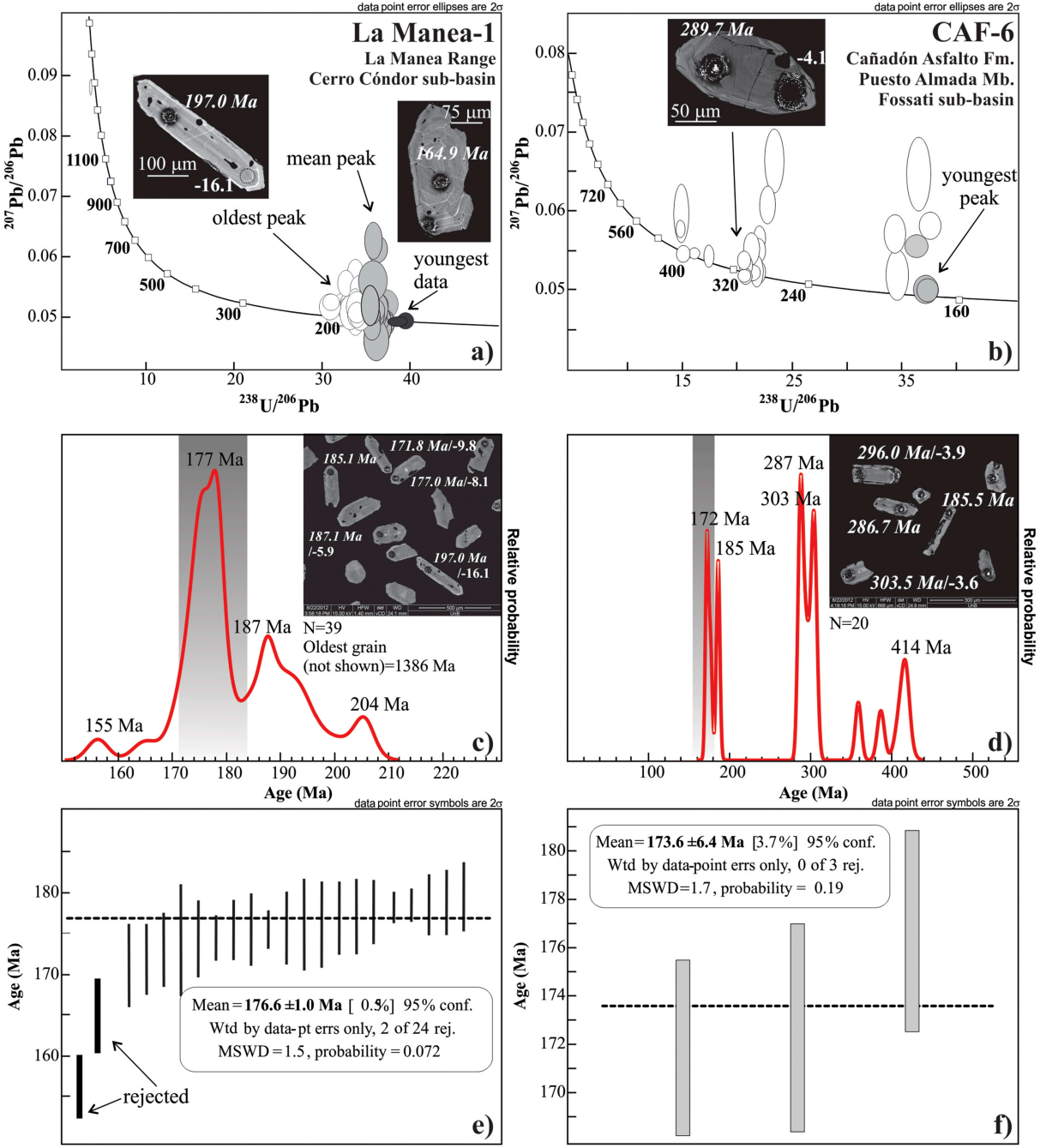
data point error ellipses are 2σ
La Manea-1
La Manea Range
Cerro Cóndor sub-basin
197.0 Ma
-16.1
100 µm
75 µm
164.9 Ma
mean peak
oldest peak
youngest data
1100
900
700
500
300
200
0.09
0.08
0.07
0.06
0.05
10
20
30
40
207Pb/206Pb
238U/206Pb
a)
data point error ellipses are 2σ
CAF-6
Cañadón Asfalto Fm.
Puesto Almada Mb.
Fossati sub-basin
289.7 Ma
-4.1
50 µm
youngest peak
720
560
400
320
240
160
0.08
0.07
0.06
0.05
15
25
35
207Pb/206Pb
238U/206Pb
b)
177 Ma
171.8 Ma/-9.8
185.1 Ma
177.0 Ma/-8.1
187.1 Ma /-5.9
197.0 Ma /-16.1
187 Ma
N=39
Oldest grain (not shown)=1386 Ma
204 Ma
155 Ma
160
170
180
190
200
210
220
Age (Ma)
Relative probability
c)
287 Ma
303 Ma
172 Ma
185 Ma
296.0 Ma/-3.9
185.5 Ma
286.7 Ma
303.5 Ma/-3.6
N=20
414 Ma
100
200
300
400
500
Age (Ma)
Relative probability
d)
data point error symbols are 2σ
180
170
160
Age (Ma)
Mean = 176.6 ±1.0 Ma [ 0.5%] 95% conf.
Wtd by data-pt errs only, 2 of 24 rej.
MSWD = 1.5, probability = 0.072
rejected
e)
data point error symbols are 2σ
Mean = 173.6 ±6.4 Ma [3.7%] 95% conf.
Wtd by data-point errs only, 0 of 3 rej.
MSWD=1.7, probability = 0.19
180
178
176
174
172
170
Age (Ma)
f)

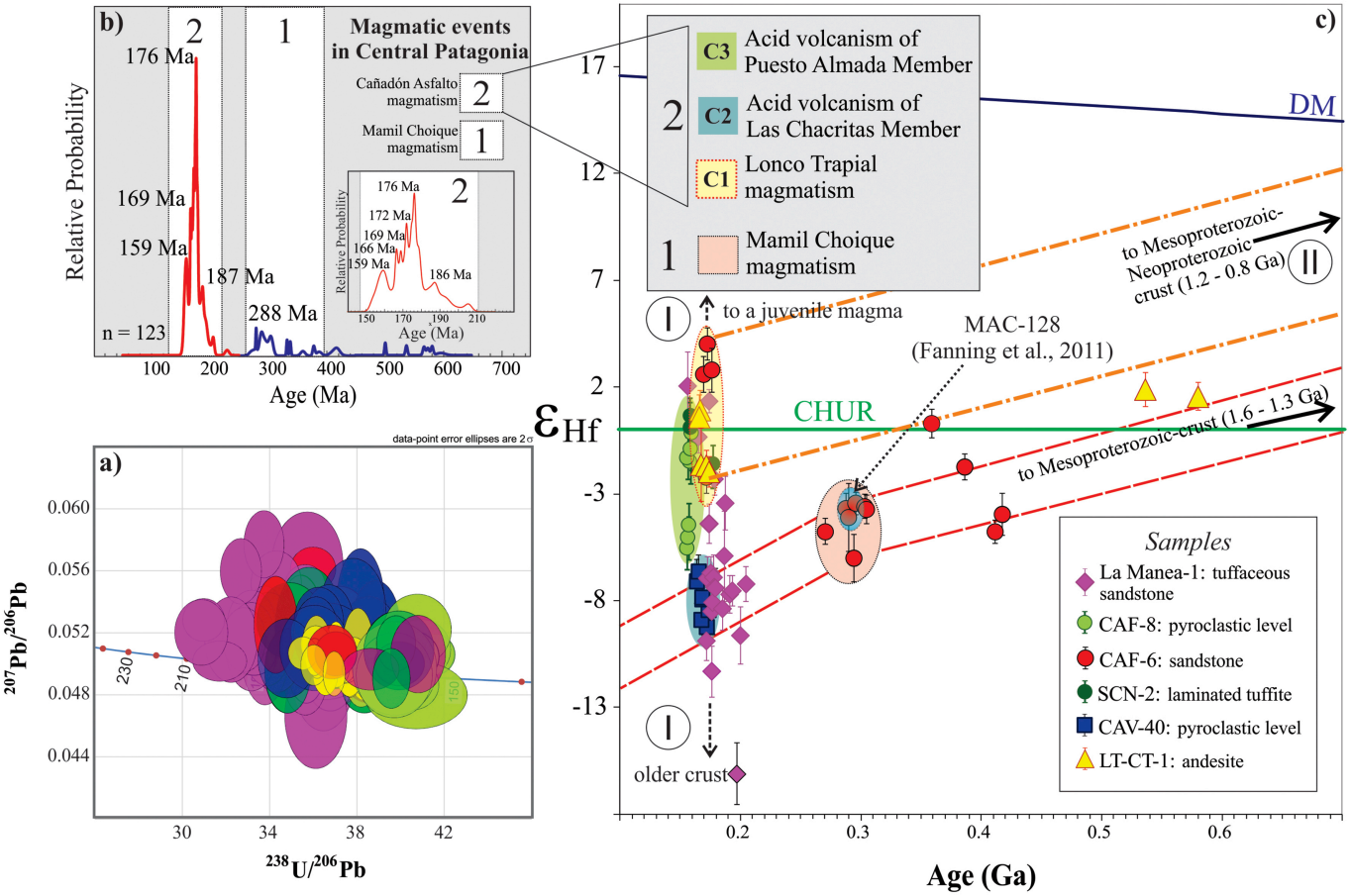
b)
Magmatic events in Central Patagonia
Cañadón Asfalto magmatism
Mamil Choique magmatism
Relative Probability
Age (Ma)
176 Ma
169 Ma
159 Ma
187 Ma
288 Ma
n = 123
172 Ma
166 Ma
186 Ma
a)
data-point error ellipses are 2σ
$^{207}Pb/^{206}Pb$
$^{238}U/^{206}Pb$
c)
C3 Acid volcanism of Puesto Almada Member
C2 Acid volcanism of Las Chacritas Member
C1 Lonco Trapial magmatism
Mamil Choique magmatism
DM
CHUR
εHf
to a juvenile magma
to Mesoproterozoic-Neoproterozoic crust (1.2 - 0.8 Ga)
to Mesoproterozoic crust (1.6 - 1.3 Ga)
MAC-128 (Fanning et al., 2011)
older crust
Samples
La Manea-1: tuffaceous sandstone
CAF-8: pyroclastic level
CAF-6: sandstone
SCN-2: laminated tuffite
CAV-40: pyroclastic level
LT-CT-1: andesite
Age (Ga)

Palynomorph
Spinicaudatans
Ostracods
Charophytes
Radimetric Ages
(Ma.)
Stratigraphic correlation
Biostratigraphy
CERRO CÓNDOR SUB-BASIN
FOSSATI SUB-B.
CAÑADON ASFALTO FORMATION
LONCO TRAPIAL FORMATION
LAS CHACRITAS MEMBER
PUESTO ALMADA MEMBER
JURASSIC
Upper
Middle
Lower
Tithonian
152.1 ± 0.9
Kimmeridgian
157.3 ± 1.0
Oxfordian
163.5 ± 1.0
Callovian
166.1 ± 1.2
Bathonian
168.3 ± 1.3
Bajocian
170.3 ± 1.4
Aalenian
174.1 ± 1.0
Toarcian
182.7 ± 0.7
Pliensbachian
190.8 ± 1.0
Sinemurian
199.3 ± 0.3
Hettangian
201.3 ± 0.2
145.0
U/Pb 172±2 Ma (LT-CT-1, this paper)
K/Ar 176±4 Ma (Stipanicic and Bonetti, 1970)
(Nullo,1983)
K/Ar 167±5 Ma (Lesta et al., 1980)
K/Ar 173±9 Ma (Silva Nieto,2005)
(Cúneo et al., 2013)
Ar/Ar 184±5 Ma (Gastre area, Zaffarana and Somoza 2013)
U/Pb 168±2 Ma (CAY-40 Asfalto Creek Locality, this paper)
K/Ar 170±4 Ma (Salani, 2007)
U/Pb 178,766±0,092 Ma (Lahuinco Creek Locality. Cúneo et al., 2013)
(Las Chacritas Creek Locality. Cabaleri et al., 2010a; Monferran, 2015)
(La Angostura - Lahuinco Creek Locality, Musacchio, 1995, 2001)
(Lahuinco Creek Locality. Volkheimer et al., 2008)
(Estancia El Torito, Puesto Almada Locality, Cabaleri et al., 2010a; Gallego et al., 2010, 2011; Monferran et al., 2013, 2016)
(Musacchio, 1989, 2001)
U/Pb 160±2 Ma (SCN-2 La Sin Rumbo Locality, this paper)
Youngest zircon grain=156±3 Ma, (La Manea-1, Sierra de La Manea Locality, this paper)
K/Ar=147±3.3 Ma (Punta Biotita Locality, Cabaleri et al., 2010a)
U/Pb 158±1 Ma (CAF-8 Cerro Bandera Locality, this paper)
(Cerro Bandera Locality, Cabaleri et al., 2013)

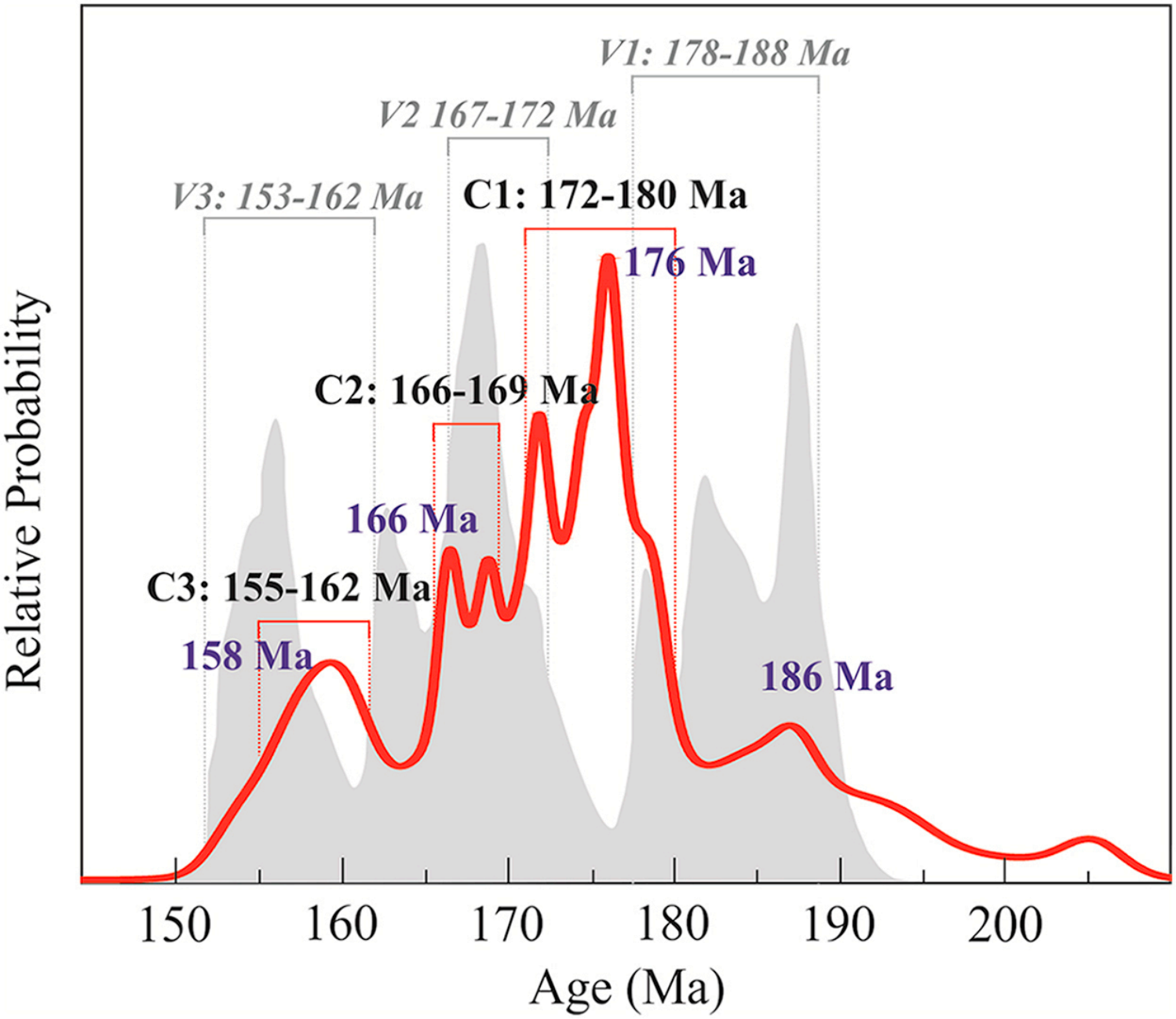
V1: 178-188 Ma
V2 167-172 Ma
V3: 153-162 Ma
C1: 172-180 Ma
176 Ma
C2: 166-169 Ma
166 Ma
C3: 155-162 Ma
158 Ma
186 Ma
Relative Probability
150
160
170
180
190
200
Age (Ma)

**Highlights**

- A combined U-Pb and Hf isotope study of the main formations related to the evolution of the Cañadón Asfalto basin, Patagonia, Argentina was carried out.
- The Mamil Choique magmatic event between 359 and 230 Ma and the Cañadón Asfalto magmatic event between 200 and 150 Ma were recognized.
- Within the younger magmatic event three magmatic/volcanic cycles with different Hf isotopic characteristics are recognized. These are related to the Lonco Trapial Formation (C1, ca. 176 Ma), as well as the Las Chacritas (C2, ca. 166 Ma) and the Puesto Almada (C3, ca. 159 Ma) members of the Cañadón Asfalto Formation.
- These events and basin evolution are discussed against crustal reworking and tectonic settings in Patagonia.